THESIS

# A FRAMEWORK FOR LIFE-CYCLE COST OPTIMIZATION OF BUILDINGS UNDER SEISMIC AND WIND HAZARDS

Submitted by

Guo Cheng

Department of Civil and Environmental Engineering

In partial fulfillment of the requirements

For the Degree of Master of Science

Colorado State University

Fort Collins, Colorado

Summer 2014

Master's Committee:

Advisor: Hussam Mahmoud

Rebecca Atadero
Kelly Strong

# ABSTRACT

A FRAMEWORK FOR LIFE-CYCLE COST OPTIMIZATION OF BUILDINGS UNDER SEISMIC AND WIND HAZARDS

The consequential life and economic impact resulting from the exposure of building structures to single hazards have been well quantified for seismic and wind loading. While it has been recognized that structures are likely to be subjected to multiple hazards during their service life, designing for such scenario has been achieved by as considering the predominant hazard. Although from a structural reliability perspective, this might be a reasonable approach, it does not necessarily result in the most optimal life-cycle cost for the designed structure. Although such observation has been highlighted in recent studies, research is still needed for developing an approach for multi-hazard life-cycle optimization of structures. This study presents a framework, utilizing structural reliability, for cost optimization of structures under wind and seismic hazards. Two example structures, on which the framework is applied, are investigated and their life-cycle cost analyzed. The structures represent typical medium and high rise residential buildings located in downtown San Francisco area. The framework comprises of using the first order reliability method (FORM), programed in MATLAB and interfaced with ABAQUS finite element software to obtain the corresponding reliability factors for the buildings under various loading intensities characterized by the probability of exceedance. The finite element analyses are carried out based on real seismic and wind pressure records using nonlinear finite element time-history dynamic analysis. The random variables selected include hazard intensity (wind load and seismic intensity) and elastic modulus of steel. Once the failure probabilities are determined for the given limit

state functions, the expected failure cost for the building service duration considering earthquake or wind hazard, or both, is calculated considering discount rate. The expected life-cycle cost is evaluated using life-cycle cost function, which includes the initial construction cost and the expected failure cost. The results show that the optimal building design considering the wind hazard alone, the seismic hazard alone or a combination of both is different. The framework can be utilized for an optimal design of both wind and seismic load for a given level of hazard intensity.

# TABLE OF CONTENTS

# LIST OF TABLES

# LIST OF FIGURES

# CHAPTER 1

# INTRODUCTION

## 1.1 Statement of the problem

The impact of single natural or man-made hazards on buildings has been studied extensively. In recent years however, there is a notable increase in the occurrence of natural hazards and the associated rise in the potential exposure of structures to multiple hazards during their service life. For example, significant life and economical loses resulted from single 2010 Haiti earthquake and the 2011 Tohoku earthquake and the subsequent tsunami in Japan. Recent events in the US also highlighted the severe impact that can be imposed on infrastructure and the resulting social impact including the 1992 Hurricane Andrew and the 2005 Hurricane Katrina. Notwithstanding, regions subjected to high level of wind hazards can also be subjected to low or moderate seismic hazard or any other hazard for that matter. However, in current design codes the predominate hazard controls the design. Such approach while might be considered reasonable from safety perspective, it does not necessarily result in the most optimized life-cycle cost of the structures considered. Therefore, a new design methodology is needed to not only protect life safety, but also minimize economic losses to an acceptable level.

For earthquake and wind loads, the design hazard level can be specified as earthquake intensity or basic wind speed with the associated return periods corresponding to a structural performance levels. However, the selection of these design levels is basically left to the professional experience and judgment of the design engineer and the building owner who has to bare the burden of cost. However, such approach might be neither safe nor economical.

Therefore, a more comprehensive performance-based design with optimized life cycle cost is needed for designing structures against multi-hazard.

Generally speaking, a structure designed based on a lower design level will subjected to a higher failure risk, which associated with a higher "future cost". On the other hand, a structure designed for a higher design level may reduce the failure risk, but will suffer a higher structural construction cost. Therefore, finding the optimal design level is needed to provide a structural design with optimized performance. In order to achieve this goal, a comprehensive method is developed in this study, which takes into the consideration of the uncertainty in loading and resistance, cost variation, and lifetime factors.

Typical medium and high rise buildings subjected to high risk of earthquake and wind hazard are assessed using the developed framework to determine the optimal structural design considering multi-hazards. The framework comprises of using the first order reliability method (FORM), programed in MATLAB and interfaced with ABAQUS finite element software to obtain the corresponding reliability factors for the buildings under various loading intensities characterized by the probability of exceedance. The finite element analyses are carried out based on real seismic and wind pressure records using nonlinear finite element time-history dynamic analysis. The random variables selected include hazard intensity (wind load and seismic intensity) and elastic modulus of steel. Once the failure probabilities are determined for the given limit state functions, the expected failure cost for the building service duration considering earthquake or wind hazard, or both, is calculated. The expected life-cycle cost is evaluated using life-cycle cost function, which includes the initial construction cost and the expected failure cost.

## 1.2 Objective and Scope of Study

As previously discussed, the significance of expanding on the implication of designing structures against multi-hazards is rather obvious. In this study, the performance of structures to various levels of wind and seismic events is assessed and the reliability factors evaluated for different limit state functions. The reliability factors are used to determine the life-cycle cost assessment of buildings considering multi-hazard risks. The specific objectives of this study include:

1. Developing the tool for determining of the structural reliability while considering uncertainties in loading and resistance.
2. Define different structural performance types and levels for the buildings considered for the given seismic and wind loading.
3. Establish a framework for life-cycle cost assessment of the structures which accounts for the different building performances, structural reliability, and other lifetime factors over building's service time.

## 1.3 Organization of Thesis

This thesis is primarily focus on presenting a framework for life-cycle cost based optimization design for medium and high rise buildings subjected to seismic and wind hazards. An approach for assessing the structural reliability using ABAQUS finite element dynamic simulation and MATLAB programming is developed. Two realistic 10- and 30-story structures are selected for the evaluation and are assumed to be located in San Francisco, CA.

The thesis includes six chapters. Chapter 1 introduces the statement of problem and objective of this study. Chapter 2 discusses the background and literature review from 1) structural design and mitigation against multi-hazards, 2) structural reliability analysis and methodology development considering earthquake and wind hazards, and 3) structural life-cycle cost based optimization design and the development of cost functions. Chapter 3 concentrates on the development of the framework, which includes 1) structure configuration and finite element model development, 2) limit state function definition, 3) cost function estimation, and 4) methodology for interfacing MATLAB with ABAQUS for the reliability-based assessment. Chapter 4 is focus on the identification of earthquake and wind load, respectively. The time-history records for both hazards are carefully selected and scaled based on code standard in order to satisfy design provisions. Chapter 5 presents the analytical investigation of this study including the results of Eigenvalue analysis, structural initial cost, basic failure cost function estimation, structural reliability, and expected life-cycle cost. The implication of the analytical results of the structural reliability and expected life-cycle cost is discussed. Chapter 6 summarizes the finding and significance of this study followed by a discussion of future research prospective.

# CHAPTER 2

# BACKGROUND AND LITERATURE REVIEW

## 2.1 Introduction

In this chapter, previous research on multi-hazard design, structural reliability, and system optimization are presented. During the last decade, studies on multi-hazard design have become one of most popular research topics for structural engineers. The majority of studies focused on one or at most two of these areas, e.g. research about investigation of structure reliability subjected to multi-hazards. The literature review for this research is concentrated on the three topics mentioned above.

## 2.2 Multiple Hazard

### 2.2.1 Overview

In this chapter, previous studies on multi-hazard design are presented. Since multi-hazard design is still relatively an unexplored subject to structural engineers, the number of previous studies in this field is limited. With the increasing occurrence of various natural hazards, multi-hazard design is becoming an essential consideration since structures are likely to be exposed to various hazards over their service life and research regarding to only individual hazards is no longer satisfactory to engineers and researchers concerned with structural safety. There is often sequent impact following a hazard event, such as flooding due to a hurricane or a tsunami after an earthquake. Technological advancements have allowed engineers to investigate structures

subjected to multiple hazards in order to insure the structure is resistant to natural or man-made hazards.

### 2.2.2 Historical Records

#### 2.2.2.1 Earthquake Hazards

Earthquakes, as one of the most threatening natural hazards to a structure's system, are always considered major catastrophes to affect human civilization. The Northridge Earthquake in California, U.S. of January 17, 1994, at 4:30 A.M. local time is regarded as one of the largest and the costliest disasters in U.S history. A magnitude of 6.8 was reported at Los Angeles, California. It caused damage to 114,000 residential and commercial structures spread over 2,100 square mile and even resulted in the collapse of buildings. This earthquake resulted in 72 deaths and more than 8,700 injuries along with initial cost estimates of total damages at U.S. $25 billion (DeBlasio and Allan J, 2004). Figure 2-1 shows the building collapse consequences made by the Northridge Earthquake.

**Figure 2-1 Building Collapse Consequences by the Northridge Earthquake**

The Kobe Earthquake event in Japan, occurred on January 17, 1995, at 5:46 A.M local time has a magnitude of 7.2 (M). The earthquake occurred within a metropolitan area of 4 million people which produced the absolute damage loss is estimated at U.S. $147 billion. In city, 100,000 building were destroyed and nearly 180,000 building were partially destroyed. The official estimation shows that more than 300,000 people were homeless on the night of the event. It has been confirmed that nearly 5,500 eventual deaths and the number of people injury reaches about 35,000 (EQE International, 1995). As a result of the earthquake – 600 to 700 in the fires, the rest in collapsing structures due to the seismic load. (Horwich, 2000). Figure 2-2 shows the collapsing structures under Kobe Earthquake.

**Figure 2-2 Collapsing Structures under Kobe Earthquake**

A report on the Great Wenchuan Earthquake in China indicates that approximately 68,000 people were killed and the property loss estimation ranges from CNY ¥150 to CNY ¥500 billion, which is around U.S. $22 to U.S. $74 billion (Zifa, 2008). A series of significant earthquake events in recent decades around the world and subsequent damages have reminded structural engineers of the necessity for earthquake mitigation.

Although, unlike Japan or the U.S., the economic loss value in other parts of the world such as the third world countries may be much less, the economic impact to these countries could be greater due to the losses being a large proportion of the Gross National Product (GNP). An economic loss report due to earthquake events from 1972 to 1990 includes three of the most significant losses as proportions of the GNP in the Central American countries is made by Coburn and Spence (2002). Their report announced that the earthquake events cost 40% of the Nicaraguan GNP, 18% of the Guatemalan GNP, and 31% of the El Salvador in 1972, 1976, and 1986 respectively.

#### 2.2.2.2 Strong Wind Hazards

Strong winds, such as those associated with hurricanes and tornadoes; also have the capability of damaging structures and its components especially in urban areas. Hurricanes are tropical storms that form over warm ocean waters and generally make landfall on the East Coast of the U.S. and the Gulf of Mexico.

In 1982, Hurricane Alicia impacted Houston, TX and resulted in extensive impact to high-rise buildings in downtown (Beer 2011). Hurricane Andrew has been named as one of the most costly natural disaster in Untied States due to an estimated U.S. $26.5 billion overall losses and 65 fatalities it has caused in 1992 (Rappaport 1993). Due to Andrew, 25,524 homes were destroyed and commercial buildings were severely damaged in Dade County, Miami (Beers 2011). Additionally, tornadoes can also cause significant damage. In 1998, the downtown area of Nashville, TN was struck by a tornado and it caused building damages. A few years later, many high-rise buildings in the downtown area of Atlanta, GA, were heavily damaged by a tornado

strike (Beers 2011). Figure 2-3 shows the damages of medium and high rise buildings in urban area made by hurricanes.

Hurricane Andrew – Miami, FL in 1992

Hurricane Alicia – Houston, TX in 1982

**Figure 2-3 Structural Damages by Hurricanes (Beer, 2011)**

### 2.2.3 Significance of Multiple Hazard

During the recent decades, rapid population growth and economic development have increased the potential threats from both man-made and natural hazards to human civilization. Structural engineers started to notice the significance of multi-hazard design at the beginning of twenty-first century, when the terrorism event of September 11, 2001 illustrated the significance of designing structures against blast loads and fire hazards. In addition, the repeated occurrence natural hazards events including earthquakes, hurricanes, and tsunamis highlighted the necessity for multi-hazard consideration.

While confronting a multi-hazard scenario the structure design becomes more complicated since the loading from different types of hazards can result in conflicts in load demands on the structure. Consider, for example, suspended ceilings in office buildings. These

ceilings can become potential safety risks when blast or wind pressure force result in ceiling tiles falling on the building's occupants (Ettouney and Glover, 2002). Another example is the structure mass, and while reinforced concrete structures may be beneficial in terms of reducing wind pressure; a large mass becomes one of the most safety-threatening weaknesses for seismic motion resistance.

In subsequent years, additional studies have continually stated that a perspective of multi-hazard effects on structural systems, such as buildings and bridges, would offer great benefits and proposed the theory of multi-hazards, which pointed out that any structural system should have an inherent resiliency to resist all type of hazards (Ettouney et al., 2005).

Later, an expanded study concluded that by considering life-cycle costs multi-hazard design and analysis are also beneficial for making appropriate engineering and economical decisions (Ettouney and Alampalli, 2006). Although Ettouney and Alampalli (2006) did not develop a method for structure multi-hazard design, their studies strongly illustrate the significance of multi-hazard design.

In 2007, it was suggested that many highly populated urban cities in coastal areas can be subjected to both seismic activity and strong winds (Zhou, 2007). Zhou (2007) presented a performance assessment of a 35-story transfer-plate high-rise building subjected to seismic and strong wind loads. Analytical methods including Equivalent Static Load Analysis (ESLA), Response Spectrum Analysis (RSA), Pushover Analysis (POA), and Linear and Nonlinear Time-History Analysis (LTHA and NTHA) were utilized to carry out the structural response in terms of the lateral global drift, inter-story drift ratio, and inter story shear force. The comparison between structural responses subjected to design wind and seismic loads is shown in Figure 2-4.

By comparing analytical results with the performance objectives of building provisions, Zhou and Xu concluded the importance of the role of multi-hazard design in structural engineering.

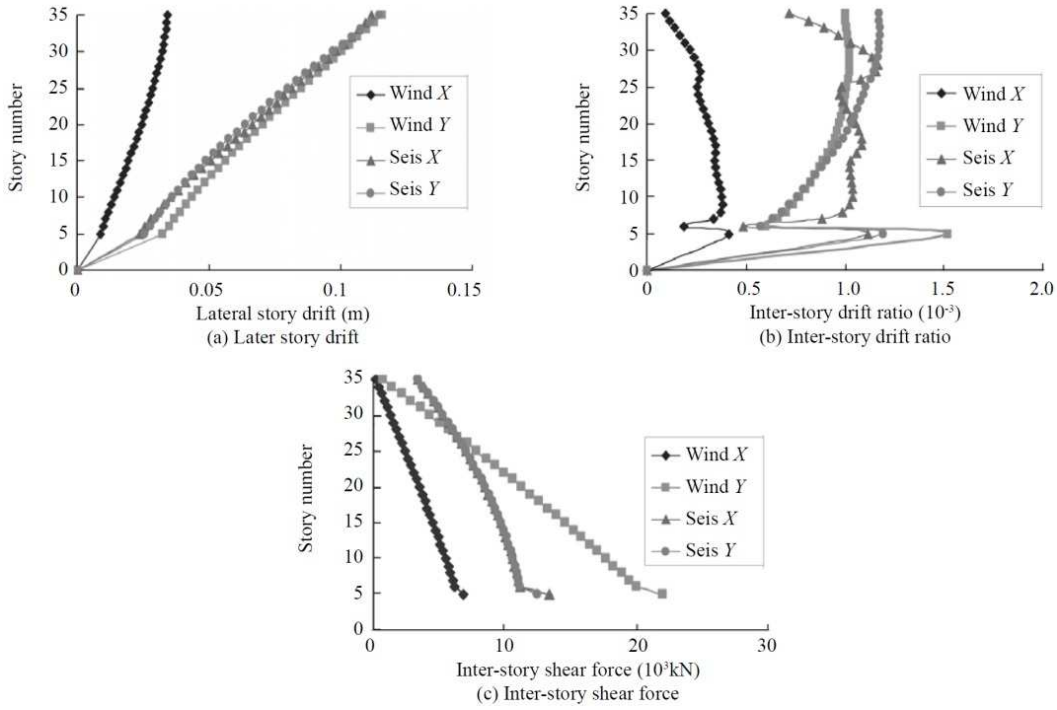


**Figure 2-4 Comparison between Structural Response under Design Wind and Seismic Loads (Zhou, 2007)**

A more recent study considered structural safety in relation to strong winds and earthquake hazards in terms of ASCE-7 standards (Duthinh & Simiu, 2009). This study concluded that structures in regions of significant wind and seismic hazards could have twice the risk of exceedance of limit states than corresponding risks present in regions where only one of these hazards dominates. Duthinh and Simiu (2009) proposed an approach to modify ASCE 7 provisions, which ensures the designs for regions where both earthquake and wind hazards are considered to be significant can satisfy the minimum requirements associated with safety implicit in provisions for regions where only one hazard matters.

## 2.3 Reliability Analysis

### 2.3.1 Overview

In a basic sense, structural reliability uses the concept of probability to expresses the structure's capacity (probability of failure) to meet pre-defined limit states when subjected to uncertain loads. By investigating this capacity, the structure can be designed intelligently so that the safety, serviceability, and durability of the structure can be guaranteed. The concept of reliability was introduced in the structural engineering field in the 1970's when engineers and researchers started to recognize that traditional structural analysis and design were no longer satisfactory in relation to natural and man-made hazards due to the corresponding uncertainty. A series of valuable research based on reliability theory was then established and completed. The details of some significant studies are presented herein.

### 2.3.2 Background and Previous Works

The structural reliability studies can be classified into two groups; namely analytical and simulation-based reliability analysis. In the analytical reliability analysis usually one or several numerical equations or functions are developed to represent the relationship between random variables and failure probability. The simulation reliability analysis combines certain reliability methods or algorithms with simulation of structural behavior under certain loading. A review of these two classifications is presented herein.

#### 2.3.2.1 Analytical Reliability Analysis

Studies based on overall structural reliability have been an active research area (Moses, 1983). A system reliability based method for analyzing nonlinear-framed structures subjected to random loads was developed (Kam, Corotis, and Rossow, 1983). An extended study for the

aforementioned method introduced uncertainty of structural materials (Lin & Corotis, 1985). Kam (1987) summarized these previous studies and proposed a reliability assessment considering the framed structures with initial geometrical imperfections of structure, which gives relative meaningful results.

Reliability theory was then utilized on the dynamic analysis of structures subjected to seismic loading (O'Connor & Ellingwood, 1987). O'Connor and Ellingwood investigated the reliability of a simple structure system by developing a method for dynamic nonlinear analysis using the single degree of freedom equation of motion and defining the limit states for damages. Two damage models have been developed to define the limit state for simple structure subjected to earthquakes; (1) the ductility factor $\mu$, and (2) the yield damage index $D$. The expressions of these two damage models are presented in Equation 2-1 and Equation 2-2, respectively.

$$\mu = \frac{u_{\max}}{u_y} \qquad \textbf{Equation 2-1}$$

In Equation 2-1, the ductility factor is defined as the ratio of the maximum displacement of an inelastic system, $u_{max}$ to its yield displacement, $u_y$

$$D = \sum_{i=1}^{n} \left( \left| \frac{\Delta \delta_{pt}}{\Delta \delta_{pf}} \right|^{1/m} \right)_i \qquad \textbf{Equation 2-2}$$

Where;

$1/m = 1 - 0.86r_1$; $r_1$ indicates the relative deflection ratio, i.e., the ratio between the compression and tension change in plastic deflection in cycle $i$; $\Delta\delta_{pt}$ is the tension change in

plastic deflection in cycle $i$; $\Delta\delta_{pf}$ is the tension change in plastic deflection in a one-cycle test to failure conducted at the relative deformation ratio of cycle $i$. For $D = 1$, a collapsed damaged state is reached. O'Connor and Ellingwood developed a limit state function, as shown in Equation 2-3, to conduct a reliability study for a simple structure sample and the results are presented in Table 2-1.

$$Z = M - C\left(\frac{1.2ASW}{RT^{2/3}}\right) - D - L = 0 \qquad \textbf{Equation 2-3}$$

in which:$A$ = peak ground acceleration; $S$ = soil factor; $W$ = weight of the structure; $R$ = system factor; $M$ = structural resistance; $C$ = influence coefficient transforming the base shear to a load effect (beam moment, column shear, etc); $D$ = dead load effect; and $L$ = live load effect. This study is reviewed because it represents a specific way for structural reliability analysis subjected to seismic loading by establishing a numerical limit state function.

**Table 2-1 Reliabilty Indices Results (O'Connor & Ellingwood, 1987)**

| Limit State | Pf | β (annual) | β (50 years) |
|---|---|---|---|
| μ = 2.0 | 0.004797 | 2.59 | 0.71 |
| μ = 3.0 | 0.002564 | 2.8 | 1.11 |
| μ = 4.0 | 0.0012065 | 3.04 | 1.55 |
| $D_1 = 1.0$ | 0.001848 | 2.91 | 1.33 |
| $D_2 = 1.0$ | 0.00971 | 3.11 | 1.66 |

The reliability studies on resisting wind effects on structures have also been investigated in recent decades. In 1990, Kareem presented a study of the reliability analysis of wind sensitive structures. In this study, several different reliability approximations and numerical methods – the Mean value First-Order Second-Moment method (MFOSM) and Advanced First-Order Second-

Moment method (AFOSM) - as well as simulation technologies - Variance Reduction Techniques - are proposed. The reliability analysis on a tall reinforced concrete chimney was examined; Figure 2-5 shows the pressure distribution on the chimney considering lifetime maximum wind at the site. The results of the deterministic and probabilistic analysis corresponding to different node levels are summarized and compared in Table 2-2. The results show the wind induced moments computed from the dynamic analysis using two different analysis concepts (code recommended values and random vibration-based analysis) and structural inherent moment capacity at each level, which is used to compute the factor of safety. The values of reliability index also are also computed by MFOSM and AFOSM respectively. The general accordance of the trends from both the factor of safety and the reliability indexes proofs the rationality of these results.

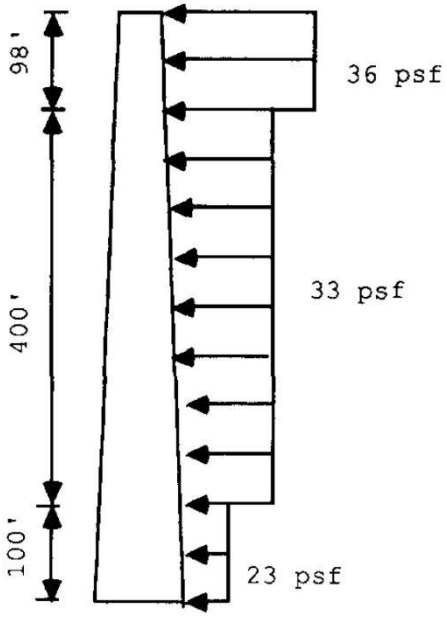


**Figure 2-5 Pressure distribution on the chimney (Kareem, 1990)**

**Table 2-2 Deterministic and probabilistic analysis (Kareem, 1990)**

| Node | Height (ft) | Diameter (ft) | Moment capacity ($\times 10^7$ lb · ft) | Wind-induced moment [a] ($\times 10^7$ lb · ft) | Factor of safety | Wind-induced moment [b] ($\times 10^7$ lb · ft) | Factor of safety | $\beta^{(1)}$ | $\beta^{(2)}$ |
|---|---|---|---|---|---|---|---|---|---|
| **2** | 538 | 37.64 | 5.4485 | 0.2361 | 23 | 0.5281 | 10.3 | 6.13 | 2.81 |
| **3** | 478 | 39.45 | 7.5343 | 0.9572 | 7.9 | 1.9937 | 3.78 | 3.68 | 2.08 |
| **4** | 418 | 41.25 | 9.9183 | 2.1552 | 4.6 | 3.6023 | 2.75 | 2.99 | 1.91 |
| **5** | 358 | 43.06 | 12.564 | 3.8434 | 3.27 | 5.3492 | 2.35 | 2.73 | 1.80 |
| **6** | 298 | 44.86 | 15.498 | 6.0430 | 2.56 | 7.9735 | 1.94 | 2.08 | 1.57 |
| **7** | 238 | 46.67 | 18.763 | 8.7758 | 2.13 | 11.033 | 1.70 | 1.62 | 1.38 |
| **8** | 178 | 48.48 | 22.803 | 12.063 | 1.89 | 14.507 | 1.57 | 1.38 | 1.25 |
| **9** | 118 | 50.28 | 29.533 | 15.926 | 1.85 | 18.324 | 1.61 | 1.49 | 1.31 |
| **10** | 84 | 51.30 | 38.166 | 18.372 | 2.08 | 20.645 | 1.85 | 1.98 | 1.53 |
| **11** | 54 | 52.21 | 42.937 | 20.651 | 2.08 | 22.685 | 1.89 | 2.08 | 1.57 |
| **12** | 34 | 52.81 | 55.886 | 22.230 | 2.51 | 24.261 | 2.31 | 2.80 | 1.81 |
| **13** | 14 | 53.41 | 47.131 | 23.858 | 1.98 | 25.600 | 1.84 | 1.98 | 1.54 |
| **14** | 0 | 53.83 | 56.815 | 25.028 | 2.26 | 27.402 | 2.07 | 2.38 | 1.69 |

**a: Code recommended values**

**b: Random vibration-based analysis**

**$\beta^{(1)}$-MFOSM**

**$\beta^{(2)}$-AFOSM**

#### 2.3.2.2 Simulation Reliability Analysis

Reliability analysis can be easily performed if a simple numerical function is able to represent the limit state function as a function in terms of the system random variables. When dealing with complex structural systems, a finite element based model can be a very valuable tool for evaluating the structure's response to different conditions and limit states. Therefore, combining structural reliability analysis with finite element analysis, often referred to as finite element reliability analysis (FE-RA) becomes necessary for assessing reliability of complex structures.

Huh and Haldar (2001), proposed a reliability estimation based on the time-history finite element method analysis of realistic structural systems subjected to seismic loading. The study included a hybrid method, which consists of the Finite Element Method, Response Surface Method, and First Oder Reliability Method, for assessing the reliability of a real nonlinear structure subjected to short duration seismic loading. Four different schemes have been developed according to the aforementioned method. By presenting a two-story nonlinear steel framed structure example subjected to seismic load and assumptions of random variables for two cases of serviceability state and one strength limit state, which is shown in Table 2-3, the reliability analysis can be carried out. The final results of reliability analysis calculated by the aforementioned four schemes are presented by comparing with the one from Monte Carlo simulation, which is presented in Table 2-4, in order to demonstrate the accuracy of these schemes. The final conclusion states that the proposed algorithm can be used to estimate the risk for both the serviceability and strength limit states for nonlinear structures subjected to seismic loading.

As this study is reviewed because it shows another for structural reliability analysis approach considering to seismic loading using concept of FE-RA. Moreover, the definition of the coefficient of variant is referred in this study herein.

**Table 2-3 Statistical Description of Random Variables for the Example (Huh & Haldar, 2001)**

| Limit State | | SERVICEABILITY STATE | | | | Strength Limit State | |
|---|---|---|---|---|---|---|---|
| | | Case 1: 9 Random Variables | | Case 2: 7 Random Variables | | | |
| Random variable | Mean value | COV | Dist. | COV | Dist. | COV | Dist. |
| $E\ (kN/m^2)$ | $1.9994 \times 10^8$ | 0.06 | LN | 0.06 | LN | 0.06 | LN |
| $A^b\ (m^2)$ | $2.045 \times 10^{-2}$ | 0.05 | LN | 0.05 | LN | – | – |
| $I_x^b\ (m^4)$ | $1.861 \times 10^{-3}$ | 0.05 | LN | 0.05 | LN | 0.05 | LN |
| $Z_x^b\ (m^3)$ | $5.670 \times 10^{-3}$ | 0.05 | LN | – | – | – | – |
| $A^c\ (m^2)$ | $3.335 \times 10^{-2}$ | 0.05 | LN | 0.05 | LN | – | – |
| $I_x^c\ (m^4)$ | $2.364 \times 10^{-3}$ | 0.05 | LN | 0.05 | LN | 0.05 | LN |
| $Z_x^c\ (m^3)$ | $8.374 \times 10^{-3}$ | 0.05 | LN | – | – | 0.05 | LN |
| $F_y\ (kN/m^2)$ | $2.482 \times 10^5$ | – | – | – | – | 0.10 | LN |
| $\xi$ | 0.02 | 0.15 | LN | 0.15 | LN | 0.15 | LN |
| | 1.0 | 0.20 | Type I | 0.20 | Type I | – | – |
| $g_e$ | 2.3 | – | – | – | – | 0.20 | Type I |

Note: b = beam, c = column, and LN = lognormal distribution

**Table 2-4 Reliability Analysis Results for the Example (Huh & Haldar, 2001)**

| | Scheme 1 | Scheme 2 | Scheme 3 | Scheme 4 |
|---|---|---|---|---|
| (a) Serviceability Limit State: Case 1 - 9 Random Variables<br>MCS [$P_f = 0.03627$ ($\beta = 1.7957$); CPU Time = 83,479 s] | | | | |
| Proposed algorithm | | | | |
| $\beta$ | 1.771 | 1.801 | 1.814 | 1.800 |
| $P_f$ | 0.03824 | 0.03583 | 0.03482 | 0.03592 |
| CPU time (s) | 54 | 1,340 | 84 | 476 |
| TNSP | 57 | 1,593 | 93 | 569 |
| Error (%) | -5.43 | 1.21 | 4.00 | 0.96 |
| (b) Serviceability Limit State: Case 2 - 7 Random Variables<br>MCS [$P_f = 0.03606$ ($\beta = 1.7984$); CPU Time = 81,890 s] | | | | |
| Proposed algorithm | | | | |
| $\beta$ | 1.772 | 1.799 | 1.822 | 1.800 |
| $P_f$ | 0.03816 | 0.03598 | 0.03424 | 0.03592 |
| CPU time (s) | 43 | 357 | 62 | 148 |
| TNSP | 45 | 429 | 66 | 173 |
| Error (%) | 5.82 | -0.22 | -5.05 | -0.39 |
| (c) Strength Limit State<br>MCS [$P_f = 0.02143$ ($\beta = 2.0251$); CPU Time = 80,686 s] | | | | |
| Proposed algorithm | | | | |
| $\beta$ | 1.981 | 2.014 | 2.054 | 2.004 |
| $P_f$ | 0.02379 | 0.02200 | 0.02001 | 0.02254 |
| CPU time (s) | 53 | 374 | 73 | 162 |
| TNSP | 45 | 429 | 66 | 173 |
| Error (%) | -11.02 | -2.66 | 6.63 | -5.16 |
| TNSP: The total number of experimental sampling points | | | | |

With the support of well-developed computer technology, advanced finite element software, such as SAP 2000 and ABAQUS, has been widely utilized in structural engineering. The computational integration of FE analysis with reliability analysis has gained much attention in recent years and the outcome of such includes open access computer software packages such as OpenSees (Haukass, 2003), FERUM (Haukaas et al., 2003), and RELSYS (Estes and Frangopol, 1998).

In recent years, advanced FE-RA software packages such as NESSUS (SwRI, 2009) and STRUREL (Gollwitzer et al., 2006) have been developed to complement existing packages. Finite Element Reliability Using MATLAB (FERUM) is a reliability analysis model developed by researchers at the UC Berkeley. It provides a platform for various reliability analyses for structural engineering (Haukaas et al., 2003). The finite element software ABAQUS is one of the most widely used commercial packages, owing to its advanced capabilities. By using an interface code between FERUM and ABAQUS, Lee (2012) developed a FE System Reliability Analysis (FE-SRA) framework and successfully demonstrated it by analyzing numerical examples of an aircraft wing torque box and a bridge pylon. Figure 2-6 shows a flow chart outlining the principle concept of this approach.. The interface code between ABAQUS and FERUM allowed for computing the probabilities of general system events and their sensitivities and provided a more versatile computing platform than other existing FE-RA software since each of the software packages represents the specialization in reliability and FE analysis (Lee, 2012).

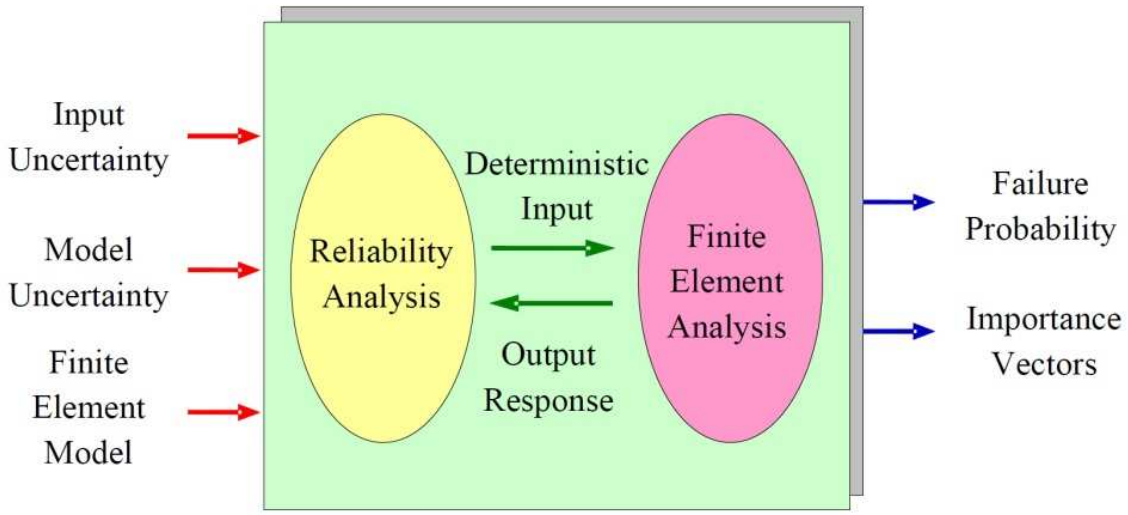


**Figure 2-6 Data Flows during Finite Element Reliability Analysis (Lee, 2012)**

## 2.4 Life-Cycle Cost Optimization Models

### 2.4.1 Overview

During the design of new buildings or retrofitting of existing buildings, cost and safety are considered the most significant factors. It is therefore necessary to consider the structural reliability and the cost of failure with the exceedances of different limit state during the entire life-cycle of a structure so that an optimal design can be achieved (Kang & Wen, 2000). In this section, previous research on structure design optimization based on cost functions will be reviewed. In the review, various cost functions are presented and the development of parameters in these cost functions as well as their analytical procedures are identified.

Kang and Wen (2000), proposed a formulation for expected life-cycle cost to design structures against multi-hazard. The study utilized finite element reliability analysis (FE-RA) to achieve a new optimal design approach. The proposed formulation included a series of significant factors such as lifetime, limit state, failure probability, discount rate, initial cost and failure cost. The basic concept of life-cycle cost optimization can be illustrated by a relationship of cost and optimal design level as shown in Figure 2-7. A design of structure which considers lower loads has a lower initial cost, but a higher expected failure cost. On the other hand, a design that reduces the expected failure cost may raise the initial cost. Therefore, the principle idea of this optimization design is to determine the point of minimum total cost. This optimal design point can be used as a target design value.

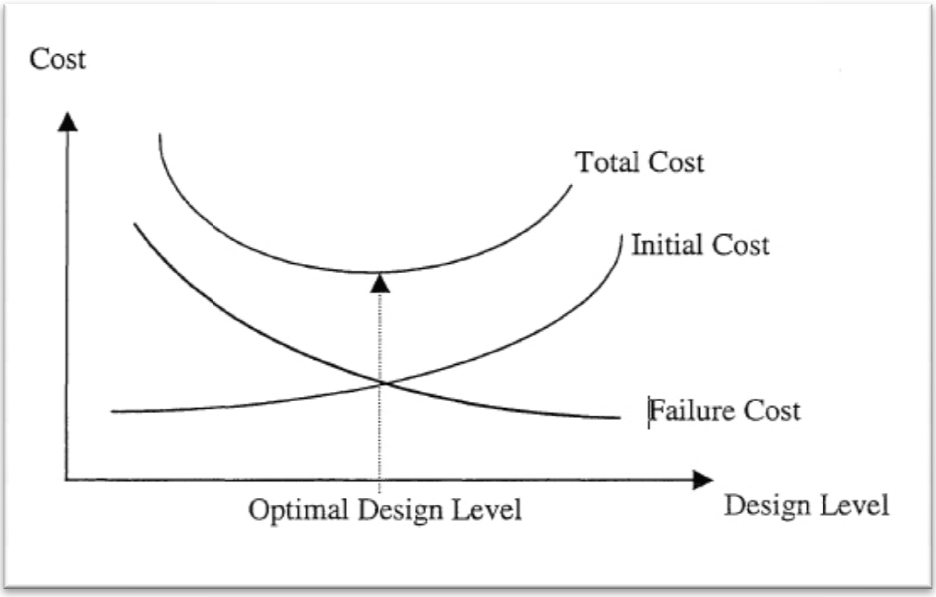


**Figure 2-7 Cost and Optimal Design Level (Kang & Wen, 2000)**

### 2.4.2 Review of Previous Cost Models

The cost-based optimal design is typically integrated with statistical or reliability analysis. Liu and Neghabat (1972) proposed a simple mathematical method for determining the optimal earthquake intensity which structures are designed to against. An objective function in terms of the variables of structural properties and earthquake intensity was identified. The optimization design considered the total construction cost of the structure and the expected cost of earthquake damage throughout the entire service life of the structure. Equation 2-4 represents the objective function aforementioned. The optimum design was achieved due to the minimization of the total expected cost of the structure.

$$K(i_0) = K_c(i_0) + K_d(i_0) \qquad \textbf{Equation 2-4}$$

where; $K(i_0)$, $K_c(i_0)$ and $K_d(i_0)$ represent the expected total construction and earthquake risk or damage costs of the structure respectively as a functions of the design intensity $i_0$.

A general cost model includes the employment of a contractor and fabricators. The cost of individual system configuration was proposed to help designers make a decision considering profit and overhead (Russell and Choudhary, 1980).

The economic-based optimal structural design along with the cost functions and models were utilized to deal with different structures in various circumstances. An introduction of a cost function and available methods which can deal with optimization design of offshore structures was presented (Vanmarcke and Angelides, 1983). Tao et al. (1994) conducted a reliability-based life-cycle cost optimization study and presented an approach to design bridges using the cost matrix for Markov Decision Process (MDP).

The life-cycle cost functions were utilized in the optimization design for entire structure systems in various studies including the work by Warszawski et al. (1996), Ang and Leon (1997), and Wen and Shinozuka (1997), which made significant contribution to the development of cost function optimization. Warszawski et al. (1996) offered an economic evaluation approach in terms of a cost function targeting the building design code against seismic load. In this cost function, the damage levels, including the damage to building and its occupants, and the corresponding costs were defined. The life-cycle cost was evaluated and considered as an annual loss. Cost parameters, such as discount ratios, were included in this cost function (Warszawski, Gluck, and Segal 1996). Ang and Leon (1997) proposed an optimization approach for structural damage control and collapse prevention during an earthquake event, which systematically integrate factors quantitatively so that a target reliability can be obtained. These factors include:

intensity of seismic hazards, probability of failures, and the structure's costs. The balance between the costs of protection versus potential future losses caused by an earthquake was also considered in this study. The life-cycle cost function proposed considered the total expected life-cycle cost and consists of the initial cost, the cost of repair or replacement, cost of contents loss, cost of economic loss due to business interruption, and the cost of injury and fatality. Lastly, the target reliability was determined on the basis of this cost function (Ang & Leon, 1997).

Sarma and Adeli (1998) summarized research of the cost optimization of concrete structures including reinforced concrete, pre-stressed concrete and fiber-reinforced concrete structures. The conclusion of the study indicated that (1) most of cost optimization studies tend to concentrate on structural elements such as beams, so there is a need to performance regard to realistic three-dimensional structures; (2) the costs are significant in industrialized countries such as the cost of the formwork, labor, and transportation and should not be ignored (3) additional research pertaining to life-cycle cost optimization of structures as well as reliability-based optimization design is necessary in the future..

### 2.4.3 Life-Cycle Cost Optimization Function

For life-cycle cost optimization design, the key issue is to find a proper treatment of loading and resistance uncertainties. The cost function, otherwise, should include the factors of construction, maintenance and operation, repair, and damage or failure consequence (loss of revenue, deaths and injuries, etc.). The discount ratio also needs to be considered due to potential future loss. By defining certain limit states, the corresponding financial consequences can be carried out due to the loadings, which can be caused by severe natural and man-made hazards that occur infrequently. The life-cycle cost function of Kang and Wen (2000) is used in this

study to consider multiple limit states under multi-hazard. The expected total cost over a time period ($t$), which is the design life of a new structure or the remaining life of a retrofitted structure, can be expressed as a function of time t and the design variable vector $X$ as follows:

$$E\left[C(t,X)\right] = C_0(X) + E\left[\sum_{i=1}^{N(t)}\sum_{j=1}^{k} C_j e^{-\lambda t_i} P_{ij}(t_i, X)\right] + \int_0^t C_m(X) e^{-\lambda\tau} d\tau \qquad \textbf{Equation 2-5}$$

In the closed form above, $C_0$ is the construction cost for the new or retrofitted structure and $C_j$ is the cost in present dollar of $j^{th}$ limit state; $X$ represents the design variable vector, e.g., design loads or resistance; $i$ is the number of hazard occurrences such as strong wind or earthquake; $t_i$ is the hazard loading period, and the total number of hazard is considered during $t$ period is expressed by $N(t)$. Both $t_i$ and $N(t)$ are regarded as random variables. The $e^{-\lambda t}$ term indicates a discount factor over time $t$ and $\lambda$, a constant, is the discount rate annually; $P_{ij}$ is the probability of exceeding the $j^{th}$ limit state when $i^{th}$ occurrence of a single hazard or joint occurrence of multi-hazards; $k$ represents the total number of limit states in consideration, and $C_m$ accounts for the operation and maintenance cost per year.

The occurrence of hazards is modeled as a Poisson Process with an annual occurrence rate of $v$. The structure resistance is assumed invariant over time. The probability of failure under multiple loadings is properly evaluated based on the event based load coincidence method (Wen, 1990). Then Equation 2-5 can be written in closed form considering multiple hazards and limit states as

$$E\left[C(t,X)\right] = C_0 + C_F \frac{\left(1-e^{-\lambda t}\right)}{\lambda} + C_m \frac{\left(1-e^{-\lambda t}\right)}{\lambda} \qquad \textbf{Equation 2-6}$$

in which, $C_F$ is the expected failure cost of exceeding limit states and can be expressed by

$$C_F = \sum_{i=1}^{k} C_i \left[ \sum_{j=1}^{n} v_j P_i^j + \sum_{j=1}^{n-1} \sum_{k=j+1}^{n} v_{jk} P_i^{jk} + \sum_{j=1}^{n-2} \sum_{k=j+1}^{n-1} \sum_{l=k+1}^{n} v_{jkl} P_i^{jkl} + \ldots \right] \qquad \textbf{Equation 2-7}$$

where,

$v_{jk} = v_j v_k (\mu d_j + \mu d_k)$, coincidence occurrence rate of hazards $j$ and $k$;

$v_{jkl} = v_j v_k v_l (\mu d_j \mu d_k + \mu d_k \mu d_l + \mu d_j \mu d_l)$, coincidence occurrence rate of hazards $j$, $k$ and $l$;

$P_i^{jk}$ = probability of exceeding of $ith$ limit state given the coincidence of hazards $j$ and $k$;

$P_i^{jkl}$ = probability of exceeding of $ith$ limit state given the joint occurrence of hazards $j$, $k$ and $l$;

$\mu d_j$ = mean duration of hazard $j$.

In this study, however, the joint occurrence of multiple hazards is out of consideration since the probability of occurrence of two severe hazards, in this case strong wind and earthquake, at the same time is nearly nothing. Therefore, the final life-cycle cost function can be expressed as:

$$E[C(t, X)] = C_0 + \sum_{i=1}^{k} C_i \sum_{j=1}^{n} v_i P_i^j \frac{\left(1 - e^{-\lambda t}\right)}{\lambda} + C_m \frac{\left(1 - e^{-\lambda t}\right)}{\lambda} \qquad \textbf{Equation 2-8}$$

## 2.5 Summary

In this chapter, previous studies related to multi-hazards, structure reliability analysis, and life-cycle cost based optimization design were reviewed. By focusing on some of recent studies, which were conducted to 1) investigate the significance and potential value of concerning the risk from multi-hazards for building structures, 2) present the development of structure reliability

analysis study, 3) introduce two general concepts (by deriving numerical function as the limit state function and by FE-RA) of solving structure reliability analysis, 4) illustrate the development of life-cycle cost optimization design for structures and the development of expect life-cycle cost function. It is found that the research in each of these fields can be sophisticated and makes great contributions to the society of structural engineering, yet, there is barely study combining all of these areas. The finding inspired us to develop a new framework combining minimum life-cycle cost structural design subjected to multi-hazards with finite element simulation based structure reliability analysis. By utilizing an innovative FE-RA method, this new framework shows its true research significance in the society of civil engineering.

# CHAPTER 3

# DEVELOPMENT OF THE FRAMEWORKS

## 3.1 Overview

In this Chapter, the framework for this study is discussed in detail. Figure 3-1 shows the general procedure of the framework. The components of this framework include – 1) structure configuration and finite element model development, 2) limit state function definition, 3) cost function estimation, and 4) methodology for interfacing MATLAB with ABAQUS for the reliability-based assessment.

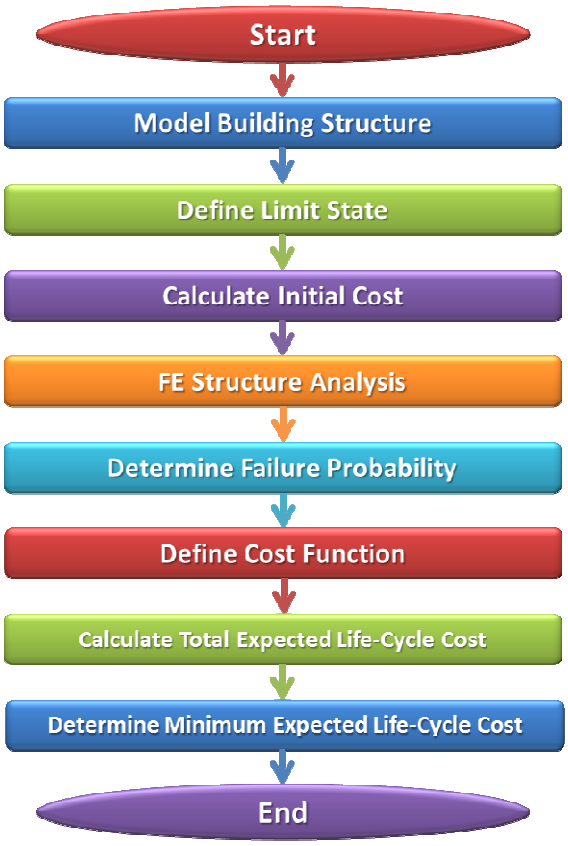


**Figure 3-1 Procedure of Determining Minimum Total Expected Life-Cycle Cost**

## 3.2 Structural Configuration and Model Development

### 3.2.1 Background Introduction

The structure considered in this study is moment frames, which are the lateral load resisting systems in a typical 3D steel structure. The moment frames, known Special Moment Resisting Frames (SMRF) are typically employed as lateral load resisting system for wind and seismic loads. Two-dimensional (2D) finite element models are used to simulate the SMRF system. Figure 3-2 shows a typical steel framed building, which presents a general concept that the analysis model refers to.


**Figure 3-2 JP Morgan-Chase building in San Francisco, CA (Structure)**

The structural analysis program used for this study is ABAQUS®, which is a general purpose commercial finite-element analytical software. Both dead load and live load are considered and applied to the models rationally and the calculation of the load combination as well as the structure mass is presented in Appendix A. The databases for dynamic time history records for wind and seismic loads are collected from Tokyo Polytechnic University (TPU) Aerodynamic Database and PEER Strong Motion Database respectively. Dynamic analysis, then, is carried out in order to assess the behaviors of building under various hazard loading conditions.

### 3.2.2 Configuration of Test Structures

The resident buildings in the city's downtown areas of San Francisco, CA were selected for the study, which are subjected to high risks of both strong wind and earthquakes in United States. Two structures are considered for this study – a 10 story structure with height of 40 meters (131 feet) and 30 story structures with height of 120 meters (393 feet). Each structure has a similar floor plan of 40 meters (131 feet) by 40 meters (131 feet) with 5 bays at 8 meters on both sides. The test structures are shown in Figure 3-3 and in this study are referred to as BM-10 for the 10-story building model and BM-30 for the 30-story building model.

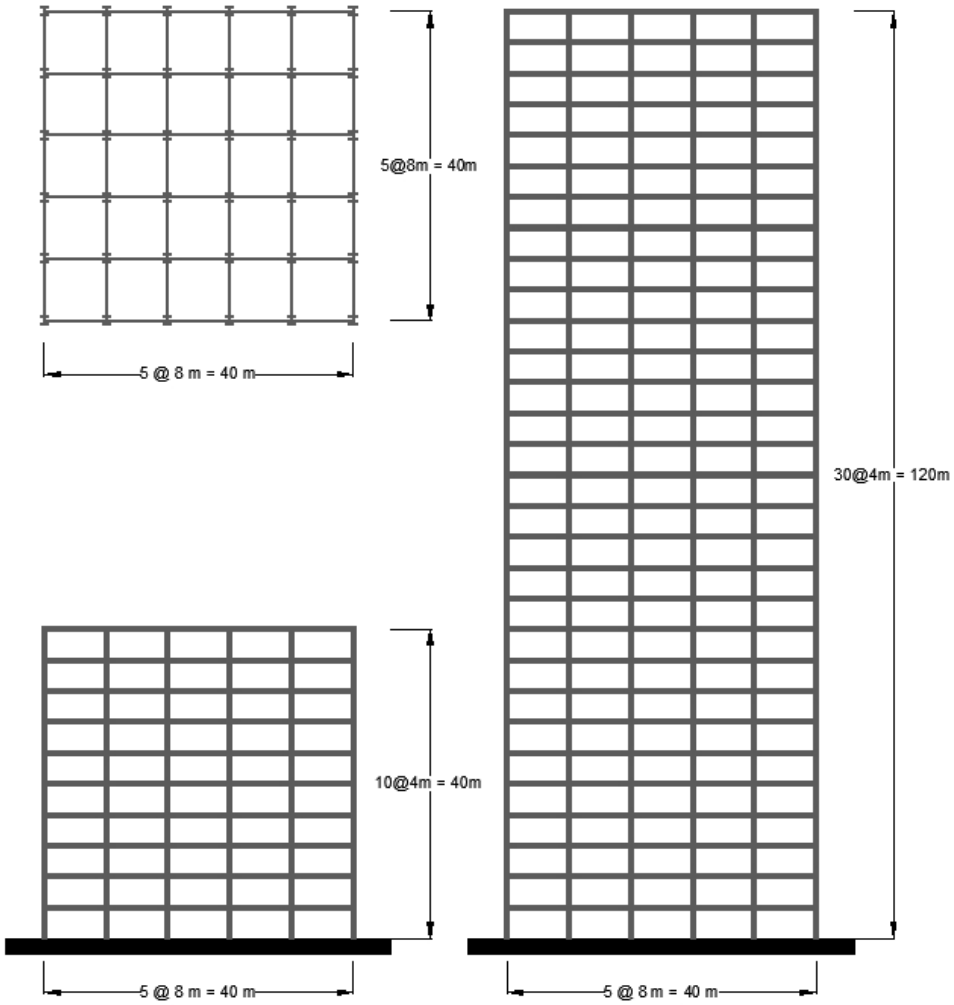


**Figure 3-3 Plan and Elevations of BM-10 and BM-30**

Since the frames considered SMRF, the structures are modeled as 2D frames without braced members. In addition, bracing members are added to the model to account for the added stiffness that is provided by partition walls, exterior walls, and cladding systems. These braced members are selected to increase the structural overall stiffness so that the fundamental period matches the approximate value defined in ASCE 7 (ASCE 7-10). The approximate equation for calculating the fundamental period in ASCE 7-10 is shown in Equation 3-1 below.

$$T_a = C_t h_n^x \qquad \textbf{Equation 3-1}$$

in which $h_n$ is the structural height, and the coefficients $C_t$ and $x$ have the value of 0.028 and 0.8 respectively for the structure type of steel moment-resisting frames (ASCE-7 10). On the basis of Equation 3-1, the approximate fundamental period of BM-10 and BM-30 are calculated and listed in Table 3-1.

**Table 3-1 Approximate Fundamental Period for BM-10 and BM-30 using ASCE 07**

| | Structural Height (feet) | Approximate Fundamental Period (sec) |
|---|---|---|
| BM-10 | 131.23 | 1.39 |
| BM-30 | 393.70 | 3.34 |

### 3.2.3 Structure Properties

All of these frames are modeled using a single steel material property. The steel, which is classified as ASTM A992 structural steel, has a Young's modulus of $2.0 \times 10^{11}$ N/$m^2$ (approximately 29,000 Kip/$in^2$) and yield strength of $3.45 \times 10^8$ N/$m^2$ (approximately 50 Kip/$in^2$). The strain hardening simulation and non-linear behavior analysis are allowed so that the inelastic can be simulated as structures subjected to intense earthquake.

For the subject frames, the beam sizes are considered to be uniform throughout the frames. The column sizes, however, change with an increased column size for the lower stories. The initial sizes of both beam and column members of the SMRF are selected based on the AISC construction manual (AISC 360-10). Figure 3-4 shows the size of beam and column for the initial column design scheme of BM-10. The procedures and details of determination of the initial structural member size are presented in Appendix B.

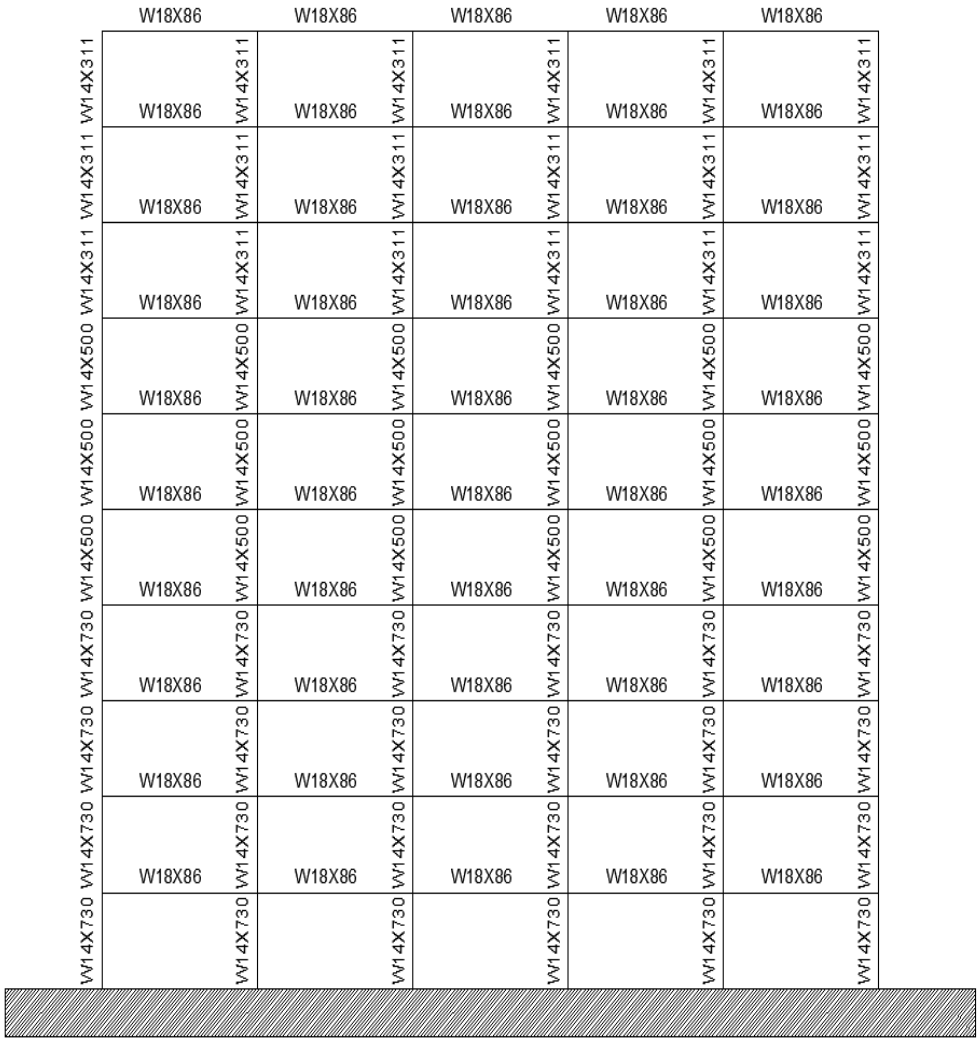


**Figure 3-4 Size of Beam and Column Member for Initial Design Scheme for BM-10**

Another five tested frames are built as extra column design schemes by ABAQUS with uniform beam sizes but different column sizes. The sizes of column are picked up based on the Wide Flange Beam Table (ASTM 6A) prior to doing the analysis, so that we can obtain a certain range of structural fundamental frequency that worked with these sizes. All the six column design schemes for the BM-10 and BM-30 are shown in Table 3-2 and the column sizes is considered to reduce from scheme *Initial* to *V* for BM-10 and from scheme *I* to *V* for BM-30.

**Table 3-2 Design Schemes of Column and Beam**

| Story Number | Column Design Schemes for BM-10 | | | | | |
|---|---|---|---|---|---|---|
| | *Initial* | *I* | *II* | *III* | *IV* | *V* |
| 1 - 4 | W14X730 | W14X455 | W14X283 | W14X176 | W14X99 | W10X100 |
| 5 - 7 | W14X500 | W14X311 | W14X193 | W14X109 | W10X100 | W10X60 |
| 8 - 10 | W14X311 | W14X193 | W14X109 | W10X100 | W10X60 | W10X39 |

| Story Number | Column Design Schemes for BM-30 | | | | | |
|---|---|---|---|---|---|---|
| | *I* | *Initial* | *II* | *III* | *IV* | *V* |
| 1 - 10 | W14X808 | W14X665 | W14X500 | W14X370 | W14X257 | W14X193 |
| 11 - 20 | W14X605 | W14X455 | W14X311 | W14X233 | W14X159 | W14X120 |
| 21 - 25 | W14X370 | W14X257 | W14X176 | W14X120 | W14X90 | W10X100 |
| 26 - 30 | W14X193 | W14X132 | W14X90 | W10X100 | W10X68 | W10X49 |

| Story Number | Beam Design Schemes for BM-10 |
|---|---|
| | *Initial* to *V* |
| 1 - 10 | W18X86 |

| Story Number | Beam Design Schemes for BM-30 |
|---|---|
| | *I* to *V* |
| 1 - 30 | W18X86 |

* The size of beam will never change for this study

Basically, the column sizes is designed based on a rule of proportional decreasing of the member's moment of inertia, e.g. the moment of inertia value of column $W14\times730$ is $14300 inch^4$ for *Initial* column design scheme. Then the moment of inertia value for column design scheme *I* is considered to be approximately ½ of $14300 inch^4$, which is $7150 inch^4$. So, $W14\times455$ that has the moment of inertia of $7190 inch^4$ can be determined to be the column size for column design scheme *I*.

As it has been indicated that the SMRF provides major contribution to resist the lateral loadings, e.g. wind pressure and seismic load, the design scheme is focus on the column member of the SMRF (exterior frame). The interior frames, however, is considered merely resist the

gravity loading, so their column sizes will be constant through these design schemes. This definition is presented as a basis for calculating the initial costs of these design schemes.

For the mesh of the structural members, a refined element with a length of about 0.1 meter (4 inches) is used at the column and beam end. The mesh is refined in the mentioned region so that realistic plastic hinges can form. Figure 3-5 shows the geometry and mesh arrangement of the first story of the models, which illustrates a common configuration and meshing for each story of both BM-10 and BM-30.

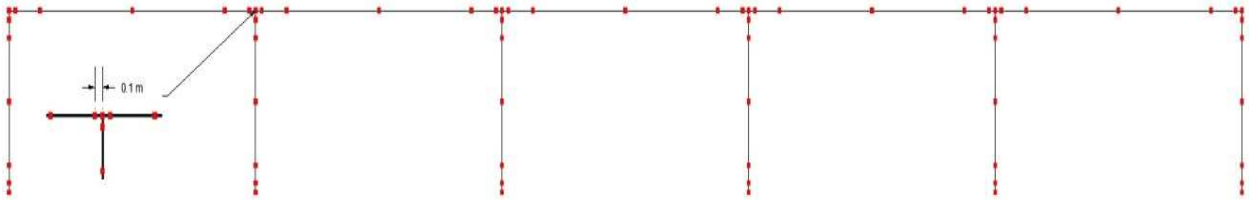


**Figure 3-5 Fist Story Geometry and FE Mesh Arrangement of Models**

### 3.2.4 Uncertainty Analysis

Reliability analysis, as the focus of this study, is used as the primary method to obtain the life-cycle cost design of structures. Therefore, it is important to properly quantify the uncertainty in the random variables since the analysis results highly depend on it. Uncertainty in structural analysis can typically be divided into two kinds; namely load as well as material uncertainty. In the context of this study load uncertainty refers to that associated with Peak Ground Acceleration (PGA) and wind speed for seismic and wind loads, respectively. For the material, the Young's modulus is chosen as the random variable. The effects of the uncertainty vary according to which structural response is considered.

The input motion and the Young's modulus of steel are selected to be the uncertainties in this study since these two factors have more direct impact on affecting the structural inter-story drift, which is considered as the limit state in this study. Take the cantilever beam as an example, the tip deformation, calculated as $\Delta_T = \frac{PL^3}{3EI}$ can be viewed as the story drift which is directly affected by the load $P$, the Young's Modulus $E$ and the moment of inertia $I$. A previous research also selected the Young's modulus, instead of the steel strength as the reliability uncertainty when the drift ratio is considered as limit state (Huh & Haldar, 2001).

The input motion, in this study, can be expressed by the scaling factor for both earthquake ground motion and wind pressure, which will be introduced in later chapter. $S_e$ and $S_w$ indicate the scaling factor of these two hazards hereafter. Both of the two random variables present in the formulation and their statistical descriptions, which include mean, coefficient of variation (C.O.V), and the type of distribution are defined rationally. The mean values of the scaling factors, however, vary depending on the probability of exceedances used in the seismic and wind simulations. Therefore, the statistical properties of the random variables are introduced later in Chapter 4 along with the analytical procedures and numerical results.

## 3.3 Limit State Definition

The limit states vary according to performance requirements. Currently, most building codes, which include ASCE, UBC and NEHRP, are generally focused on life safety. However, other consequences such as the economic losses caused by building damages are usually ignored. In this study the limit state considered are: 1) deformation limit state including the structural

overall deflection and inter-story drift, and 2) motion perception limit state including the vibration or peak acceleration.

For seismic assessment, three performance levels or limit states are widely accepted. These are Serviceability, Damage Control, and Collapse Prevention. Although both deformation and motion perception limit states are sensitive to probabilistic analysis subjected to earthquake load, structural engineers usually focus more on story drift limit state because story drift can directly lead to structural damage. Recent studies have considered acceleration limit states to prevent damage to nonstructural systems.

For the limit state definition under strong wind hazard, however, the structure's serviceability performance is often more of a concern. When a building is subjected to strong wind load, the displacement and acceleration responses as well as damage caused by flying debris are all under consideration. For steel and RC structures, most strong wind hazards including hurricanes and tornados mainly cause damages to non-structure parts, such as building cladding; therefore, the structural deformation is usually out of consideration. Motion perception may not lead structural damage or economic loss directly, but its consequences, such as human discomfort, can be another issue that engineers concern about.

### 3.3.1 Deformation Limit State

A review of previous work indicated that various limit states defined in the literature. A five inter-story drift ratio limit states were proposed to express the damage of entire building and as it shown in Table 3-3 (Whitman et al. 1975). The Federal Emergency Management Agency (FEMA) report 227 and 228 (FEMA 1992) descripted seven limit states according to overall building damage states as shown in Table 3-4. However, for calculating the failure probability

and failure cost, a quantitative measurement of damage state in terms of structural inter-story drift ratio response is needed to describing the performance level.

**Table 3-3 Damage Description of Damage Performance Level (Whitman et al. 1975)**

| Performance Level | Overall Building Damage |
|---|---|
| I | No Damage |
| II | Light Damage |
| III | Moderate Damage |
| IV | Heavy Damage |
| V | Total Damage or Collapse |

**Table 3-4 Description of Damage State (FEMA 227, 1992)**

| Damage State | Description of Damage |
|---|---|
| None | No Damage |
| Slight | Limited localized minor damage not requiring repair |
| Light | Significant localized damage of some components generally not requiring repair |
| Moderate | Significant localized damage of many components warranting repair |
| Heavy | Extensive damage requiring major repairs |
| Major | Major widespread damage that may result in the facility being razed, demolished, or repaired |
| Destroyed | Total destruction of the majority of the facility |

For that reason, Kang and Wen (2000) developed an advanced life-cycle cost optimization approach and suggested a general damage description of the performance level and drift ratio as shown in Table 3-5. This definition of limit state not only includes all limit states so

that the details of damage performances can be presented elaborately, but also introduced the quantitative limit inter-story drift ratios, which have made the relevant economic loss estimation calculations more reasonable and explainable. The seven limit states and six permissible drift ratios (PDRs) are used to define the limit states in this study.

**Table 3-5 General Damage Description of the Performance Level and Drift Ratio (Kang and Wen, 2000)**

| Performance Level | Damage State | Permissible Drift Ratio (%) |
|---|---|---|
| I | None | $\Delta < 0.2$ |
| II | Slight | $0.2 < \Delta < 0.5$ |
| III | Light | $0.5 < \Delta < 0.7$ |
| IV | Moderate | $0.7 < \Delta < 1.5$ |
| V | Heavy | $1.5 < \Delta < 2.5$ |
| VI | Major | $2.5 < \Delta < 5.0$ |
| VII | Destroyed | $\Delta > 5.0$ |

### 3.3.2 Wind Motion Vibration Perception Limit State

The motion perception is often expressed by human response to acceleration. Research has been conducted related to the topic of determining perception threshold values for acceleration caused by structure motion in the last 20 years. Various studies were aimed at formulating guidelines of tolerance thresholds for tall and slender building design. An early study quantified the human response to motion in tall buildings (Chang, 1973). By extrapolating from data in the aircraft industry, Chang proposed a series of peak acceleration limits for different comfort levels as shown in Table 3-6.

**Table 3-6 Peak Acceleration Limits for Different Comfort Levels (Chang 1973)**

| Peak Acceleration | Comfort Limit |
|---|---|
| < 0.5% g | No Perceptible |
| 0.5% to 1.5% g | Threshold of Perception |
| 1.5% to 5.0% g | Annoying |
| 5.0% to 15.0% g | Very Annoying |
| > 15.0% g | Intolerable |

A more comprehensive study of defining the human response to building motion was carried out in Japan with a wider range of variables (Sfintesco, 1981). Figure 3-6 shows the relationship between the peak acceleration and building period, which is explained below.

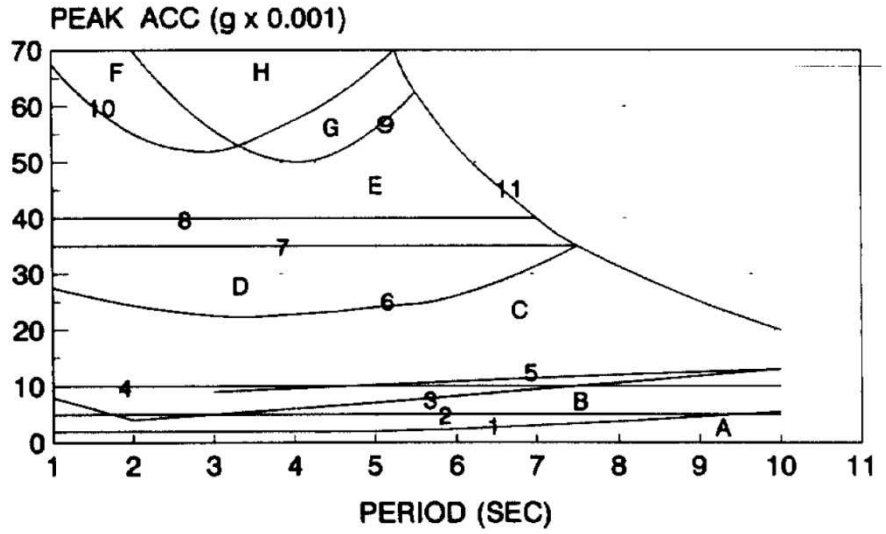


**Figure 3-6 Perception Thresholds (Peak Acceleration) (Sfintesco, 1981)**

1. Zone A, below Curve 1: the peak acceleration is less than 0.5% g, which indicates a human cannot perceive motion. Curve 1 defines the perception threshold for an average population.

2. Curve 2: the peak acceleration is 0.5% g, which defines the threshold at which some building objects, such as furniture, hanging lights may begin to move.

3. Curve 3: divides the zones between “very normal walking” and “nearly normal walking”.

4. Zone B: the peak acceleration is between 0.5% g and 1.0% g, which identifies the region where some people can perceive motion and some building objects may begin to move slightly.

5. Curve 4: the peak acceleration of 1% g, defines the threshold that the desk working can be affected.

6. Curve 5: defines the threshold that people may subjected to motion sickness for extended periods.

7. Zone C: the peak acceleration between 1.0% g and 2.5% g, which identifies most of people can perceive motion with general motion sickness and desk working is affected.

8. Curve 6: divides the zones between normal and hindered walking.

9. Zone D: the peak acceleration between 2.5% g and 4.0% g, which defines the range that desk working becomes difficult and at times impossible.

10. Curve 7: the peak acceleration of 3.5% g, defines the threshold that desk working is difficult.

11. Curve 8: the peak acceleration of 4.0% g, defines the threshold that furniture and fixtures start to motion and make sounds, which may make people annoying.

12. Zone E: defines a range that people can strongly perceive motion and it is hard to walk naturally.

13. Curve 9: identifies the threshold that people are unable to walk.

14. Curve 10: defines the maximum tolerance for motion.

15. Zone F and G: the peak acceleration is above 5.0% g and it defines the range of people's walking ability in which most of people cannot tolerate the motion.

16. Zone H: defines the range that people cannot walk at all. Motion is intolerable.

Griffis (1993) summarized considerable previous works related to serviceability limit states under the wind load, including the two studies above, and concluded that the current practice of tall building design has targeted design values for acceleration motion at 2.1% g of peak acceleration for office buildings and 1.5% g of peak acceleration for residential buildings.

The review of previous research indicated that a peak acceleration response value around 1.5% g is the limit defining human's annoyance (Chang, 1973) or the threshold of effect for desk working (Sfintesco, 1981). The conclusion of Griffis's study provided evidence that it is important to control the building peak acceleration response blow 1.5% g. In this study, the limit state of peak acceleration is defined as 3.0% g. A cost function is used in this study to reduce the acceleration response to the target level (1.5% g) using Smart Tuned Mass Damping system. The detail of the cost function is introduced later.

## 3.4 Cost Function Estimation

### 3.4.1 Cost Function Formulation

As previously mentioned, the cost function, defined by Kang and Wen (2000) is a closed form equation and it is considered for calculating the expected life-cycle cost in this study. The derivation process and calculation method have been introduced in Chapter 2.

For a proper utilization of the cost function in this study, additional information is needed. First, the earthquake and wind hazard should be considered separately, which means the joint occurrence of these two hazards is ignored for the expected life-cycle cost calculation. Secondly, an assumption is made where the maintenance cost function, $C_m$, is not considered in this specific study. The discount ratio $\lambda$ is used for considering the present value of benefits that will occur in the future. For the failure cost estimation under wind hazard, however, the cost of failure is defined as an approximated potential initial investment on damping devices, which have the capability of mitigating the effect of the probable wind hazard that would occur in certain duration. Therefore, the discount ratio factor is not considered in the failure cost function for wind hazard and, instead of considering the occurrence rate $v$, the probability of occurrence in the total duration (50 years in this study) is used herein. The final close forms for earthquake and wind hazard are presented in Equation 3-2 and Equation 3-3, respectively.

$$E\left[C_e(t,X)\right] = C_0 + (C_1P_1 + C_2P_2 + \cdots + C_kP_k)\frac{v}{\lambda}\left(1 - e^{-\lambda t}\right) \qquad \textbf{Equation 3-2}$$

$$E\left[C_w(t,X)\right] = C_0 + (C_1P_1 + C_2P_2 + \cdots + C_kP_k)\,p_t \qquad \textbf{Equation 3-3}$$

in which $C_k$ indicates the $k$-th limit state failure cost, $P_k$indicates the failure probability of $k$-th limit state, and $p_t$ indicates the probability of hazard occurrence during time $t$.

### 3.4.2 Initial Costs

The initial cost can be understood as the construction cost for a new or retrofitted facility. Generally speaking, the initial cost includes the costs of all components that the building consists of. In optimization design, however, the nonstructural components are usually out of consideration since it has no effect on the optimal design of the main structural elements. Therefore, the main contribution to the initial cost is the cost of steel, shear connectors, metal decking, concrete, beam and column fireproofing. In this study and for simplicity, only the costs of steel, beam and column fireproofing are considered since the optimization design is based on changing the structural member size. The costs of steel material are calculated based on 1997 Building Construction Cost Data (BCCD), and the cost of fireproofing of structural members (beams and columns), otherwise, are calculated according to 1996 Means BCCD by Georgetown Laboratory Cost Estimation. For the cost of steel material, it consists of two parts: the bare cost (Material, labor and equipment costs) and overhead and profit (O & P).

The initial calculation cost hereinabove is considered as a national average value. Thus, a location factor is needed here to adjust the initial cost to the city of concern, which is chosen in this study as San Francisco, CA. The equation of this adjustment is shown below:

$$Cost\,in\,City\,A = \frac{City\,Index(A)}{100} \times National\,Average Cost \qquad \textbf{Equation 3-4}$$

During the cost evaluation, the historical cost index is also needed to convert national average building costs in a given year to that of current year. An example of converting 1990 cost to 2013 cost can be expressed by following formula:

$$Cost\,in\,year\,2013 = \frac{Index\ for\ year\,2013}{Index\ for\ year\,1990} \times Cost\,in\,year\,1990 \qquad \textbf{Equation 3-5}$$

The detail of location factors and historical index in this research is collected and presented in Table 3-7. This table lists the RSMeans® historical cost index based on Jan. 1, 1993 = 100.

**Table 3-7 RSmeans® Historical Cost Index**

| Year | Historical Cost Index Jan.1, 1993 = 100 | | Year | Historical Cost Index Jan.1, 1993 = 100 | Year | Historical Cost Index Jan.1, 1993 = 100 |
|---|---|---|---|---|---|---|
| | Estimated | Actual | | Actual | | Actual |
| Jul. 2014 | | | Jul. 1998 | 115.1 | Jul. 1980 | 62.9 |
| Apr. 2014 | | | 1997 | 112.8 | 1979 | 57.8 |
| Jan. 2014 | 202.7 | | 1996 | 110.2 | 1978 | 53.5 |
| Jul. 2013 | | 201.2 | 1995 | 107.6 | 1977 | 49.5 |
| Jul. 2012 | | 194.6 | 1994 | 104.4 | 1976 | 46.9 |
| 2011 | | 191.0 | 1993 | 101.7 | 1975 | 44.8 |
| 2010 | | 183.5 | 1992 | 99.4 | 1974 | 41.4 |
| 2009 | | 180.1 | 1991 | 96.8 | 1973 | 37.7 |
| 2008 | | 180.4 | 1990 | 94.3 | 1972 | 34.8 |
| 2007 | | 169.4 | 1989 | 92.1 | 1971 | 32.1 |
| 2006 | | 162.0 | 1988 | 89.9 | 1970 | 28.7 |
| 2005 | | 151.6 | 1987 | 87.7 | 1969 | 26.9 |
| 2004 | | 143.7 | 1986 | 84.2 | 1968 | 24.9 |
| 2003 | | 132.0 | 1985 | 82.6 | 1967 | 23.5 |
| 2002 | | 128.7 | 1984 | 82.0 | 1966 | 22.7 |
| 2001 | | 125.1 | 1983 | 80.2 | 1965 | 21.7 |
| 2000 | | 120.9 | 1982 | 76.1 | 1964 | 21.2 |
| 1999 | | 117.6 | 1981 | 70.0 | 1963 | 20.7 |

### 3.4.3 Failure Cost Functions for Earthquake Hazards

The aforementioned failure cost (Equation 3-2) for structural buildings subjected to seismic load consists of six cost functions; namely damage and repair ($C^{Dam}$), contents loss ($C^{Con}$), relocation cost ($C^{Rel}$), economic loss ($C^{Eco}$), cost of human injury ($C^{Inj}$), and fatality

($C^{Fat}$). According to FEMA reports (1992), each of these functions is estimated and presented as follows:

#### 3.4.3.1 Damage and Repair Cost Function and Content Loss

Damage/repair cost and contents loss cost are considered as a mean damage index function and can be obtained by a unit cost multiplied by the floor area. A value of $\$85/ft^2$ is recommended in FEMA 227 as a typical damage and repair unit cost for general medium rise office buildings for commercial, professional, technical and business services. For contents loss cost, $\$28.9/ft^2$ is considered as the unit cost.

#### 3.4.3.2 Relocation Cost Function

Relocation cost is considered when the function of the facility is partially or entirely lost because of building damage. The overall relocation cost depends on unit relocation cost, gross leasable area, and estimated function-loss duration. The FEMA handbook No. 174 (1989) suggested a value of $\$1.50/month\ /ft^2$ as the unit relocation cost.

#### 3.4.3.3 Economic Loss Cost

Economic losses consist of two parts: rental cost and income loss. An average rental rates per square per month for typical buildings can be estimated. However, the rental rates vary according to the location under consideration. In the study, a value of $\$\,0.61/month/ft^2$ is suggested in FEMA 228 (1992) as the rental rate for Seattle and by applying the location factor according to BCCD (1998), the average rental rate can be calculated as $\$\,0.58/month/ft^2$. The income loss can be defined as a disruption of income based on business and social function of the building. When the damage of building interrupts commercial activity, the income loss arises. Two factors, which are the income generation level and the disruption duration, control the

estimation of the cost associated with income losses. Similar to rental rate, income losses are considered as a proportion of the duration of partial or full function lost. On the basis of FEMA 228 (1992), an income loss rate of $\$100/year/ft^2$ is suggested for buildings with commercial, professional, technical and business services.

#### 3.4.3.4 Injury and Fatality Costs

The overall injury cost is evaluated by product of injury rate for a certain limit state, occupancy rate, and cost for each person and floor area. According to the study of Wen and Kang (2000), a value of $2\ person/1{,}000ft^2$ is used as the occupancy rate, and cost of minor injury and serious injury make up the cost for each person and the values are $\$1{,}000/person$ and $\$10{,}000/person$, respectively. Similar to the injury cost, the cost of fatality is calculated by multiplying the expected death rate (depending upon limit state) with the number of occupants and fatality cost for each person and floor area. FEMA 227 (1992) report suggests a value of $\$1{,}740{,}000/person$ as the fatality cost for each person.

All the failure cost functions and their basic costs are summarized in Table 3-8. All of these costs are regarded as U.S. dollars in 1992. Therefore, the aforementioned historical cost index is needed to convert the costs from 1992 to 2013.

**Table 3-8 Failure Cost Functions, Equations and Basic Costs (FEMA 227 and 228, 1992)**

| Failure Cost Function | | Equation | Basic Cost |
|---|---|---|---|
| Damage / Repair | $C^{Dam}$ | Replacement Cost × Floor Area × Mean Damage Index | \$85/ for replacement cost |
| Contents Loss | $C^{Con}$ | Unit Contents Cost × Floor Area × Mean Damage Index | \$28.9/ for unit contents cost |
| Relocation | $C^{Rel}$ | Relocation Cost × Gross Leasable Area × Loss of Time | \$1.5/month/ |
| Economic Loss | $C^{Eco}$ | Rental Cost($C^{Ren}$) + Income Cost($C^{Inc}$) | |
| Rental | $C^{Ren}$ | Rental Rate × Gross Leasable Area × Loss of Function | 0.58/month/ |
| Income | $C^{Inc}$ | Rental Rate ×Gross Leasable Area × Out of Business | \$100/year/ |
| Injury (Minor) | $C^{Inj}$ | Minor Injury Cost per person × Expected Injury Rate (Minor) | \$1,000 |
| Injury (Serious) | $C^{Inj}$ | Serious Injury Cost per person × Expected Injury Rate (Serious) | \$10,000 |
| Human Fatality | $C^{Fat}$ | Death Cost per person × Expected Death Rate | \$1,740,000 |

### 3.4.4 Factors for Failure Cost Calculation

#### 3.4.4.1 Discount Rate

Discount rate is another important factor in the cost function, which expresses the value of present in the future benefits. The higher value of discount rate makes a lower present value for future benefits. Previous studies regarding the evaluation of discount rate have shown that despite the various approaches used, the values are typically in the range of 3% to 6% (Wen and Kang, 2000). On the basis of FEMA 227 (1992), discount rate of 4% to 6% is suggested for private buildings consideration. Therefore, in this study, a medium value 5% is considered as the discount rate.

#### 3.4.4.2 Other Factors

During the calculation of expected failure cost, several crucial factors need to be included such as 1) the mean damage index factor, 2) the costs of relocation and economic loss, 3) the occupancy injury and fatality rate. The mean damage index factor is used to calculate damage/repair and content loss costs. On the basis of FEMA 227 (1992), mean damage index factors corresponding to different limit states are shown in Table 3-9. For evaluating the costs of relocation and economic loss, consensus opinions about expected loss of function and restoration period were developed in Earthquake Damage Evaluation Data for California (Applied Technology Council, 1985), commonly called ATC-13, which is in this study. Table 3-10 shows the weighted statistics for loss of function period for professional business service facilities. The Occupancy injury and fatality rate is also needed in injury and fatality costs calculation. Values of death and injury rates for seven limit states are obtained from FEMA 227 and presented in Table 3-11.

**Table 3-9 General Damage Description of the Limit State Level and Central Damage Factor (%) (FEMA 227, 1992)**

| Limit State Level | Damage State | Damage Factor Range (%) | Central Damage Factor (%) |
|---|---|---|---|
| I | None | 0 | 0 |
| II | Slight | 0 - 1 | 0.5 |
| III | Light | 1 - 10 | 5 |
| IV | Moderate | 10 - 30 | 20 |
| V | Heavy | 30 - 60 | 45 |
| VI | Major | 60 - 100 | 80 |
| VII | Destroyed | 100 | 100 |

**Table 3-10 Weighted Statistic for Loss of Function and Restoration Time (days) of Social Function Classifications (ATC-13, 1985)**

| Limit State Level | Central Damage Factor (%) | Mean Time (days) of Total loss of Function to Restore |
|---|---|---|
| I | 0 | 0 |
| II | 0.5 | 3.4 |
| III | 5 | 12.08 |
| IV | 20 | 44.72 |
| V | 45 | 125.66 |
| VI | 80 | 235.76 |
| VII | 100 | 346.93 |

**Table 3-11 Expected Injury and Death Rates for Existing Building (FEMA 227, 1992)**

| Limit State Level | Central Damage Factor (%) | Fraction Injured | | Fraction Death |
|---|---|---|---|---|
| | | Minor | Serious | |
| I | 0 | 0 | 0 | 0.000001 |
| II | 0.5 | 0.00003 | 0.000004 | 0.00001 |
| III | 5 | 0.003 | 0.00004 | 0.0001 |
| IV | 20 | 0.003 | 0.0004 | 0.001 |
| V | 45 | 0.03 | 0.004 | 0.001 |
| VI | 80 | 0.3 | 0.04 | 0.01 |
| VII | 100 | 0.4 | 0.4 | 0.2 |

### 3.4.5 Failure Costs for Wind Hazard

As mentioned previously, the failure cost considering wind load is related to the cost of the damping system for reducing the acceleration response to a target value. For this study, the failure cost for structural analysis under wind load is defined as the approximated potential cost of dampers, which is needed to control the peak acceleration of the building as to not exceed the target acceleration.

A study on the performance and cost evaluation of a Smart Tuned Mass Damper (STMD) for reducing wind-induced motion of tall building is proposed (Tse et al., 2012). The paper introduced an estimation cost for STMD. By carrying out a sensitivity analysis to evaluate the combined effects of the generalized mass of a building and the designated acceleration reduction on the effective mass and, hence, the cost of the STMD that gives the reduction, a mathematical relationship between the total cost of the STMD ($Cost_{STMD}$), generalized mass of the building ($m^*$), and the designated acceleration reduction level ($\gamma$) can be written as

$$Cost_{STMD} = \left(16.1\gamma^2 - 6.8\gamma + 1.5\right)m^* + \left(1.9\gamma^2 - 1.7\gamma + 2.2\right) \quad \textbf{Equation 3-6}$$

in which the building generalized mass $m^*$can be regarded as the total mass of the building in this case and the designated acceleration reduction $\gamma$ has a range of 0.2 – 0.8 and can be calculated as

$$\gamma = 1 - \frac{PAR_{controlled}}{PAR_{uncontrolled}} \quad \textbf{Equation 3-7}$$

in which, in this study, the $PAR_{controlled}$ indicates the peak acceleration response with control (STMD), which is considered as the target peak acceleration that has been defined earlier as 1.5% g; and the $PAR_{unControlled}$ indicates the peak acceleration response without control (STMD), which is considered as the pre-defined limit state acceleration response (3.0% g).

In summary, the STMD will be assumed to make the major contribution to suppress the acceleration motion of building under wind load in this study. The cost of the STMD can be calculated using Equation 3-6 involving the building mass and the designated acceleration reduction factor used to reduce the limit state acceleration response to the target acceleration response. The probability of failure is defined as the probability of the building acceleration response exceeding the pre-defined acceleration limit state. Therefore, the failure cost for wind

hazard is calculated by multiplying the probability of failure and cost of the STMD, which is needed for the designated acceleration reduction.

## 3.5 Methodology Development

### 3.5.1 Introduction of First Order Reliability Method (FORM)

Common analytical methods that have been developed to deal with structural reliability analysis include Monte Carlo Simulation (MCS) and as known as the sampling-based methods and the First Order Reliability Method (FORM), among others. In this section, the basic conception of FORM is presented and the technique of reliability analysis by connecting FORM with finite element dynamic analysis is introduced. At last, the accuracy of this method is tested on by a simple structure example by comparing the results obtained using Monte Carlo Simulation with those obtained by integrating FORM with finite element methods.

### 3.5.2 Overview

The first order reliability method (FORM) is an approximation technique used to evaluate the probability of failure or reliability index of components or systems. In a structural reliability analysis based on FORM, $g(x)$ represents the limit-state function and the exceedance of the limit states (often considered as "failure") can be expressed as $g(x) \leq 0$, where $x$ is a vector of the random variables under consideration. Then the probability of failure $P_f$ is

$$P_f = P[g(\boldsymbol{x}) \leq 0] = \int_{g(\boldsymbol{x}) \leq 0} f_x(\boldsymbol{x})\, d\,\boldsymbol{x} \qquad \textbf{Equation 3-8}$$

in which $f_x(\boldsymbol{x})$ is the joint probability density function (PDF) of $\boldsymbol{x}$. The FORM provides a way to linearize each limit state function in the standard normal space at an optimal point so that the

probability of failure $P_f$ can be obtained. The fundamental assumption of this method is that the limit state functions are continuous and differentiable, at least in the neighborhood of the optimal point (Der Kiureghian, 2005). By transforming the variables into the standard normal space, the probability of failure $P_f$ can be written as

$$P_f = P[G(\boldsymbol{u}) \le 0] = \int_{G(\boldsymbol{u}) \le 0} \varphi_{\boldsymbol{u}}(\boldsymbol{u}) d\,\boldsymbol{u} \qquad \textbf{Equation 3-9}$$

in which $G(\boldsymbol{u}) = g(\boldsymbol{T}^{-1}(\boldsymbol{u}))$ is considered the limit state function in the standard normal space, $\boldsymbol{u}$ is the vector of standard normal variables, and $\boldsymbol{T}$ represents the transformation matrix according to different distributions of the variables. By using the FORM, the approximated value of the probability of failure $P_f$ can be obtained by linearizing the function $G(\boldsymbol{u})$ at a point $\boldsymbol{u}^*$ that defined by the constrained optimization problem

$$\boldsymbol{u}^* = argmin\{\|\boldsymbol{u}\| | G(\boldsymbol{u}) = 0\} \qquad \textbf{Equation 3-10}$$

in which "$\arg min$" denotes that argument of the minimum of a function and $\|*\|$ presents the $L^2$-Norm. In the Equation 3-10, $\boldsymbol{u}^*$ is located on the limit state edge, which satisfies $G(\boldsymbol{u}^*) = 0$, and is the minimum distance from the origin point in the standard normal space. Figure 3-7 shows the approximated limit state function in two-dimensional space. The equal probability density contour in the standard normal space is represented by a concentric circle centered at the origin point, $\boldsymbol{u}^*$ has the highest probability density compare to all of the points in the failure domain $G(\boldsymbol{u}) \le 0$. In the reliability community, point $\boldsymbol{u}^*$ is commonly known as the *design point* or *most probable point* (MPP).

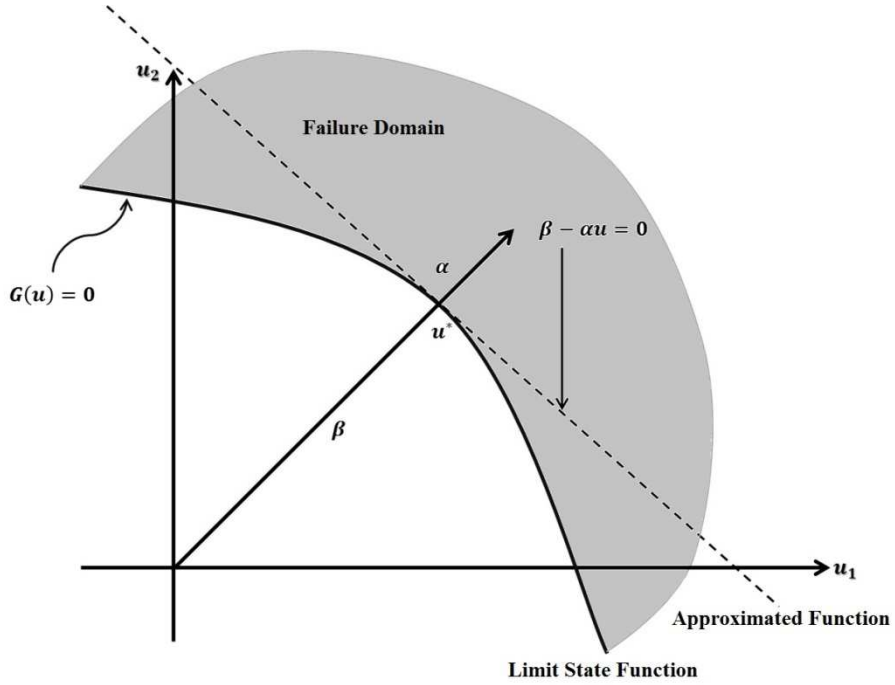


**Figure 3-7 First-order Reliability Method Approximation**

Noting that $G(\boldsymbol{u}^*)= 0$, the linearized limit state function can be expressed at MPP as

$$G(\boldsymbol{u}) \cong \nabla G(\boldsymbol{u}^*)(\boldsymbol{u} - \boldsymbol{u}^*) = \left\|\nabla G(\boldsymbol{u}^*)\right\|(\beta - \alpha \boldsymbol{u}) \qquad \textbf{Equation 3-11}$$

in which $\nabla G(\boldsymbol{u}) = \left[\frac{\partial G}{\partial u_1}, \frac{\partial G}{\partial u_2}, \ldots, \frac{\partial G}{\partial u_n}\right]$ denotes the gradient row vector, $\alpha = -\frac{\nabla G(\boldsymbol{u}^*)}{\|\nabla G(\boldsymbol{u}^*)\|}$ represents the normalized negative vector at MPP (a unit vector normal to the limit state surface at MPP and toward the failure domain), and $\beta = \alpha \boldsymbol{u}^*$ is the *reliability index*. Once $\beta$ is determined, the first-order approximation of the failure probability can be given as

$$P_f = \Phi(-\beta) \qquad \textbf{Equation 3-12}$$

in which $\Phi(*)$ denotes the standard normal cumulative density function (CDF). All the details of the FORM are found in Der Kiureghian (2005).

### 3.5.3 Utilization of FORM with ABAQUS Dynamic Model

In this study, the HL-RF algorithm (Song, 2007) is used as the framework for the interface between first order reliability method (FORM) and the ABAQUS dynamic models. Figure 3-8 shows the basic procedure of the HL-RF algorithm. Basically, the algorithm takes the idea of the FORM. By evaluating the limit state function and its gradient, the normalized vector at MPP ($\alpha$) can be obtain as well as the reliability index ($\beta$), which is considered to be the coefficient conducts the probability of failure ($P_f$). In order to gain accurate results, convergence tolerance parameters - $\varepsilon_1$, $\varepsilon_2$, and $i_{\max}$ are defined. In this research, , , and are assumed to be 0.05, 0.05, and 20, respectively.

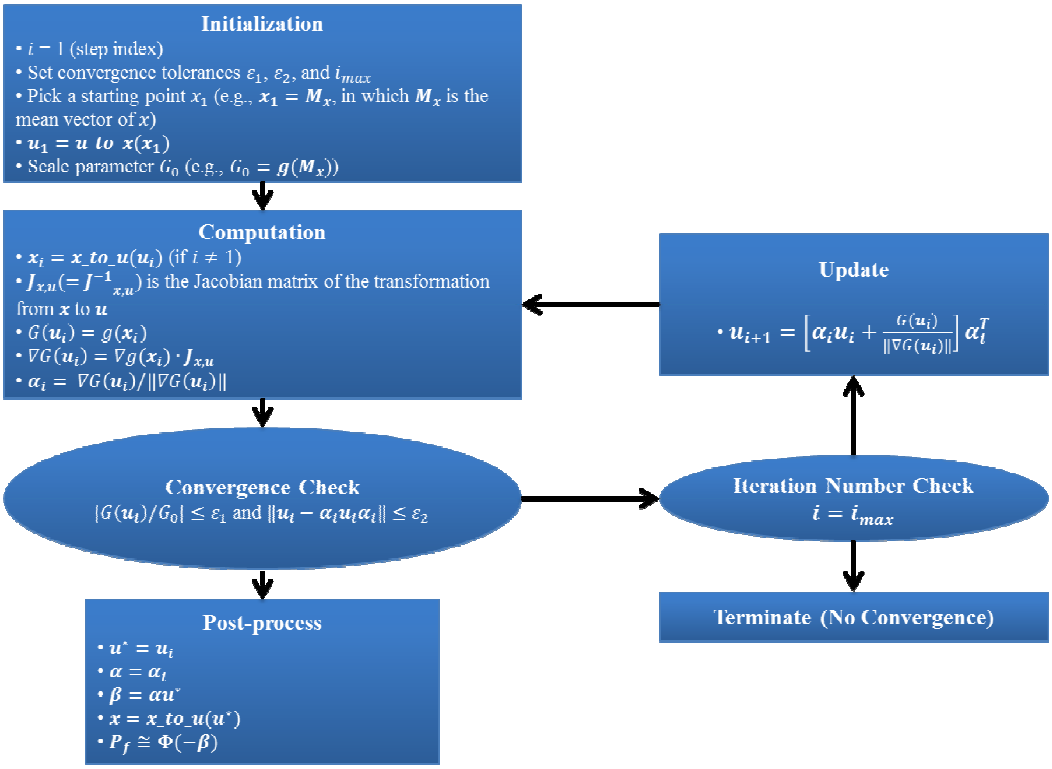


**Figure 3-8 FORM by HL-RF Algorithm (Song, 2007)**

The data flow of between the FORM by HL-RF algorithm and ABAQUS® is shown in Figure 3-9. In this study, a MATLAB code is written to provide such interface

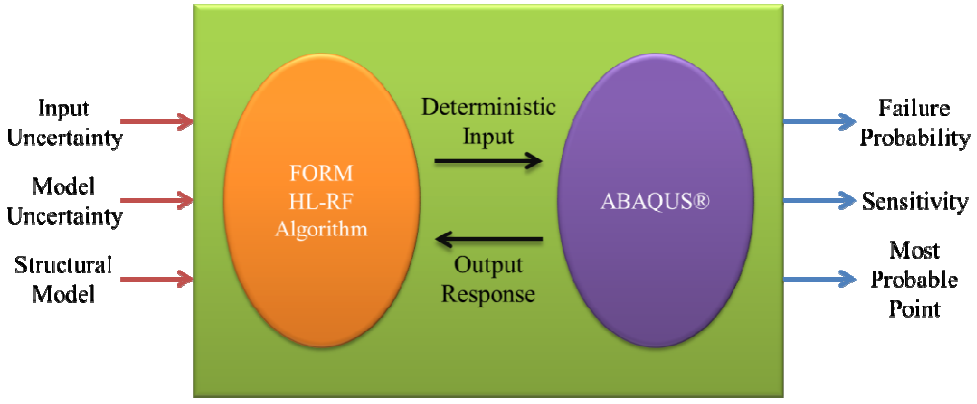


**Figure 3-9 Data Flow of FORM by HL-RF Algorithm and ABAQUS®**

In order to find the solution of the constrained optimization problem aforementioned in Equation 3-11 using FORM, and (the values of the limit state function and its gradients in the standard normal space respectively) are needed to be calculated in each step of the iteration. It is available to obtain the value of gradient analytically if the limit state function is expressed as an analytical function of random variable . Unfortunately, for a global dynamic finite element analysis using ABAQUS, it is impossible to establish an analytical function to express the mathematical relationships between the random variables, for instance the PGA and Young's Modulus, and structure system response, the inter-story drift in this study, so the values of gradients become no way to determine. The interface module between FORM by HL-RF algorithm and ABAQUS is developed so that the limit state function values can be obtained from the responses output (e.g., force or displacement responses evaluated by the finite element analysis performed by ABAQUS), as well as the gradient values numerically.

### 3.5.4 Example and Accuracy Test

In order to test the accuracy of this methodology, a numerical example is presented using the interface module between FORM by HL-RF algorithm and ABAQUS. The example problem is set up as a simple cantilever beam and its configuration is shown in Figure 3-10. The length of this cantilever beam is ( ), cross-section geometry is . This cantilever beam is considered homogenous and made of steel material. The steel's density of is assumed. A concentrated force is loaded at the end of this beam and the deformation at the beam's tip is considered as the target interest and the limit state is assumed to be herein.

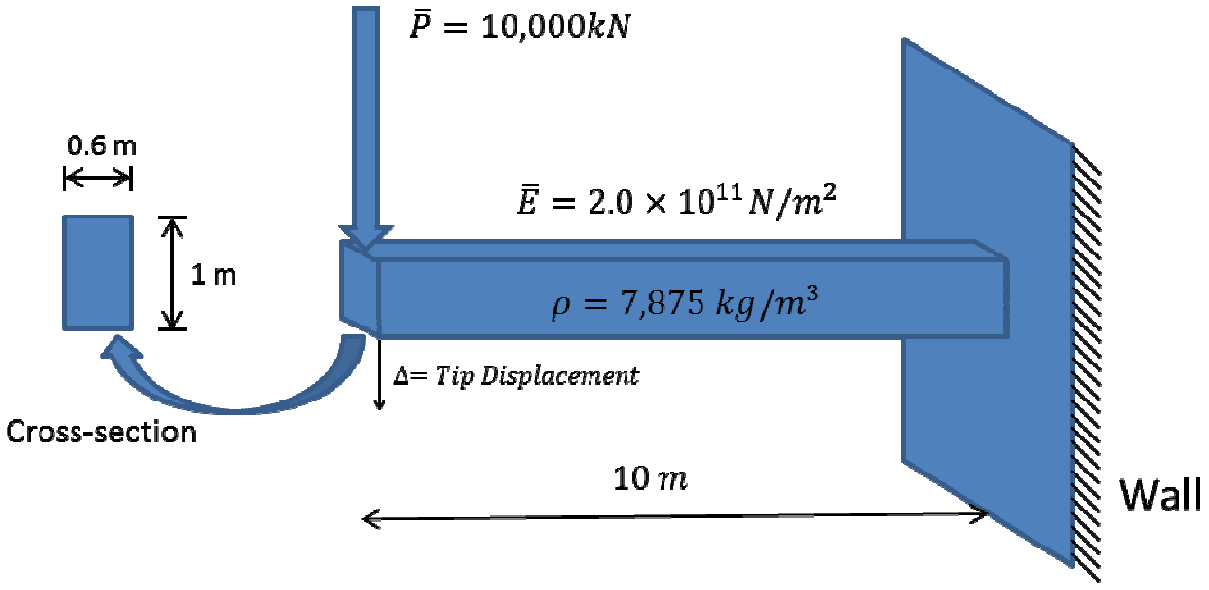


**Figure 3-10 Cantilever Beam Example for Accuracy Test**

Unlike the real problem, the example is tested using static analysis. The random variables in this example are (1) magnitude of the concentrated force, and (2) the Young's Modulus of the cantilever beam. Other parameters are considered constants. The statistical values of these two

variables, including mean, coefficients of variation, and the type of at distribution are presented in Table 3-12

**Table 3-12 Statistic Properties of Random Variables for Accuracy Test**

| | Mean Value | C.O.V | Distribution Type |
|---|---|---|---|
| Concentrated Force ( P ) | $10{,}000\ kN$ | 0.2 | Normal |
| Young's Modulus ( E ) | $2.0 \times 10^{11}\ N/m^2$ | 0.06 | Normal |

The reliability analysis is carried out using the proposed algorithm and MCS with sample number of 1,000 and 10,000, respectively. The computer used for the analysis is a Windows PC with 6 GB memory. The results, including the value of reliability index, failure probability, and the CPU time, obtain from these two methods is shown in Table 3-13.

**Table 3-13 Results Comparison between Proposed Algorithm and MCS with 1,000 and 10,000 Samples**

| | Proposed Algorithm | MCS with 1,000 Samples | MCS with 10,000 Samples |
|---|---|---|---|
| $\beta$ | 2.234 | 2.170 | 2.238 |
| $P_f$ | 0.01275 | 0.01500 | 0.012600 |
| CPU time | 134 sec | 2.2 Hrs. | 20 Hrs. + |
| Error compare with MCS test (1,000 sample) (%) | | | 15.03 |
| Error compare with MCS test (10,000 sample) (%) | | | 1.19 |

# CHAPTER 4

# DYNAMIC LOAD DEFINITION

## 4.1 Seismic Ground Motion Records

### 4.1.1 Ground Motion Record Selection

The selection of earthquake ground motion records is an important parameter in structural dynamic analysis. Improper selection of ground motions can lead to unpresentable results. As alluded to previously, the study is focused on the building structures located in urban areas subjected to various levels of earthquake and wind loads. The downtown of San Francisco, CA stands for the typical urban area, which subjected to the identified multi-hazards risks. The selected location has a specific site condition (soil classification) and other earthquake characteristics. Therefore, the ground motion record for this location is carefully selected in order to obtain reasonable and convictive results. The site condition information is collect from the United States Geological Survey (USGS) Global $V_s{}^{30}$ (the shear wave velocity in the first 30 meter of subsoil) Map Server section by inputting the coordinates of the selected location, a map with a color bar that indicates the detail of the $V_s{}^{30}$ in downtown are of San Francisco is obtained and shown in Figure 4-1. According to the map, the $V_s{}^{30}$ value in San Francisco downtown area can be determined as larger than $760\ \mathrm{m/s}$.

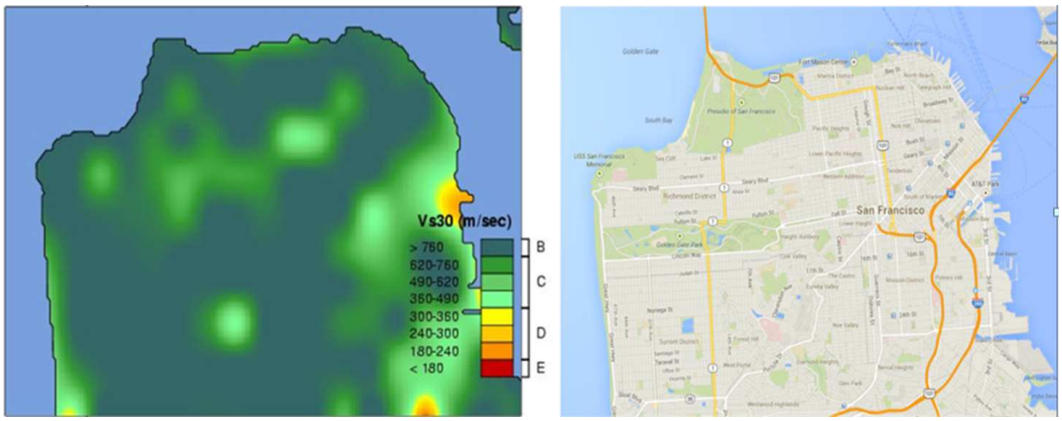


**Figure 4-1 Map of $V_s^{30}$ in San Francisco Downtown Area (USGS)**

Before selecting the ground motion records, several assumptions are needed. First, records from a location near San Francisco should be considered due to the potential similarities in fault mechanism, topography, and site conditions. Secondly, the source magnitudes of the earthquake events under consideration in this research are assumed to be limited from 6.0 to 8.0. For simplicity, only near field ground motions are considered and the source-to-site distance is assumed to range from to . While previous research has confirmed that the is greater than , the site condition can be assumed as rock classification, which is known as Site Class B (ASCE 7) with ranging from to . A summary list of the aforementioned conditions is listed in Table 4-1.

**Table 4-1 Summary List for Ground Motion Selection**

| Parameter | Assumptions |
|---|---|
| Location | Near to San Francisco |
| Lowest Usable Frequency | Hz |
| Fault Mechanism | Strike-Slip or Reverse |
| Magnitude | |
| Source-to-Site Distance | |
| Site Classification | – |

Since the purpose of this research is to highlight the analysis framework, only one earthquake is selected. It is however recognized that a general or in-depth conclusion cannot be made based on simulations using only one seismic record. For this study, the Loma Prieta earthquake is selected on the basis of all the parameters identified in Table 4-1. The record was obtained from the Pacific Earthquake Engineering Research (PEER) Ground Motion Database which is maintained by the University of California, Berkeley (PEER, 2010). Details of the record are presented in Table 4-2. The un-scaled acceleration time-history series and the elastic acceleration response spectrum of this selected ground motion record are shown in Figure 4-2 and Figure 4-3, respectively. For simplification, only the first 15 seconds of the time-history series is used in the finite element dynamic analysis.

**Table 4-2 Details of the Selected Earthquake Record**

| Event | Year | Station | Mechanism | Magnitude | $R_{rup}$(km) | Vs30(m/s) | Low.freq(Hz) |
|---|---|---|---|---|---|---|---|
| Loma Prieta | 1989 | Gilroy Array #1 | Reverse-Oblique | 6.93 | 9.6 | 1428 | 0.25 |

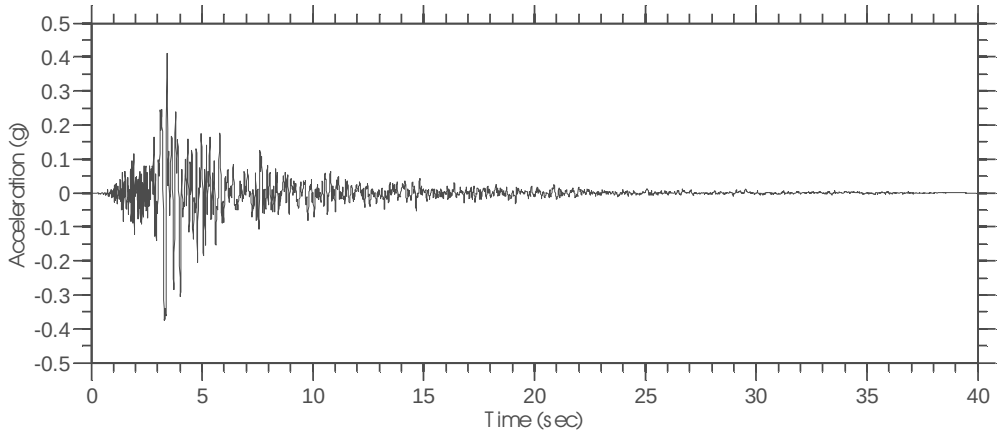


**Figure 4-2 Unscaled Acceleration Time-history Record for the Loma Prieta Earthquake**

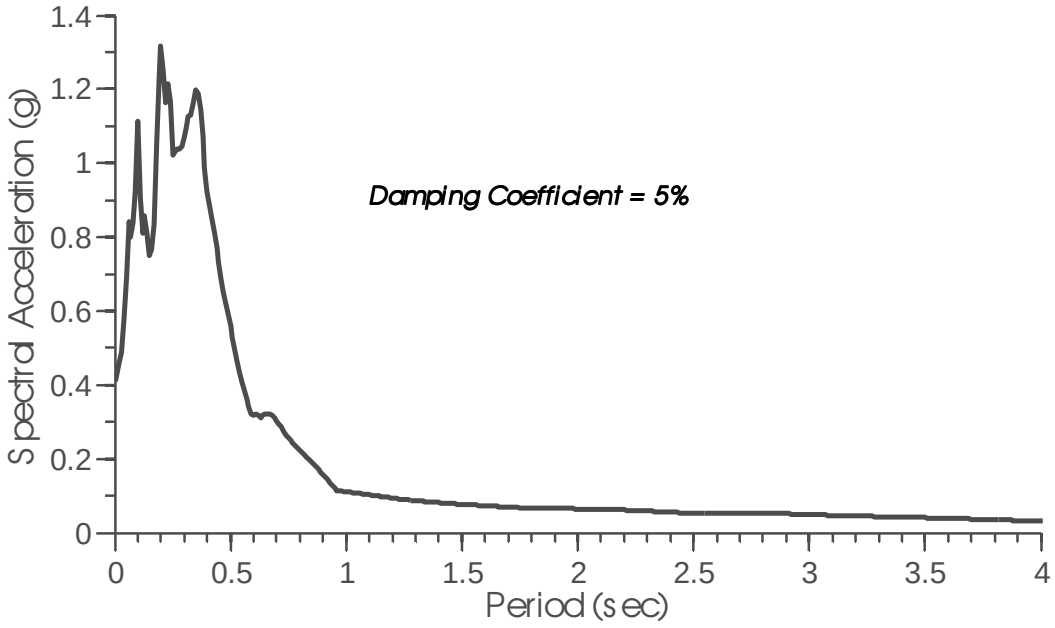


**Figure 4-3 Elastic Response Spectra for the Loma Prieta Earthquake with a Damping Value 5%**

### 4.1.2 Ground Motion Record Scaling

. Scaling of the ground motions is based on the process outlined in the Federal Emergency Management Agency P-695 report (FEMA P695, 2009). Details of the ground motion scaling process are listed below:

Initially, each record is normalized by the median of the series of peak ground velocities of the records. Equation 4-1 shows the formula for obtaining the normalization factor (FEMA P695, 2009). For individual ground motion record, the value of normalization factor is considered as 1.

$$NM_i = \frac{Median(PGV_{PEER,i})}{PGV_{PEER,i}} \qquad \textbf{Equation 4-1}$$

in which:

$NM_i$ = Normalization factor of the $i^{th}$ record (of the set of interest),

$PGV_{PEER,i}$ = Peak ground velocity of the $i^{th}$ record (from PEER database),

$Median(PGV_{PEER,i})$ = Median of $PGV_{PEER,i}$ values of records in the set.

In addition to normalizing the records, the design spectrum needs to be constructed so that the normalized records can be scaled to the design spectrum at the structural period. The construction of the design spectrum depends on several parameters which are listed in ASCE-7. Among these parameters is $S_S$ and $S_1$, which are the Risk-adjusted Maximum Considered Earthquake ($MCE_R$) ground motion parameters for 0.2 sec (short period) and 1.0 sec spectral response acceleration, respectively. These values can be collected from 2008 United States Geological Survey National Seismic Hazard Maps (USGS-NSHM, 2008). By inputting the coordinates of San Francisco downtown area, the corresponding values of $S_S$ and $S_1$considering 2%, 5%, and 10% probability of exceedance in 50 years can be obtained as shown in Table 4-3.

**Table 4-3 $MCE_R$ Parameters for San Francisco Downtown Area**

| | $S_S$ | $S_1$ |
|---|---|---|
| 2% Probability of Exceedance in 50 years | 2.158 | 0.803 |
| 5% Probability of Exceedance in 50 years | 1.566 | 0.564 |
| 10% Probability of Exceedance in 50 years | 1.167 | 0.406 |

The site classification of the location of interest (San Francisco downtown area) is assumed as Site Class B, which result in site coefficients values, $F_a$ and $F_v$, of 1.0. The site coefficient values are determined according to *Table 11.4-1* and *Table 11.4-2* in ASCE-7 10.

The $MCE_R$ spectral response acceleration parameter for short periods ($S_{MS}$) and at 1 sec ($S_{M1}$), adjusted for Site Class effects, can be determined by Equation 4-2 and Equation 4-3, respectively (ASCE-7).

$$S_{MS} = F_a S_S \qquad \textbf{Equation 4-2}$$

$$S_{M1} = F_v S_1 \qquad \textbf{Equation 4-3}$$

Once the $MCE_R$ spectral response acceleration parameters are obtained, the $MCE_R$ design response spectrum is generated using ASCE-7 10. Figure 4-4 shows the curves of the $MCE_R$ design response spectrum associated with different probability of exceedance in 50 years for this study and the values of $MCE_R$ design spectral acceleration corresponding to three different probability of exceedance in 50 years for both BM-10 and BM-30 is calculated and the results are shown in Table 4-4.

**Table 4-4 $MCE_R$ Design Spectral Acceleration Values for BM-10 and BM-30**

| | BM-10 | BM-30 |
|---|---|---|
| 2% Probability of Exceedance in 50 years | 0.578g | 0.240g |
| 5% Probability of Exceedance in 50 years | 0.406g | 0.169g |
| 10% Probability of Exceedance in 50 years | 0.292g | 0.122g |

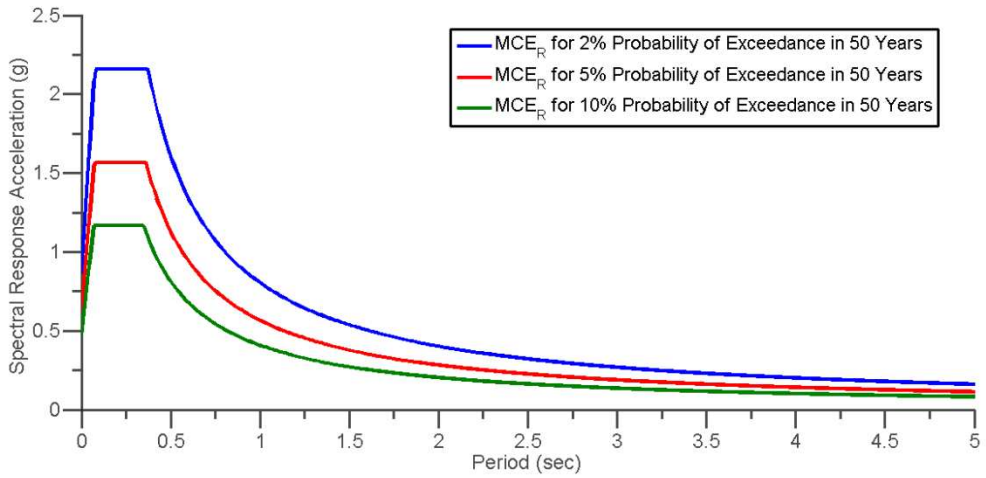


**Figure 4-4 $MCE_R$ Design Response Spectrums for Different Probability of Exceedance in 50 Years**

After constructing the design spectra, the SEISMOSIGNAL software is used to determine the normalized response spectrum for the selected record and the spectral acceleration values

corresponding to the fundamental periods of BM-10 and BM-30 can be obtained as shown in Figure 4-5.

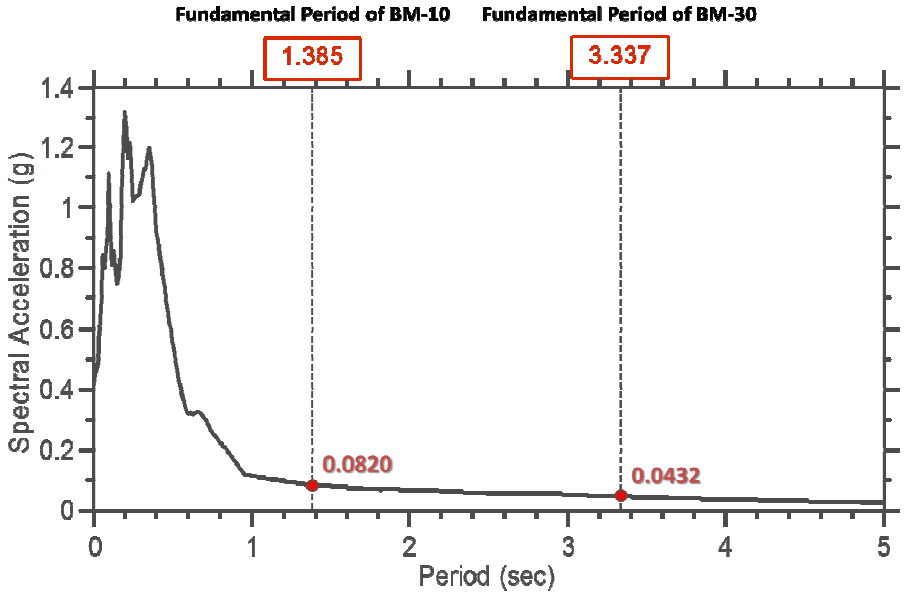


**Figure 4-5 Normalized Response Spectrum and Spectral Acceleration Values for BM-10 and BM-30**

Eventually, the scaling factors for ground motion records corresponding to three different probability of exceedance in 50 years for BM-10 and BM-30 can be calculated by Equation 4-4, and their values are presented in Table 4-5.

$$Scaling\ Factor_E = \frac{Spectral\ Acceleration_{MCE_R}}{Spectral\ Acceleration_{Normalized}} \qquad \textbf{Equation 4-4}$$

**Table 4-5 Scaling Factors for Ground Motion Records Values for BM-10 and BM-30**

| | BM-10 | BM-30 |
|---|---|---|
| 2% Probability of Exceedance in 50 years | 7.049 | 5.567 |
| 5% Probability of Exceedance in 50 years | 4.951 | 3.910 |
| 10% Probability of Exceedance in 50 years | 3.564 | 2.814 |

## 4.2 Wind Speed/Pressure Records

### 4.2.1 Design Wind Speed Selection and Wind Load Calculation

The design wind speed, which also known as the basic wind speed,  , is used to determine the design wind loads on buildings and other structures (ASCE-7). The wind speed maps for different probability of exceedance in 50 years for the U.S.  (Fig. 26.5-1 of ACSE 7-10), is shown in Figure 4-4 to Figure 4-6. The default unit of these basic wind speeds is mile per hour. The gray areas in the maps indicate special wind regions and are not of interest in this study.

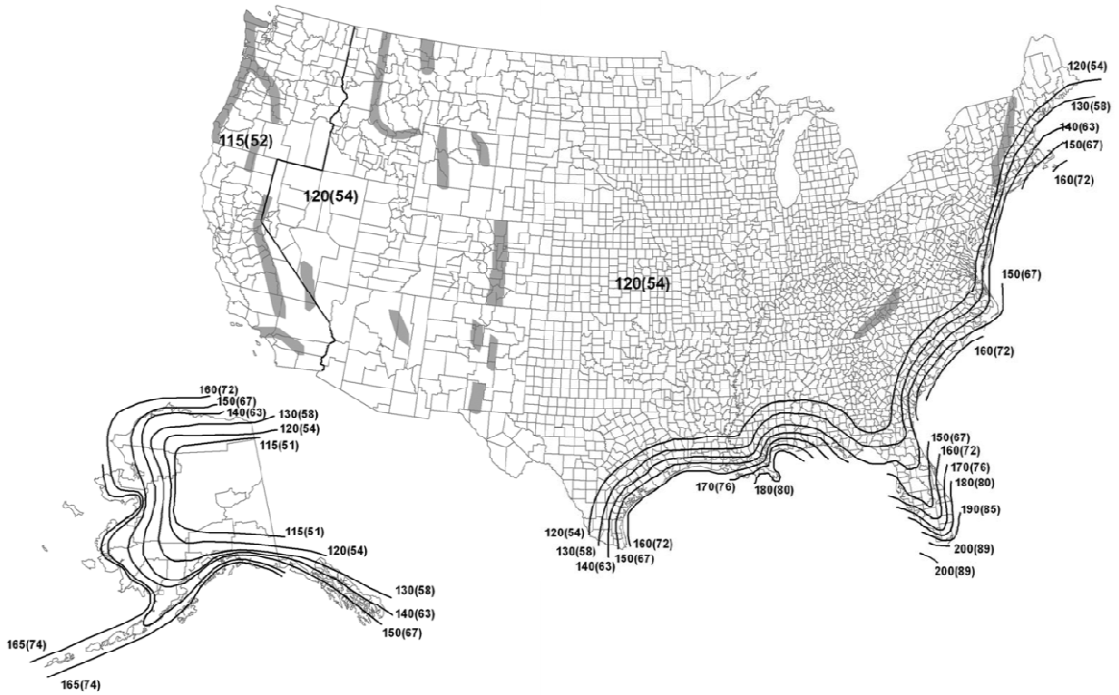


**Figure 4-6 Basic Wind Speeds Correspond to Approximately a 3% Probability of Exceedance in 50 Years**

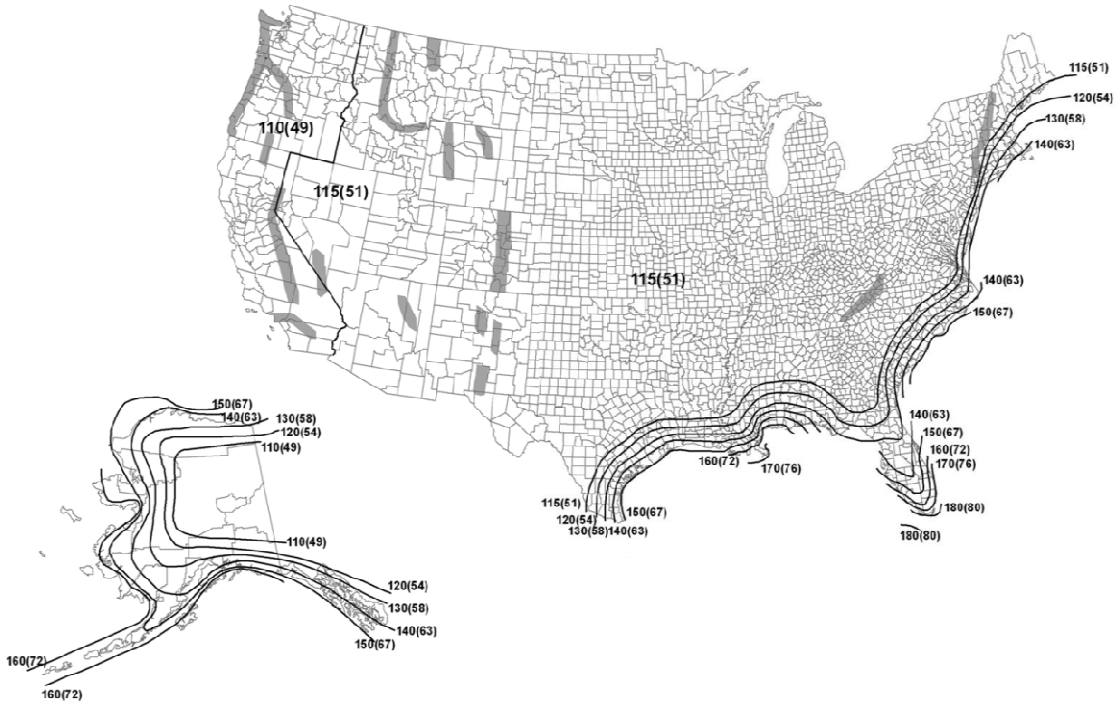


**Figure 4-7 Basic Wind Speeds Correspond to Approximately a 7% Probability of Exceedance in 50 Years**

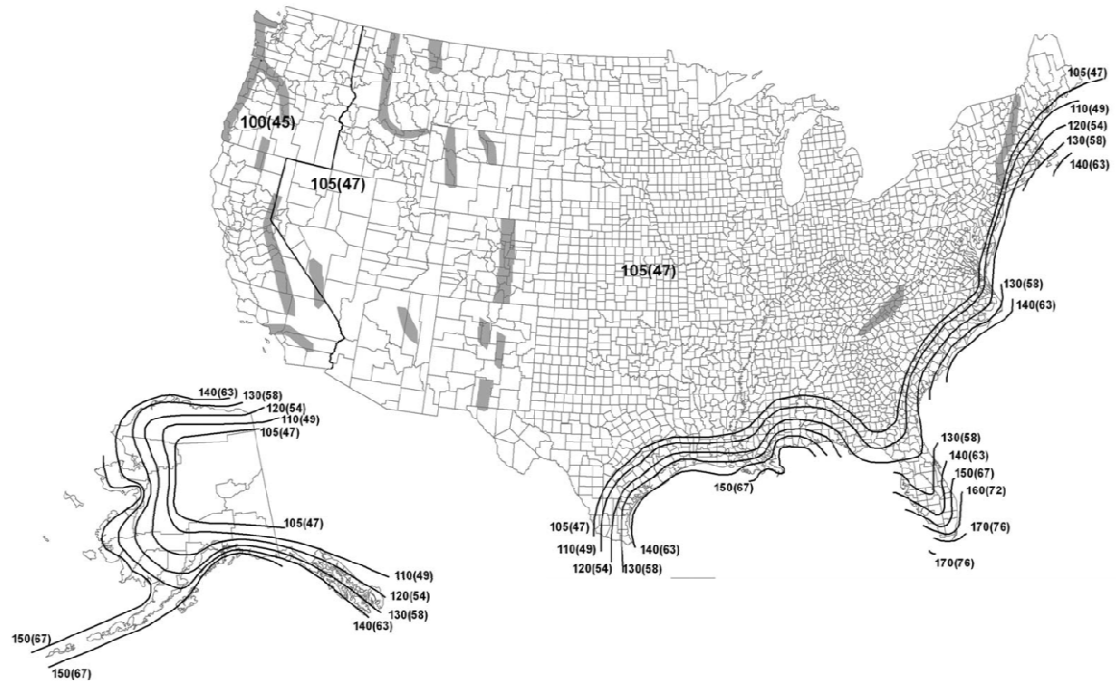


**Figure 4-8 Basic Wind Speeds Correspond to Approximately a 15% Probability of Exceedance in 50 Years**

According to the information from these maps, the basic wind speeds in San Francisco downtown area can be obtained and shown in follow:

$V_{3\%\ exceedance\ in\ 50\ yrs} = 115\ mph$

$V_{7\%\ exceedance\ in\ 50\ yrs} = 110\ mph$

$V_{15\%\ exceedance\ in\ 50\ yrs} = 100\ mph$

The wind load, then, can be calculated based on the basic wind speeds that have been determined. Steps to determine Main Wind Force Resisting System (MWFRS) wind loads for enclosed buildings of all heights are introduced in ASCE-7:

- First, a series of related wind load parameters need to be determined:
  1. The directionality factor, $K_d = 0.85$ since the structure type is considered as the MWFRS (Section 26.6 and Table 26.6-1, ASCE-7 10)
  2. The exposure category is assumed to be category C so the velocity pressure exposure coefficient, $K_d = 0.85$ at the height meters above ground level $z = 4\ m$ (Table 27.3-1, ASCE-7 10)
  3. The topographic factor $K_{zt} = 1.0$ (Section 26.8, ASCE-7 10)
  4. The gust effect factor, $G = 0.85$ (Section 26.9, ASCE-7 10)
  5. The enclosure classification is define as enclosed buildings herein (Section 26.10, ASCE-7 10)
  6. The internal pressure coefficient, $GC_{pi} = \pm 0.18$ and it is based on enclosure buildings classification
  7. The external pressure coefficient, $C_p = 0.8$ for the windward wall surface
- Using the above information, the velocity pressure $q_z$ can be determined according to Equation 4-5 (Section 27.3.2, ASCE-7 10).

$$\boldsymbol{q_z = 0.00256\, K_z\, K_{zt}\, K_d V^2\ (lb/ft^2)} \qquad \textbf{Equation 4-5}$$

- Finally, the design wind pressure for the MWFRS of building for all heights can be calculated using Equation 4-6 (Section 27.4.1, ASCE-7 10).

$$\boldsymbol{p = q_z GC_p - q_z(GC_{pi})\ (lb/ft^2)} \qquad \textbf{Equation 4-6}$$

In this study, only the design wind pressure at the height of 4 meters on the windward wall will be calculated. It is because the 4 meter is considered as a typical height of the wind pressure time-history record from TPU Aerodynamic Database was acquired. Then, the design values of the wind pressure of interest associated with the wind speeds considering different probability of exceendance in 50 years can be determined as shown in Table 4-6 and these values will be used to determine the scaling factors for time-history wind loads.

**Table 4-6 Design Windward Wall Surface Wind Pressures at the Height of 4 meters ( $p_4^w$ )**

| | $p_4^w\,(lb/ft^2)$ | $p_4^w\ (N/m^2)$ |
|---|---|---|
| 2% Probability of Exceedance in 50 years | 16.63 | 796.41 |
| 5% Probability of Exceedance in 50 years | 15.22 | 728.67 |
| 10% Probability of Exceedance in 50 years | 12.58 | 602.20 |

$w$: Windward Wall Surface Pressure

### 4.2.2 Time-History Wind Pressure Record

The time-history wind pressure record is collected from the TPU Aerodynamic Database, which is maintained by the school of Architecture and Wind Engineering of Tokyo Polytechnic University. The objective of this program is to provide structural engineers with the aerodynamic database of high-rise buildings in terms of wind loads, which based on wind tunnel test data so that the wind induced building dynamic analyses can be carried out.

#### 4.2.2.1 Record Introduction

Take the 10-story building model as an example, by entering the geometry information of the building (breadth: height: depth = 1: 1: 1) and the exposure factor (Assumed to be 1/6), a group of data including the averaged wind pressure coefficients on the wall surface, graphs of wind pressure distribution on the wall face, and time series data can be obtained.

Figure 4-9 presents the graph of wind pressure distribution on the wall face of a building model with height, breadth, and depth are all 0.1 meter. As it shows that the Model Scale is equal to 1/400, this model can be considered as the scaled model of 40 meters by 40 meters by 40 meters building, which has the same configuration with our 10-story building model. The Surface 1, 2, 3, and 4 indicate the four facades of the building model, in which Surface 1 and 3 represent the front face and back facade, and Surface 2 and 4 represent two side facades herein.

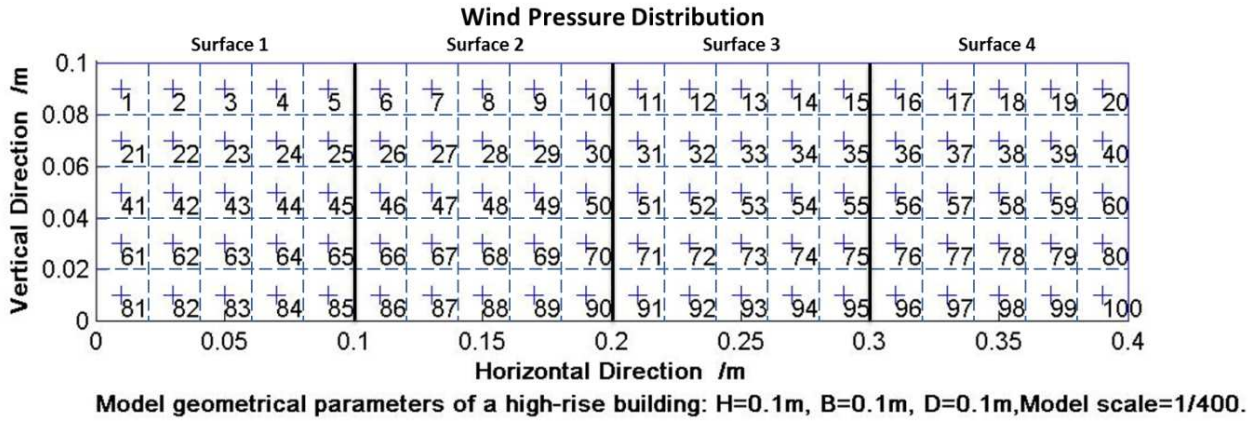


**Figure 4-9 Graph of Wind Pressure Distribution with Location Factors for 10-Story Building Model**

Those numbers, which have been arranged in sequence in Figure 4-9, are called location factors. Each of these factors identifies a certain area, in which the wind pressure is considered to be a constant and the value of this pressure can be found in the corresponding averaged wind pressure coefficients data. For the 10-story building model, the averaged wind pressure

coefficients data is presented as a matrix with a dimension of 32,768 × 100 and partially shown in Table 4-7. Each of the columns indicates the time history averaged wind pressure coefficients for a certain location factor from 0.001 to 32.768 second. Each of the rows identifies the averaged wind pressure coefficients for the entire wall surface of the building at a certain moment.

As the TPU Aerodynamic Database is on the basis of three-dimensional (3D) model test, a post-process becomes necessary in order to gain the wind pressure records for 2D structural analysis for this study.

**Table 4-7 Partial Wind Pressure Coefficients Data for 10-Story Building Model**

| | | **Location Factors** | | | | | | | |
|---|---|---|---|---|---|---|---|---|---|
| | | **1** | **2** | **3** | **4** | **5** | **……** | **99** | **100** |
| **Time (sec)** | **0.001** | 0.775 | 0.740 | 0.654 | 0.646 | 0.348 | …… | -1.220 | -0.914 |
| | **0.002** | 0.731 | 0.812 | 0.765 | 0.784 | 0.399 | …… | -1.010 | -0.747 |
| | **0.003** | 0.651 | 0.731 | 0.757 | 0.828 | 0.402 | …… | -1.107 | -0.885 |
| | **0.004** | 0.600 | 0.894 | 0.993 | 0.929 | 0.534 | …… | -0.893 | -0.805 |
| | **0.005** | 0.638 | 0.991 | 1.175 | 1.022 | 0.680 | …… | -1.02 | -0.873 |
| | **0.006** | 0.714 | 1.117 | 1.349 | 1.222 | 0.861 | …… | -0.100 | -0.853 |
| | **0.007** | 0.651 | 1.068 | 1.294 | 1.226 | 0.862 | …… | -1.140 | -0.930 |
| | **0.008** | 0.667 | 1.101 | 1.298 | 1.248 | 0.953 | …… | -1.052 | -0.879 |
| | **0.009** | 0.646 | 1.060 | 1.175 | 1.160 | 1.095 | …… | -1.078 | -0.933 |
| | **0.010** | 0.746 | 1.123 | 1.168 | 1.223 | 1.178 | …… | -0.965 | -0.874 |
| | ⋮ | ⋮ | ⋮ | ⋮ | ⋮ | ⋮ | …… | ⋮ | ⋮ |
| | **32.766** | 0.893 | 0.694 | 0.642 | 0.664 | 0.631 | …… | -1.383 | -0.984 |
| | **32.767** | 0.832 | 0.624 | 0.556 | 0.560 | 0.499 | …… | -1.537 | -1.030 |
| | **32.768** | 0.881 | 0.742 | 0.657 | 0.600 | 0.410 | …… | -1.219 | -0.873 |

#### 4.2.2.2 Post-Process

At the beginning, a decision has to be made that either the along- wind or the cross-wind should be chosen for the study. A sensitivity analysis indicates that the effect of the along-wind load, which considers wind pressure of Surface 1 and 3, is larger than the cross-wind load, which includes wind pressure of Surface 2 and 4.

An approximated calculation is carried out in order to transform the wind pressure coefficients for 3D building models to the ones for 2D models. The transformation process is presented in follow as well as in Figure 4-10 and Figure 4-11:

1. Transform the wind pressure coefficients to concentrated wind load coefficients by multiplying the wind pressure coefficient with the surface area.
2. Sum up the wind load coefficients at the same height on the wall surface.
3. Make an assumption that the SMRF system is the only lateral load resisting system and that each of the frames takes half of the summed load (gravity frames do not resist later load).s Input the summed wind load coefficients (Step 1) at the same height of the 2D building model.

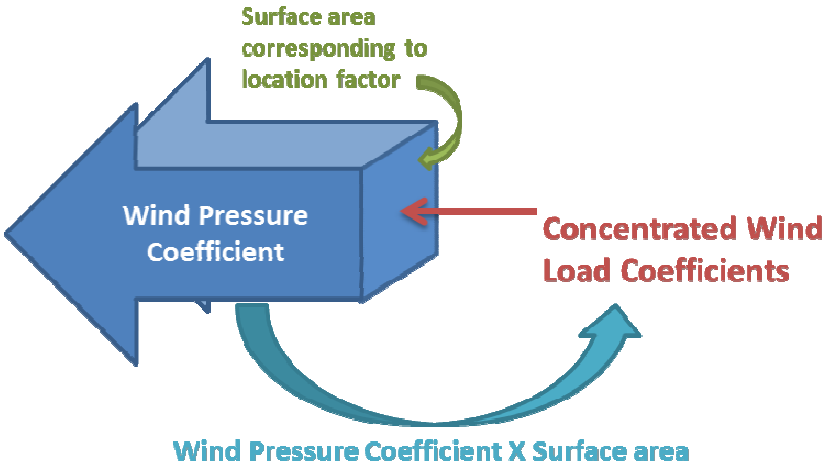


**Figure 4-10 Transformation Process of Wind Pressure Coefficient to Concentrated Wind Load Coefficient**

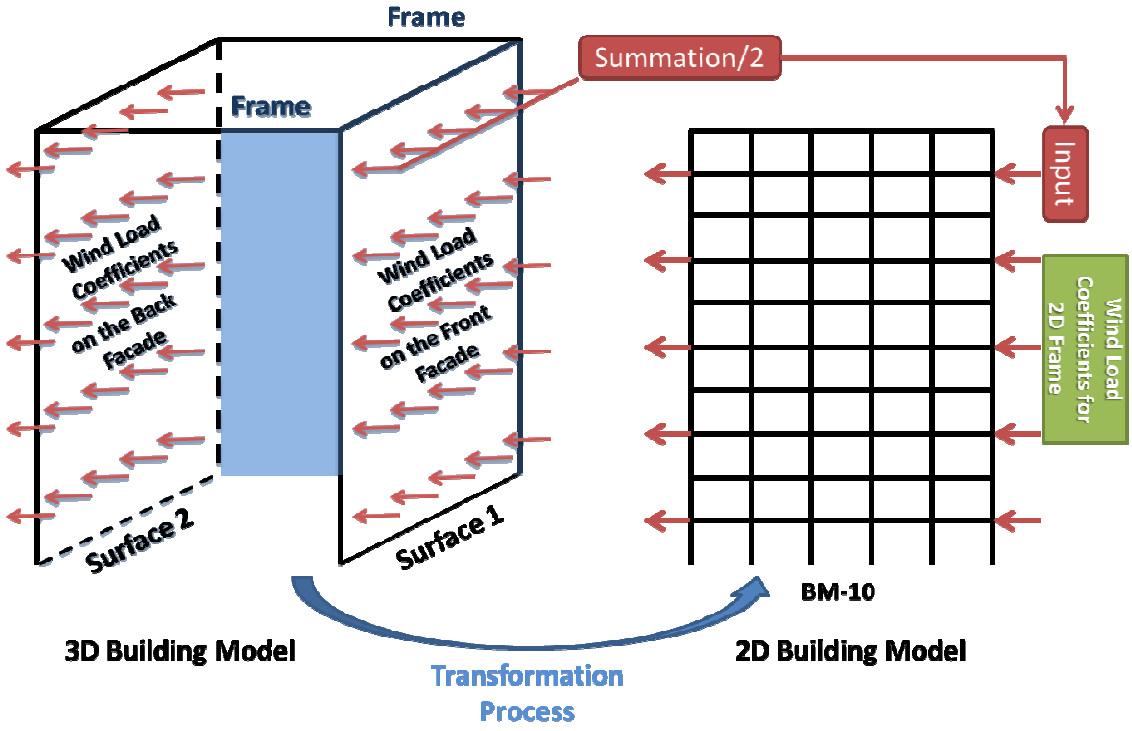


**Figure 4-11 Transformation Process of Wind Pressure Coefficients from 3D to 2D Building Model**

Finally, the time increment for the time-history dynamic analysis is defined as 0.1 second and the wind load coefficients data and the corresponding time history records for this study can be carried out. Figure 4-12 shows the post-processed wind load coefficient profile at 16$^{th}$ second of time-history record on the BM-10.

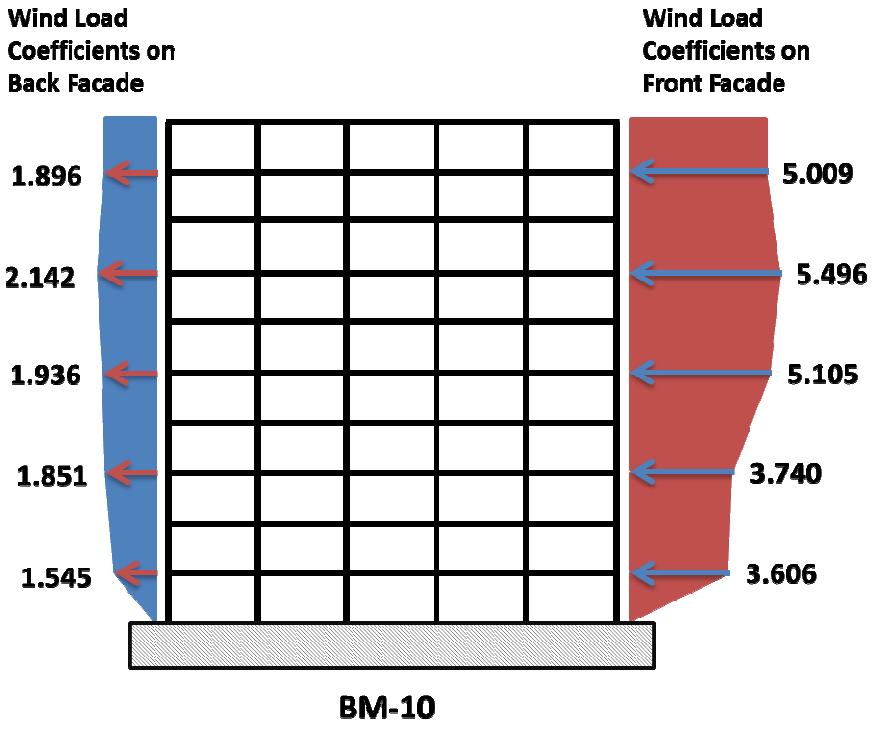


**Figure 4-12 Wind Load Coefficient Profile at 16th Second on BM-10**

### 4.2.3 Wind Load Scaling

The scaling process for wind loads is defined as an approximation. Two coefficients are needed to determine the scaling factor. The first coefficient is the design wind pressure values, which have been determined in earlier investigation. $p_4^w$, the expression of this coefficient, indicates the design wind pressure at 4 meters height on the windward wall surface, which also can be known as the front façade. The second coefficient is defined as the maximum wind pressure coefficient value at 4 meters height (same height of the design wind pressure) on the front façade (Surface 1) during the entire period of time-history records and can be referred to as $MWPC_4^{S1}$ in this study.

The scaling factors for wind load records corresponding to three different probability of exceedance in 50 years for BM-10 and BM-30 is calculated using Equation 4-7 and their values are summarized in Table 4-8.

$$Scaling\ Factor_w = \frac{p_4^w}{MWPC_4^{S1}} \qquad \textbf{Equation 4-7}$$

**Table 4-8 Scaling Factors for Wind Load Records Values for BM-10 and BM-30**

| | BM-10 | BM-30 |
|---|---|---|
| 2% Probability of Exceedance in 50 years | 370.098 | 429.960 |
| 5% Probability of Exceedance in 50 years | 338.615 | 393.385 |
| 10% Probability of Exceedance in 50 years | 279.847 | 325.111 |

# CHAPTER 5

# ANALYSIS RESULTS AND DISCUSSION

## 5.1 Eigenvalue Calculation

The eigenvalue calculations then are carried out for all of the column design schemes on both BM-10 and BM-30 by ABAQUS® and the results are shown in Table 5-1.As it has seen mentioned that extra braced members are included in finite element models (non-structural components) so that the values of the fundamental periods calculated by eigenvalue analysis can be close to the ones obtained from Equation 3-1, the approximate fundamental period equation (ASCE 7-10), for BM-10 and BM-30.

**Table 5-1 Eigenvalue Results of Column Design Schemes for BM-10 and BM-30**

| BM | Fundamental Period for Column Design Schemes (Sec) | | | | | |
|---|---|---|---|---|---|---|
| 10 | *Initial* | *I* | *II* | *III* | *IV* | *V* |
| | 1.38462 | 1.52492 | 1.70164 | 2.03537 | 2.27588 | 2.39498 |
| 30 | *I* | *Initial* | *II* | *III* | *IV* | *V* |
| | 3.17692 | 3.33845 | 3.60685 | 3.9119 | 4.34915 | 4.74541 |

An additional study, then, can be carried out in order to enhance the reality of the building models by adding physical damping to the structural system. The classical Rayleigh damping, is used to simulate the inherent damping effect of the building models. The coefficients, $\alpha$ and $\beta$, are constants used to define the mass and stiffness proportionality of damping. Equation 5-1 shows the relationship between $\alpha$, $\beta$, the natural frequency, and the damping ratio.

$$\alpha + \beta\omega_n{}^2 = 2\omega_n\xi_n \qquad \textbf{Equation 5-1}$$

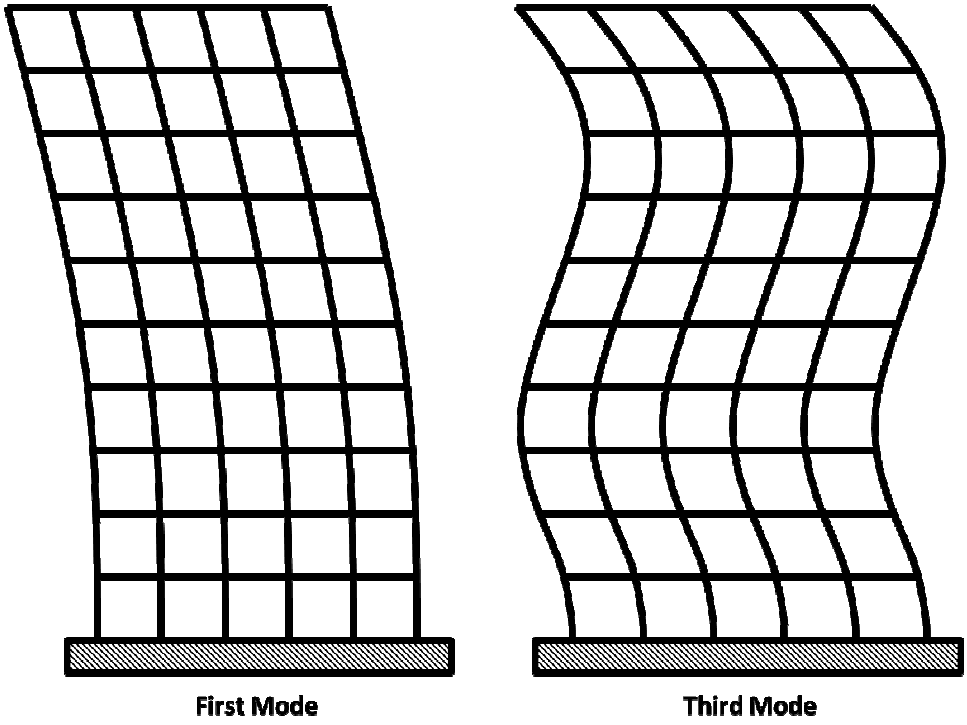


**Figure 5-1 Mode Shapes of the 1st and 3rd modes**

in which $\omega_i$ is the frequency of the $n^{th}$ mode. The value of $\alpha$ and $\beta$ can be determined by prescribing damping ratio of $\xi_i$ and $\xi_j$ corresponding to the $i^{th}$ and $j^{th}$ modes with frequencies of $\omega_i$ and $\omega_j$, respectively. In this study, the damping ratio of $i^{th}$ and $j^{th}$ modes is assumed to be the same ( $\xi$ ) and the 1st and 3rd modes, whose basic shapes are shown in Figure 5-1, is considered herein ( ; ), then $\alpha$ and $\beta$ can be computed as

$$\alpha = \xi\frac{2\omega_1\omega_3}{\omega_1+\omega_3} \;;\quad \beta = \xi\frac{2}{\omega_1+\omega_3} \qquad \textbf{Equation 5-2}$$

and eventually the results of the $\alpha$ and $\beta$ coefficients are presented in Table 5-2.

**Table 5-2 Results of the Damping coefficients $\alpha$ and $\beta$**

| Building Model | $\alpha$ | $\beta$ |
|---|---|---|
| BM-10 | 0.0612 | 0.0211 |
| BM-30 | 0.0259 | 0.0454 |

## 5.2 Initial Cost Calculation

As introduced in Chapter 3, the initial cost of a building comprises of the costs of all structural components that make up the building. Nonstructural components are assumed to remain unchanged since there is no effect on optimization design intensity by increasing or decreasing the cost of nonstructural components. In this study, the main structural components considered in the initial cost are steel and fireproofing of beams and columns. Steel costs are calculated according to 1997 Building Construction Cost Data (BCCD, 1997), and the cost is measured based on 1996 Means BCCD by Georgetown Laboratory Cost Estimate.

The calculation of the initial cost is on the basis of 3-D models, which include all the beam members and column members from the interior and exterior frames. For the steel cost calculation, bare cost and overhead and profit (O&P) are both considered. Bare cost for steel structure is the sum of material base price, labor rate, and equipment cost. With the exception of the e bare cost, the total cost also includes O&P, which is a crucial component in a construction project. The adjustments for different construction scenarios and for bare cost and total cost including O&P is given in the 1997 BCCD and is shown in Table 5-3. All of these costs are used as general national average cost in U.S. dollar per ton and are based on 1997 BCCD.

**Table 5-3 Cost Adjustment for Steel Structure (BCCD, 1997)**

| Adjustment to the Costs | Bare Cost | Total Cost Inl. O&P |
|---|---|---|
| For 3 to 6 story building, add per ton | $70.00 | $130.00 |
| For 7 to 15 story building, add per ton | $90.00 | $167.00 |
| For over 15 story building, add per ton | $105.00 | $195.00 |

For calculating of beam and column fireproofing, the unit cost can be found from 1996 Means BCCD by Georgetown Laboratory Cost Estimate. The united cost for beam and column fireproofing is $ 1.14 per square foot and $ 1.46 per square foot, respectively. The areas of beam and column fireproofing can be measured as follow:

in which , , and are depth, flange width, and distance, respectively. Figure 5-2 shows the shape of steel member and important parameters for initial cost calculation.

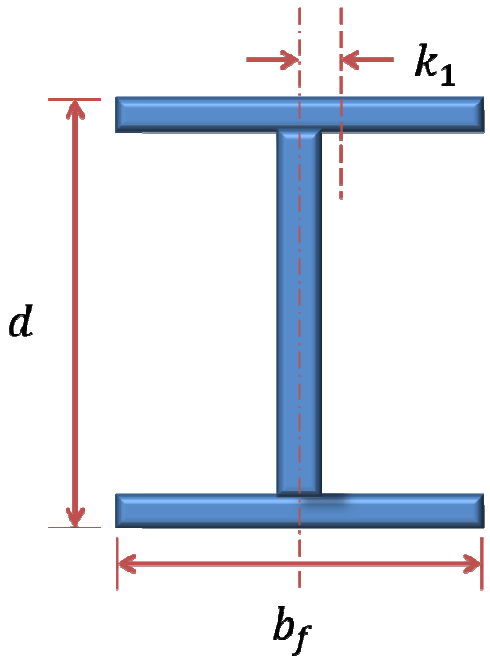


**Figure 5-2 Shape of the Steel Member for Initial Cost Calculation**

The initial cost calculations for buildings in this study can be carried out in accordance with the standards given above. The initial column design schemes for each of the 10-story and 30-story building models are considered as examples here to demonstrate the procedures of estimating initial cost calculation. Historical cost index from Table 3-7 is imported to convert the costs in 1996 and 1998 to 2013 costs. Finally, Table 5-4 to Table 5-9 shows the calculation process and the historical adjusted results of initial costs (by using Equation 3-5) for the two building models.

**Table 5-4 Structural Member Weight Estimation for BM-10**

| | | Floor | I-Beam Number | Length (ft.) | lb./ft. | Weight (lb.) | Weight (ton) |
|---|---|---|---|---|---|---|---|
| **10-Story Building Model** | Interior Column | 1 - 4 | W10X77 | 839.90 | 77 | 64672 | 32 |
| | | 5 - 7 | W10X49 | 629.92 | 49 | 30866 | 15 |
| | | 8 - 10 | W10X33 | 629.92 | 33 | 20787 | 10 |
| | | | | | | | |
| | Exterior Column | 1 - 4 | W14X730 | 1049.87 | 730 | 766404 | 383 |
| | | 5 - 7 | W14X500 | 787.40 | 500 | 393701 | 197 |
| | | 8 - 10 | W14X311 | 787.40 | 311 | 244882 | 122 |
| | | | | | | | |
| | Beam | 1 - 10 | W18X86 | 15748.03 | 86 | 1354331 | 677 |
| | | | | | | | |
| | **SUM** | | | | | | **1438** |

**Table 5-5 Structural Member Fireproofing Area Estimation for BM-10**

| | | Floor | I-Beam Number | Length (ft.) | d | bf | k1 | Area ($ft^2$) |
|---|---|---|---|---|---|---|---|---|
| **10-Story Building Model** | Interior Column | 1 - 4 | W10X77 | 839.90 | 0.8833 | 0.8492 | 0.0677 | 4109.19 |
| | | 5 - 7 | W10X49 | 629.92 | 0.8317 | 0.8333 | 0.0573 | 3003.15 |
| | | 8 - 10 | W10X33 | 629.92 | 0.8108 | 0.6633 | 0.0573 | 2548.56 |
| | | | | | | | | |
| | Exterior Column | 1 - 4 | W14X730 | 1049.87 | 1.8683 | 1.4908 | 0.1823 | 9418.20 |
| | | 5 - 7 | W14X500 | 787.40 | 1.6333 | 1.4333 | 0.1458 | 6627.30 |
| | | 8 - 10 | W14X311 | 787.40 | 1.4267 | 1.3525 | 0.1094 | 6162.07 |
| | | | | | | | **Total Column Fireproofing Area =** | **31868.46** |
| | Beam | 1 - 10 | W18X86 | 15748.03 | 1.5325 | 0.9242 | 0.0729 | 87335.96 |
| | | | | | | | **Total Beam Fireproofing Area =** | **87335.96** |

**Table 5-6 Total Initial Cost Estimation for BM-10**

| | Item | BCCD 1997 Unit Costs Total Cost Inl. O&P | Weight (ton) | Cost | Adjusted Cost by Historical Index (2013) |
|---|---|---|---|---|---|
| **10-Story Building Model** | Steel | $1,956 | 1438 | $2,812,379 | $5,016,406 |
| | | | | | |
| | Item | BCCD1996 Unit Costs | Area ($ft^2$) | Cost | Adjusted Cost by Historical Index (2013) |
| | Beam fireproofing | $1.14 | 87335.96 | $99,563 | $181,779 |
| | Column fireproofing | $1.46 | 31868.46 | $46,528 | $84,949 |
| | | | | **Total Initial Cost =** | **$5,283,135** |

**Table 5-7 Structural Member Weight Estimation for BM-30**

| | | Floor | I-Beam Number | Length (ft.) | lb./ft. | Weight (lb.) | Weight (ton) |
|---|---|---|---|---|---|---|---|
| **30-Story Building Model** | Interior Column | 1 - 10 | W14X193 | 2099.74 | 193 | 405249 | 203 |
| | | 11 - 20 | W14X120 | 2099.74 | 120 | 251969 | 126 |
| | | 21 - 25 | W10X77 | 1049.87 | 77 | 80840 | 40 |
| | | 26 - 30 | W10X45 | 1049.87 | 45 | 47244 | 24 |
| | | | | | | | |
| | Exterior Column | 1 - 10 | W14X808 | 2624.67 | 655 | 1719160 | 860 |
| | | 11 - 20 | W14X605 | 2624.67 | 455 | 1194226 | 597 |
| | | 21 - 25 | W14X370 | 1312.34 | 257 | 337270 | 169 |
| | | 26 - 30 | W14X193 | 1312.34 | 132 | 173228 | 87 |
| | | | | | | | |
| | Beam | 1 - 30 | W18X86 | 47244.10 | 86 | 4062992 | 2031 |
| | | | | | | | |
| | **SUM** | | | | | | **4136** |

**Table 5-8 Structural Member Fireproofing Area Estimation for BM-30**

| | | Floor | I-Beam Number | Length (ft.) | d | bf | k1 | Area ($ft^2$) |
|---|---|---|---|---|---|---|---|---|
| **30-Story Building Model** | Interior Column | 1 - 10 | W14X193 | 2099.74 | 0.8417 | 0.6683 | 0.1042 | 4136.48 |
| | | 11 - 20 | W14X120 | 2099.74 | 0.8833 | 0.8492 | 0.1250 | 4895.89 |
| | | 21 - 25 | W10X77 | 1049.87 | 1.2067 | 1.2225 | 0.1354 | 14197.73 |
| | | 26 - 30 | W10X45 | 1049.87 | 1.2900 | 1.3092 | 0.1771 | 14925.63 |
| | | | | | | | | |
| | Exterior Column | 1 - 10 | W14X808 | 2624.67 | 1.2217 | 1.2271 | 0.0781 | 9237.75 |
| | | 11 - 20 | W14X605 | 2624.67 | 1.3650 | 1.3329 | 0.0990 | 10060.15 |
| | | 21 - 25 | W14X370 | 1312.34 | 1.5833 | 1.4029 | 0.1354 | 21618.55 |
| | | 26 - 30 | W14X193 | 1312.34 | 1.8033 | 1.4708 | 0.1719 | 23103.68 |
| | | | | | | | **Total Column Fireproofing Area =** | **102175.86** |
| | Beam | 1 - 30 | W18X86 | 47244.10 | 1.5325 | 0.9242 | 0.0729 | 262007.88 |
| | | | | | | | **Total Beam Fireproofing Area =** | **262007.88** |

**Table 5-9 Total Initial Cost Estimation for BM-30**

| 30-Story Building Model | Item | BCCD 1997 Unit Costs Total Cost Inl. O&P | Weight (ton) | Cost | Adjusted Cost by Historical Index (2013) |
|---|---|---|---|---|---|
| | Steel | $1,984 | 4136 | $8,206,001 | $14,636,946 |
| | | | | | |
| | Item | BCCD1996 Unit Costs | Area ($ft^2$) | Cost | Adjusted Cost by Historical Index (2013) |
| | Beam fireproofing | $1.14 | 262007.88 | $298,689 | $545,338 |
| | Column fireproofing | $1.46 | 102175.86 | $149,177 | $272,363 |
| | | | | **Total Initial Cost =** | **$15,454,646** |

Eventually, the city cost index, also known as location factor, is needed to adjust the national average to selected site. The city cost index for San Francisco is obtained from 1997 Building Construction Cost Data (BCCD). The location adjustment is according to Equation 3-4. The selected city cost index and the initial costs considering the cost of steel and fireproofing for all the column design schemes for the 10-story and 30-story building models are presented in Table 5-10 and Table 5-11.

**Table 5-10 Initial Costs of Column Design Schemes for BM-10**

| Column Design Scheme | Initial Cost (steel and fireproofing) | City Cost Index | Adjusted Initial Cost (San Francisco) |
|---|---|---|---|
| *Initial* | **$5,283,135** | 125.7 | **$6,640,901** |
| *I* | **$4,353,752** | | **$5,472,666** |
| *II* | **$3,758,081** | | **$4,723,908** |
| *III* | **$3,428,252** | | **$4,309,313** |
| *IV* | **$3,214,082** | | **$4,040,101** |
| *V* | **$3,124,827** | | **$3,927,908** |

**Table 5-11 Initial Costs of Column Design Schemes for BM-30**

| Column Design Scheme | Initial Cost (steel and fireproofing) | City Cost Index | Adjusted Initial Cost (San Francisco) |
|---|---|---|---|
| *I* | **$17,271,876** | 125.7 | **$21,710,748** |
| *Initial* | **$15,501,087** | | **$19,484,867** |
| *II* | **$13,773,946** | | **$17,313,850** |
| *III* | **$12,689,774** | | **$15,951,046** |
| *IV* | **$11,670,955** | | **$14,670,391** |
| *V* | **$11,153,563** | | **$14,020,029** |

## 5.3 Expected Failure Cost Calculation

The expected failure cost, as another primary component for building expected life-cycle cost calculation, has been generally introduced in the Chapter 3. Since the discrepancies in the definition of limit states and failure costs, the failure cost functions and related coefficients subjected to earthquake and wind hazard are developed in different ways and presented separately. By using the aforementioned measurements and methods, the expected failure cost can be calculated and presented as shown in the following sections.

### 5.3.1 Failure Cost Functions for Earthquake Hazard

For the calculation of the expected failure costs under seismic load, the definitions of different failure cost functions is listed and explained in Chapter 3 and the corresponding equations and basic costs can provided in Table 3-8. Other key factors are needed for calculating the expected value of failure costs corresponding to seven limit states, which have been defined in Chapter 3. These factors, include mean damage index, mean time of total loss of function of restore, expected injury rate (minor and serious), and expected death rate. The factors are

collected from ATC-13 (1985) and FEMA report 227 (1992) and are shown in Table 3-9, Table 3-10, and Table 3-11.

During the process of estimating the failure cost, the floor area is another necessary factor in determining the final result of the failure costs. For simplification purpose, the floor area is considered as the total area of all the floor of the building. In the case of the 10-story building model, the floor area is calculated by multiplying the area of each floor ($40m \times 40m = 1{,}600m^2$) with the number of story (10 stories). Therefore, the floor area, which is used in calculating the failure cost of the 10-story building model, is $16{,}000m^2$ ($172{,}223ft^2$). Similarly, the floor area of the 30-story building model can be calculated as $48{,}000m^2$ ($516{,}668ft^2$).

The aforementioned failure cost functions corresponding to the pre-defined limit states can be calculated based on the equations given in Table 3-8 listed below.

**Table 5-12 Failure Cost Functions Estimation for BM-10**

| Limit State Level | $C^{Dam}$ | $C^{Con}$ | $C^{Rel}$ | $C^{Eco}$ | |
|---|---|---|---|---|---|
| | | | | $C^{Ren}$ | $C^{Inc}$ |
| I | $0 | $0 | $0 | $0 | $0 |
| II | $73,195 | $24,886 | $29,278 | $11,321 | $160,427 |
| III | $731,946 | $248,862 | $104,022 | $40,222 | $569,986 |
| IV | $2,927,784 | $995,446 | $385,090 | $148,901 | $2,110,080 |
| V | $6,587,513 | $2,239,754 | $1,082,074 | $418,402 | $5,929,175 |
| VI | $11,711,135 | $3,981,786 | $2,030,160 | $784,995 | $11,124,162 |
| VII | $14,638,918 | $4,977,232 | $2,987,459 | $1,155,151 | $16,369,637 |

| Limit State Level | $C^{Inj}$ | | $C^{Fat}$ | $C^{Sum}$ (w/ injury and fatality) | $C^{Sum}$(w/ injury and fatality) |
|---|---|---|---|---|---|
| | Minor | Serious | | | |
| I | $0 | $0 | $0 | $0 | $0 |
| II | $10 | $14 | $599 | $299,729 | $299,106 |
| III | $1,033 | $138 | $5,993 | $1,702,202 | $1,695,038 |
| IV | $1,033 | $1,378 | $59,933 | $6,629,646 | $6,567,301 |
| V | $10,333 | $13,778 | $599,335 | $16,880,365 | $16,256,919 |
| VI | $103,334 | $137,778 | $5,993,345 | $35,866,694 | $29,632,237 |
| VII | $137,778 | $1,377,781 | $119,866,906 | $161,510,862 | $40,128,397 |

| Limit State Level | Adjusted $C^{Failure}$ (w/ injury and fatality) to 2013 | Adjusted $C^{Failure}$ (w/o injury and fatality) to 2013 |
|---|---|---|
| I | $0 | $0 |
| II | $606,696 | $605,434 |
| III | $3,445,504 | $3,431,002 |
| IV | $13,419,364 | $13,293,169 |
| V | $34,168,303 | $32,906,359 |
| VI | $72,599,385 | $59,979,941 |
| VII | $326,921,382 | $81,225,689 |

**Table 5-13 Failure Cost Functions Estimation for BM-30**

| Limit State Level | $C^{Dam}$ | $C^{Con}$ | $C^{Rel}$ | $C^{Eco}$ | |
|---|---|---|---|---|---|
| | | | | $C^{Ren}$ | $C^{Inc}$ |
| I | $0 | $0 | $0 | $0 | $0 |
| II | $219,584 | $74,658 | $87,834 | $33,962 | $481,280 |
| III | $2,195,838 | $746,585 | $312,067 | $120,666 | $1,709,958 |
| IV | $8,783,351 | $2,986,339 | $1,155,269 | $446,704 | $6,330,241 |
| V | $19,762,540 | $6,719,263 | $3,246,223 | $1,255,206 | $17,787,524 |
| VI | $35,133,404 | $11,945,357 | $6,090,479 | $2,354,985 | $33,372,487 |
| VII | $43,916,755 | $14,931,697 | $8,962,376 | $3,465,452 | $49,108,911 |

| Limit State Level | $C^{Inj}$ | | $C^{Fat}$ | $C^{Sum}$ (w/ injury and fatality) | $C^{Sum}$(w/ injury and fatality) |
|---|---|---|---|---|---|
| | Minor | Serious | | | |
| I | $0 | $0 | $0 | $0 | $0 |
| II | $31 | $41 | $1,798 | $899,188 | $897,318 |
| III | $3,100 | $413 | $17,980 | $5,106,607 | $5,085,114 |
| IV | $3,100 | $4,133 | $179,800 | $19,888,938 | $19,701,904 |
| V | $31,000 | $41,333 | $1,798,004 | $50,641,094 | $48,770,757 |
| VI | $310,001 | $413,334 | $17,980,036 | $107,600,082 | $88,896,712 |
| VII | $413,334 | $4,133,342 | $359,600,719 | $484,532,585 | $120,385,190 |

| Limit State Level | Adjusted $C^{Failure}$ (w/ injury and fatality) to 2013 | Adjusted $C^{Failure}$ (w/o injury and fatality) to 2013 |
|---|---|---|
| I | $0 | $0 |
| II | $1,820,087 | $1,816,301 |
| III | $10,336,512 | $10,293,007 |
| IV | $40,258,092 | $39,879,508 |
| V | $102,504,910 | $98,719,077 |
| VI | $217,798,155 | $179,939,823 |
| VII | $980,764,147 | $243,677,066 |

### 5.3.2 Failure Cost Functions for Wind Hazard

The failure cost functions considering wind hazard is treated entirely different than the ones for earthquake hazard. As mentioned in Chapter 3, the failure cost for wind is defined as an approximated potential initial investment on damping system, which has the capability of mitigating the high accelerations due to wind loading. In addition, the limit state is defined as human motion perception thresholds that indicate the toleration of the occupancy in the building. According to previous studies, a target value of structural acceleration response under wind load is 1.5g %. Therefore, an acceleration limit state with value of 3.0g % is assumed to be the typical limit state in this study. Eventually, the failure cost can be defined as the approximated potential

costs on STMD system with the ability to offer a reduction of structural acceleration response from the 3.0% g limit state to the target acceleration response of 1.5% g.

For the calculation of the failure cost under wind hazard, the total cost of STMD ($Cost_{STMD}$) is assumed to represent the failure cost function ($C_k$ in Equation 3-3). Two important parameters are introduced before calculating $Cost_{STMD}$: 1) the building general mass ($m^*$) is assumed to be the building's total mass, which is calculated in Appendix A; 2) the designed acceleration reduction level ($\gamma$) is calculated based on Equation 3-7, by considering the limit state acceleration of 3.0% g as the peak acceleration response without controls, and the target acceleration as peak acceleration response with controls. As there is only one limit state considered, the designed acceleration reduction level is 0.5 ($\gamma = 0.5$).

Finally, Equation 3-6, which provides a mathematical relationship between the total cost of the STMD ($Cost_{STMD}$), generalized mass of the building ($m^*$), and the designated acceleration reduction level ($\gamma$), can be used to obtain value of failure cost functions ($Cost_{STMD}$) under wind load. The results of the failure cost functions for 10-story and 30-story building model are presented in Table 5-14.

**Table 5-14 Cost of STMD for BM-10 and BM-30**

| | $Cost_{STMD}$ |
|---|---|
| 10-Story Building Model | \$16,279,154 |
| 30-Story Building Model | \$49,651,378 |

## 5.4 Reliability (Probability of Failure) Results

As it has been descripted in Equation 3-2 and Equation 3-3, the probability of failure associated with different limit state ($P_k$) also plays a significant role in the expected life-cycle cost calculation. The methodology for carrying out the probability of failure results has been

introduced in early chapter. Finite element software ABAQUS® is used as an analytical tool to investigate the dynamic response (deformation and acceleration) under the seismic and wind load. An interface is established between MATLAB and ABAQUS using concept of FORM to estimate the approximated failure probability results. The data flow is given in Figure 3-9, which demonstrates the cooperation of these two packages.

The uncertainty analysis mentioned in Chapter 3 offers a general idea on how random variables are defined in this study. As previously discussed, the scaling factors for both seismic and wind load and steel Young's modulus are considered as the random variables. Also, the values of the scaling factors for both hazards, however, were determined in Chapter 4. By combining all the aforementioned results, the final statistical properties of random variables are presented in Table 5-15.

Another important factor for this reliability analysis is the limit state, which has been fully defined and developed in Chapter 3. According to the review of previous studies and structural provisions, Kang and Wen (2000) summarized a proper definition of limit state associated with permissible drift ratio (PDR) for reliability analysis subjected to seismic load, which is listed in Table 3-5 and is used in this study. The limit state for reliability analysis subjected to wind load, however, has been defined as a human motion perception. Only one limit state is used for the wind load reliability and its value is determined as 3.0% g. Based on the identified limit states, the probability of failure results, are calculated and presented in follow.

**Table 5-15 Statistic Details of Random Variables**

| | | Random Variables (RVs) | Mean | C.O.V | Distribution Type | Number of RVs |
|---|---|---|---|---|---|---|
| **10-Story Building Model** | **Seismic Load** | $S_e$ -2% Probability of Exceedance | 7.049 | 0.2 | Normal Distribution | 1 |
| | | $S_e$ -5% Probability of Exceedance | 4.951 | 0.2 | Normal Distribution | 1 |
| | | $S_e$ -10% Probability of Exceedance | 3.564 | 0.2 | Normal Distribution | 1 |
| | **Wind Load** | $S_w$ -3% Probability of Exceedance | 370.098 | 0.2 | Normal Distribution | 1 |
| | | $S_w$ -7% Probability of Exceedance | 338.615 | 0.2 | Normal Distribution | 1 |
| | | $S_w$ -15% Probability of Exceedance | 279.847 | 0.2 | Normal Distribution | 1 |
| **30-Story Building Model** | **Seismic Load** | $S_e$ -2% Probability of Exceedance | 5.567 | 0.2 | Normal Distribution | 1 |
| | | $S_e$ -5% Probability of Exceedance | 3.910 | 0.2 | Normal Distribution | 1 |
| | | $S_e$ -10% Probability of Exceedance | 2.814 | 0.2 | Normal Distribution | 1 |
| | **Wind Load** | $S_w$ -3% Probability of Exceedance | 429.96 | 0.2 | Normal Distribution | 1 |
| | | $S_w$ -7% Probability of Exceedance | 393.385 | 0.2 | Normal Distribution | 1 |
| | | $S_w$ -15% Probability of Exceedance | 325.111 | 0.2 | Normal Distribution | 1 |
| **Both Mode and Hazards** | | Young's Modulus | $2.0 \times 10^{11}$ | 0.06 | Normal Distribution | 1 |

### 5.4.1 Reliability Results under Seismic Load

The reliability results, herein, are presented in the form of probability of failure. The failure probability can be defined as the probability of the structural overall behavior in terms of inter-story drift exceeding the limit states that have been defined in Chapter 3. Each of these limit states are corresponding to a certain PDR. Seven limit states and six PDRs are used in this

study. The details of definition of these seven limit states and values of these six PDRs can be found in Table 3-5.Reliability analyses associated with the different limit state function using these six PDRs are carried out. These reliability analyses are conducted by dynamic nonlinear time-history analysis using ABAQUS®. The time-history ground motion record for both the 10-story and 30 story building models is the 1989 Loma Prieta earthquake as mentioned in Chapter 4. The scaling factors, however, vary according to the different building models and (P.O.E's) probability of exceendances in 50 years under consideration.

Traditional reliability analysis often uses the probability of failure ($P_f$) to indicate how reliable the target structure is. For modern structural engineering study, however, the reliability index (β) is more commonly used instead of probability of failure for safety measures. The value of the reliability index increases when the probability of failure is low. In this study, the reliability index is used as the main tool to identify the reliability of building models. The transformation between reliability index (β) and probability of failure ($P_f$) is conducted using Equation 3-12.

For offering a more relevant presentation of the results, the structural fundamental frequency ( $f$ ) is utilized as an index and substitutes the column design schemes (from scheme *Initial* to scheme *V*), which was used in previous discussions. This is because the structural fundamental frequency ( $f$ ) represents the structural dynamic property, which can be more relevant to design engineers. For determination of the structural fundamental frequency, an eigenvalue analysis is carried out using ABAQUS®. All column design schemes for the BM-10 and BM-30 are considered and the result of $f$ are presented in Table 5-16.

**Table 5-16 Approximated Overall Structural Lateral Stiffness Results for BM-10 and BM-30**

| | Column Design Schemes | $f$ (Hz) |
|---|---|---|
| 10-Story Building Model | *Initial* | 0.7220 |
| | *I* | 0.6557 |
| | *II* | 0.5875 |
| | *III* | 0.4914 |
| | *IV* | 0.4394 |
| | *V* | 0.4175 |

| | Column Design Schemes | $f$ (Hz) |
|---|---|---|
| 30-Story Building Model | *I* | 0.3148 |
| | *Initial* | 0.2996 |
| | *II* | 0.2772 |
| | *III* | 0.2556 |
| | *IV* | 0.2299 |
| | *V* | 0.2107 |

Figure 5-3 to Figure 5-5 show the reliability index (β) verses the structural fundamental frequency ( $f$ ) considering six permissible inter-story drift ratio for the 10-story building model subjected to different intensity of seismic load with 2%, 5%, and 10% P.O.E in 50 years, respectively. In general, the tendencies of the reliability index curves are increasing as the structural fundamental frequency increases. This is because of the increase in the structural fundamental frequency changes the structural overall stiffness so that the structure becomes stiffer and less sensitive to the seismic load. Additionally, it is not difficult to recognize the reduction in the slopes of the curves as the permissible inter-story drift ratio increases. In summary, it can be concluded that the reliability analysis is more sensitive when dealing with larger permissible inter-story drift ratio limit state.

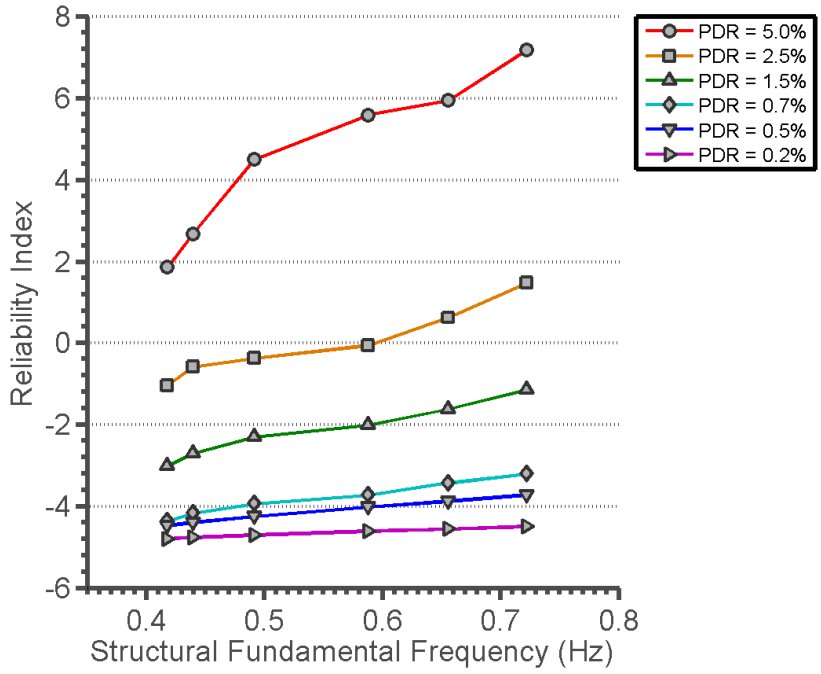


**Figure 5-3 Reliability Index Results of BM-10 Considering Seismic Load of 2% P.O.E in 50 Years**

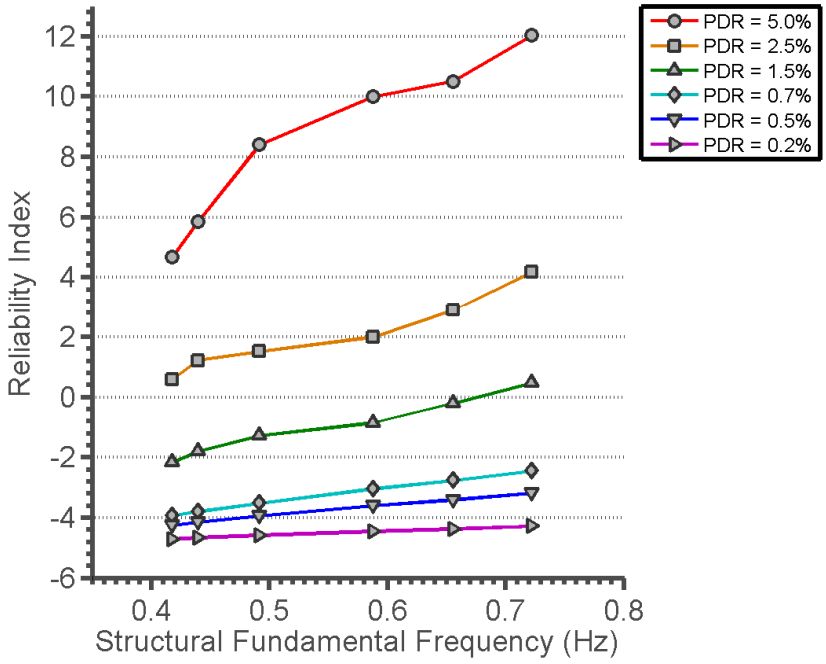


**Figure 5-4 Reliability Index Results of BM-10 Considering Seismic Load of 5% P.O.E in 50 Years**

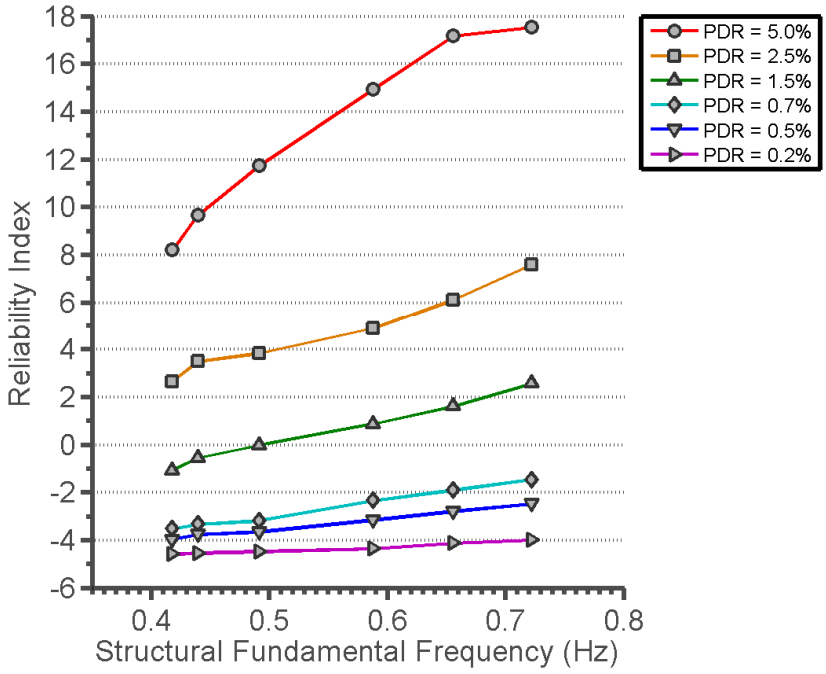


**Figure 5-5 Reliability Index Results of BM-10 Considering Seismic Load of 10% P.O.E in 50 Years**

Figure 5-6 to Figure 5-8, present the reliability index (β) results verses the fundamental frequency considering the six permissible inter-story drift ratio for the 30-story building model subjected to different intensity of seismic load according to P.O.Es (2%, 5%, and 10%) in 50 years, respectively.

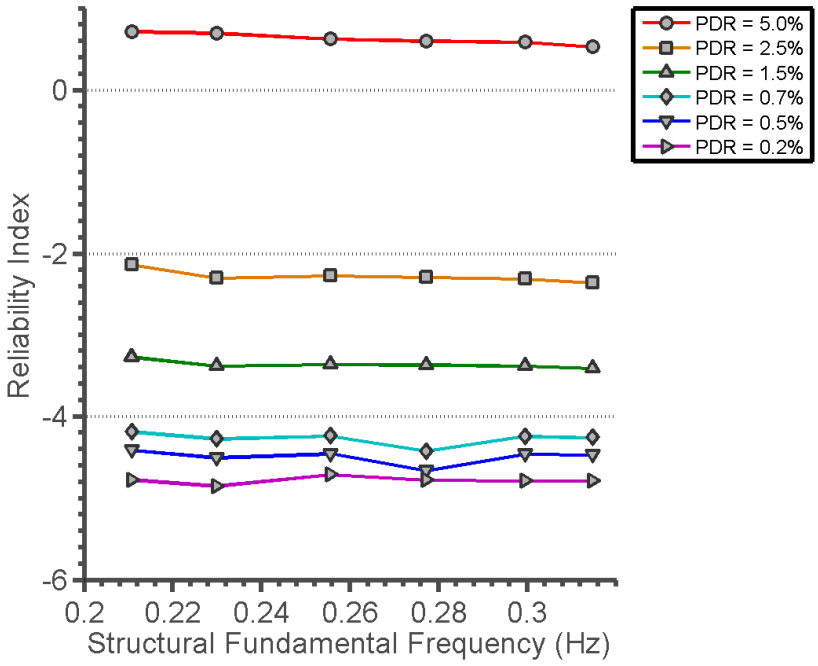


**Figure 5-6 Reliability Index Results of BM-30 Considering Seismic Load of 2% P.O.E in 50 Years**

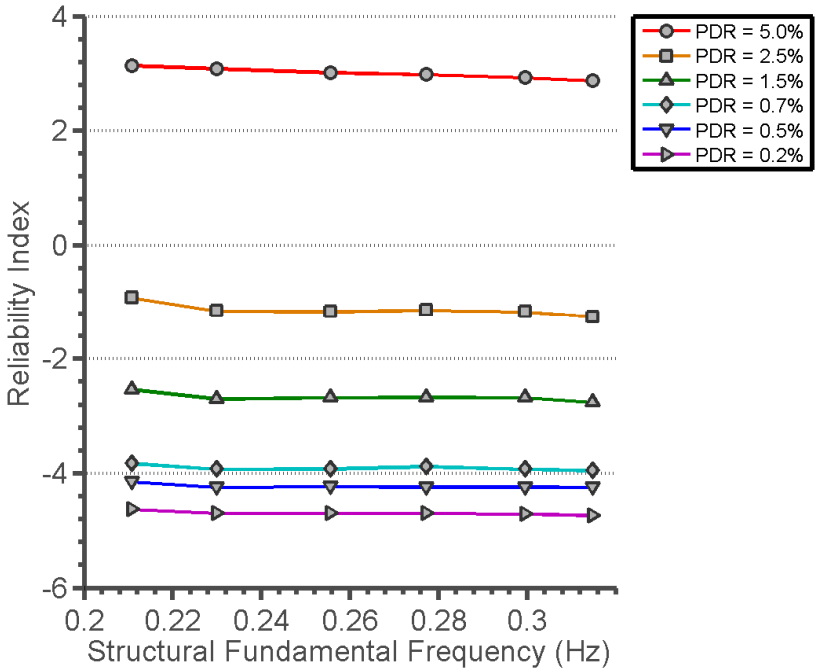


**Figure 5-7 Reliability Index Results of BM-30 Considering Seismic Load of 5% P.O.E in 50 Years**

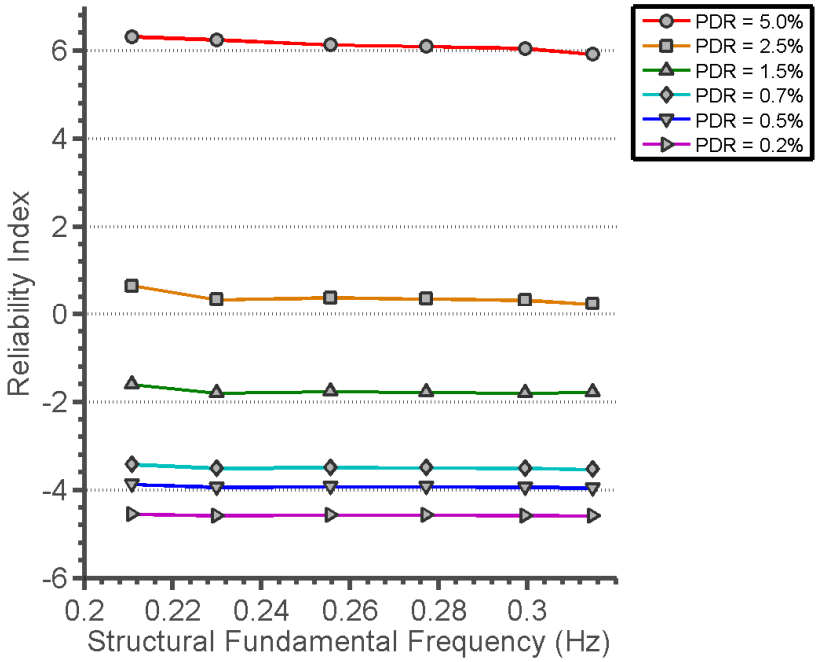


**Figure 5-8 Reliability Index Results of BM-30 Considering Seismic Load of 10% P.O.E in 50 Years**

Unlike the previous results, these reliability indecies herein, show mainly increasing trend and relatively less slope, which indicate the structure becomes less reliable as the overall structural stiffness is reduced. In addition, the 30-story building is less senstive to the the change the 10-story building.

### 5.4.2 Reliability Results under Wind Load

The reliability index results carried out by reliability analysis subjected to wind load for 10-story and 30-story building models are present in Figure 5-9 and Figure 5-10, respectively. As mentioned previously, the reliability index under wind hazard is defined by the structural peak acceleration response. Unlike the results from reliability analysis subjected to seismic load, a unique trend is realized in the reliability index results for both the 10-story and 30-story building models. The reliability indices reach a maximum values at a fundamental frequency of 0.5875 Hz and 0.2556 Hz for the 10-story and 30-story building model, respectively. This indicates that

the structure with column design *II* and *III* obtain relatively less acceleration responses subjected to same wind load intensity.

Moreover, reliability index values from the analysis of the 30-story building model are on average smaller than the ones from the reliability analysis of the 10-story building model, which indicate that the taller structures may suffering from a larger failure probability in terms of acceleration response subjected to wind load.

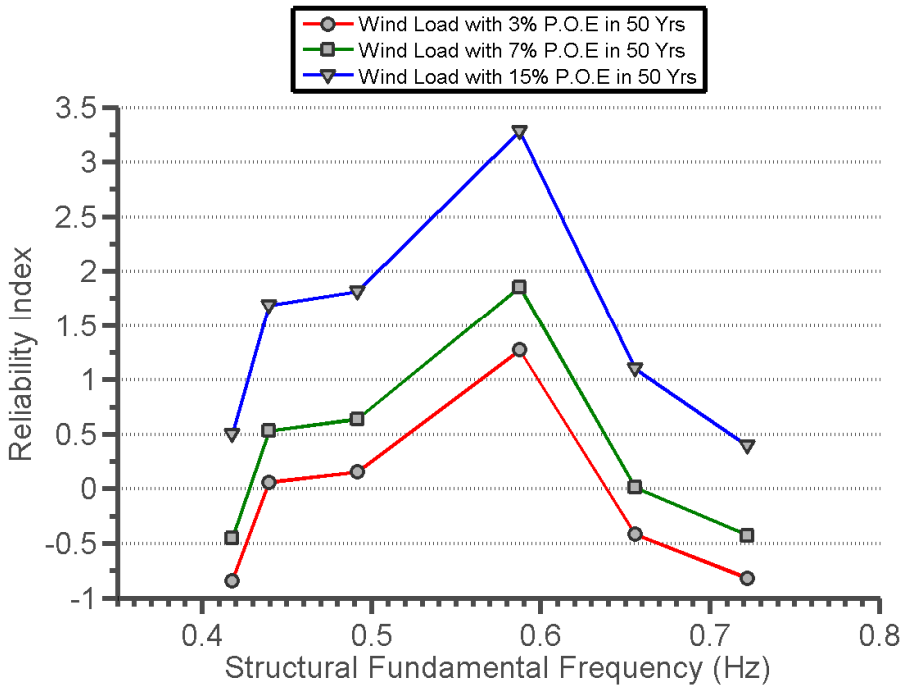


**Figure 5-9 Reliability Index Results of BM-10 Considering Wind Load**

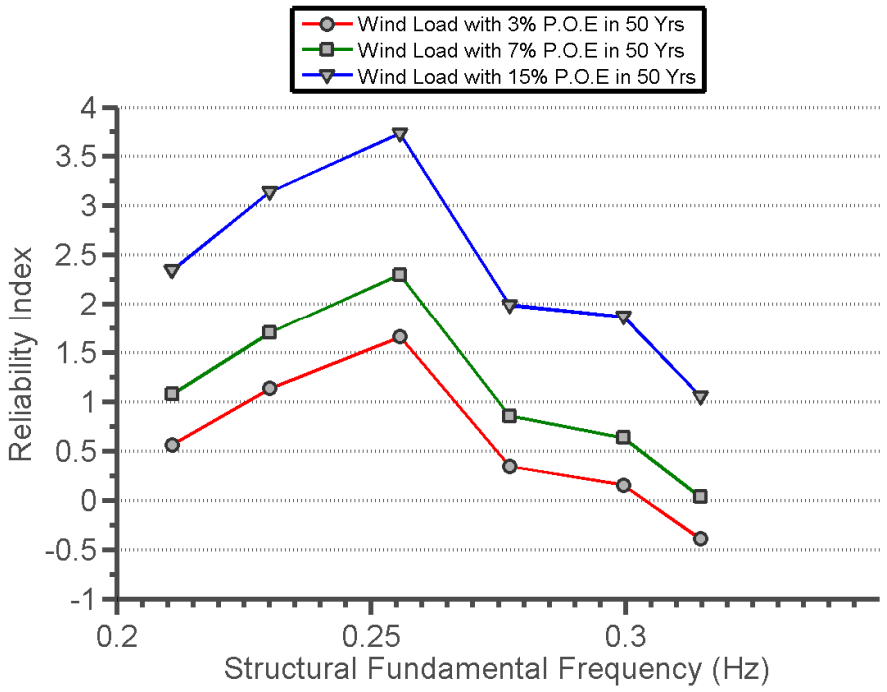


**Figure 5-10 Reliability Index Results of BM-30 Considering Wind Load**

## 5.5 Expected Life-Cycle Cost Results

Once all reliability analysis are completed and all reliability indices are obtained, the expected failure costs for earthquake and wind hazard are conducted by the aforementioned close form solution provided in Equation 3-2 and Equation 3-3, respectively, in which the corresponding failure probability $P$ concerning six permissible inter-story drifts can be calculated and expressed as percentages using Equation 3-12. Moreover, the basic failure cost functions corresponding to the pre-defined six permissible inter-story drift (limit states), as well as the factors of $v$ and $\lambda$, have been carried out in an earlier part of this chapter. Eventually, the expected life-cycle costs are able to be evaluated and the results are presented with initial costs and expected failure costs associated with different column design schemes.

### 5.5.1 Expected Failure Cost Results

First the initial costs and expected failure costs of all six column design schemes associated with their structural fundamental frequencies ( $f$ ) considering single hazard risk is presented. In Figure 5-12, the color bars show the expected failure costs associated with structural fundamental frequencies considering only seismic load intensity with 2%, 5%, and 10% P.O.E in 50 years, respectively, for the 10-story building model, with consideration of injury and death of building occupants.

In order to investigate the trends of failure costs of the structures with higher or smaller fundamental frequency, a prediction can be made by fitting the known failure cost value into a numerical function. For obtaining a decent prediction, a Fast Fourier transform (FFT) analysis is introduced to foresee a rational failure cost tendency. Figure 5-11 shows the FFT analysis for the scaled Loma Prieta earthquake time-history record marked by the fundamental frequencies of the column design scheme (*Initial* to *V*) for 10-story building model. It can be seen that considering the range of frequency from 0.3 to 1.0 Hz, the spectrum amplitude is higher when smaller frequency is obtained, which indicates that the structural with smaller fundamental frequency (less stiffness) are easier to be excited by the Loma Prieta earthquake and vice versa. Therefore, the prediction can be made that for the structure with fundamental frequency from 0.3 to 1.0 Hz, the failure cost is considered to be fitted as a monotone decreasing numerical function. Eventually, the exponential function is assumed to fit the failure cost for BM-10 and the fitted curves and functions are shown in Figure 5-12.

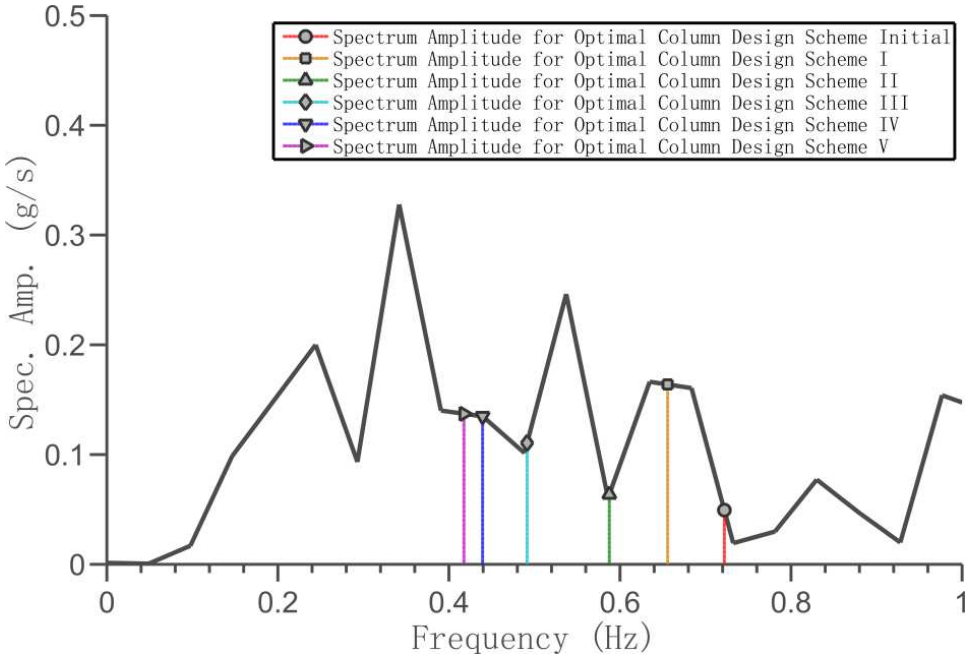


**Figure 5-11 |FFT| Analysis for Scaled Loma Prieta Earthquake (BM-10)**

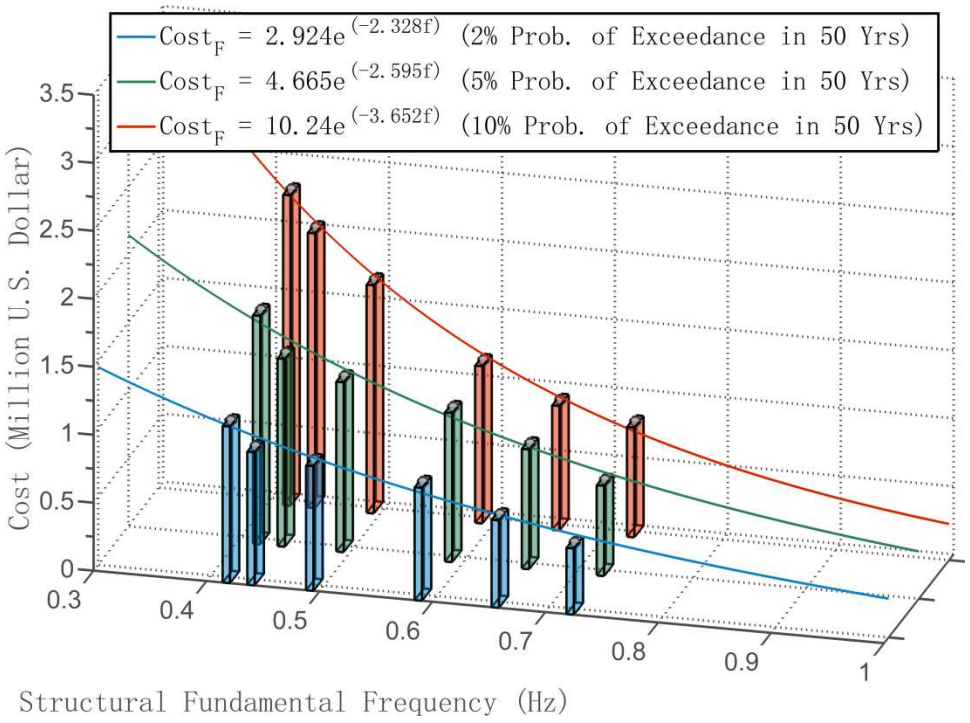


**Figure 5-12 Expected Failure Costs (Fitting Curves) for BM-10 Considering Earthquake Hazard**

The FFT analysis for the scaled Loma Prieta earthquake time-history record marked by the fundamental frequencies of the column design scheme (*Initial* to *V*) for 30-story building

model has been shown in Figure 5-13. If only considering the frequency from 0.1 to 0.5 Hz, the spectrum amplitude increases as the frequency increases when considering the frequency from 0.1 to 0.3 Hz and the spectrum amplitude is decreasing while the frequency is increasing when considering frequency from 0.3 to 0.5 Hz. Therefore it is reasonable to fit the failure cost with the function, which is not considered as monotone function in a certain internal region. Then the second-order polynomial function is assumed to fit the failure cost for BM-30 and the fitted curves and functions are shown in Figure 5-14.

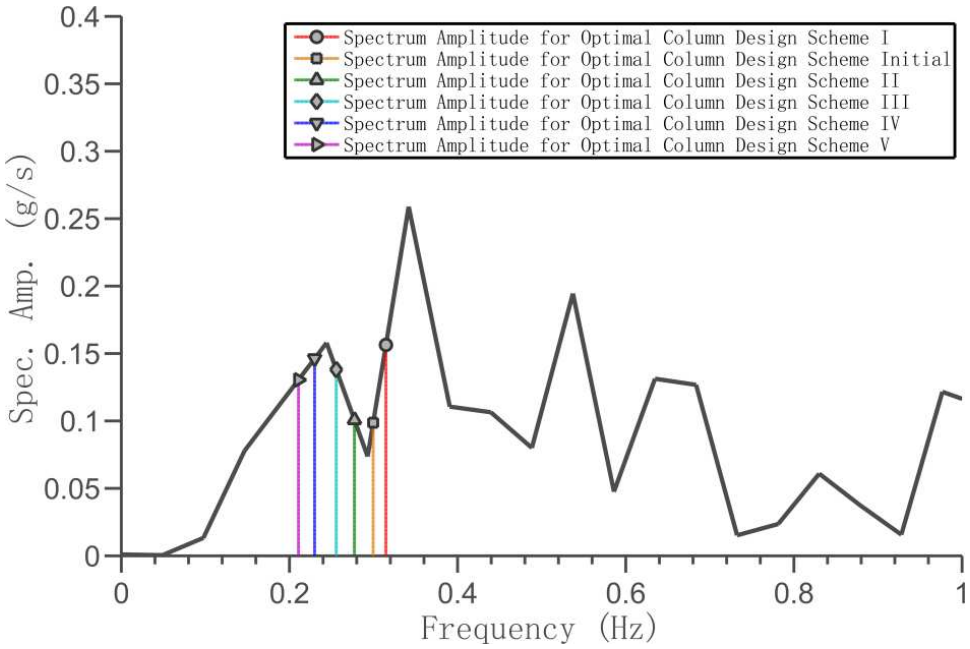


**Figure 5-13 |FFT| Analysis for Scaled Loma Prieta Earthquake (BM-30)**

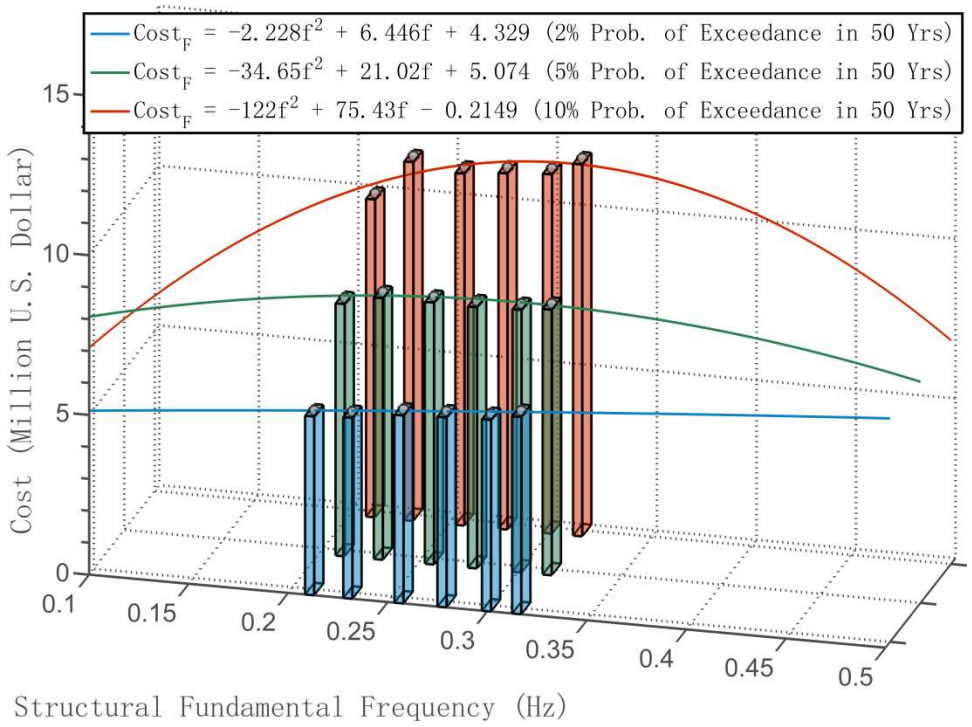


**Figure 5-14 Expected Failure Costs (Fitting Curves) for BM-30 Considering Earthquake Hazard**

According to the expected failure cost results, it can be recognized that the intensity of variation of the failure costs considering earthquake loading for the 10-story building model is turns out to be more significant than the one for 30-story building model. It is explainable that the fundamental frequencies of the six column design schemes for 30-story building model are corresponding to six similar spectrum amplitude values by FFT analysis (Figure 5-12), which indicates that all of these column design frames may be subjected to a similar excitation level considering Loma Prieta earthquake.

For the failure cost results considering earthquake loading, it is interesting to note that the expected failure costs considering relatively higher P.O.E earthquake level, e.g. 10% P.O.E in 50 years, generates an integrally larger cost compare to those considering lower P.O.E, e.g. 2% P.O.E in 50 years. The ratios between the failure costs considering different P.O.E, however, change along with the structural fundamental frequency as shown in Table 5-17. As it can be

seen that the ratio of the failure cost considering 2%, 5%, and 10% P.O.E earthquake loading for the 10-story building model is generally less when the structural fundamental frequency is decreasing. The ratio of the failure cost considering 2%, 5%, and 10% P.O.E earthquake loading for the 30-story building model, however, does not show an obvious tendency.

**Table 5-17 The Ratio of Failure Costs**

| | Column Design Schemes | $f$ (Hz) | Probability of Exceedance | | |
|---|---|---|---|---|---|
| | | | 10% | 5% | 2% |
| 10-story Building Model | *Initial* | 0.722 | 1.98 : | 1.46 : | 1.00 |
| | *I* | 0.6557 | 2.06 : | 1.41 : | 1.00 |
| | *II* | 0.5875 | 1.42 : | 1.37 : | 1.00 |
| | *III* | 0.4914 | 1.83 : | 1.36 : | 1.00 |
| | *IV* | 0.4394 | 1.66 : | 1.36 : | 1.00 |
| | *V* | 0.4175 | 1.39 : | 1.32 : | 1.00 |

| | Column Design Schemes | $f$ (Hz) | Probability of Exceedance | | |
|---|---|---|---|---|---|
| | | | 10% | 5% | 2% |
| 30-story Building Model | *I* | 0.3148 | 1.78 : | 1.41 : | 1.00 |
| | *Initial* | 0.2996 | 1.98 : | 1.45 : | 1.00 |
| | *II* | 0.2772 | 1.87 : | 1.39 : | 1.00 |
| | *III* | 0.2556 | 1.87 : | 1.38 : | 1.00 |
| | *IV* | 0.2299 | 1.88 : | 1.37 : | 1.00 |
| | *V* | 0.2107 | 1.89 : | 1.35 : | 1.00 |

Although it has been shown that the structure considering earthquake load with higher P.O.E may be subjected to higher failure cost, the fitted curve (corresponding to fitted numerical function) made prediction that the failure cost considering earthquake load with lower P.O.E may become dominated as the considering structural fundamental frequency varies.

Therefore, the expected failure costs considering merely wind load intensity with 3%, 7%, and 15% P.O.E in 50 years for the 10-story and 30-story building models, respectively, are

presented in Figure 5-15 and Figure 5-16, respectively. Since there is not confidence to develop a FFT analysis based on the wind pressure time-history record, the failure costs considering wind load, in this study, will not be fitted in numerical functions and further prediction of the failure cost is not included herein.

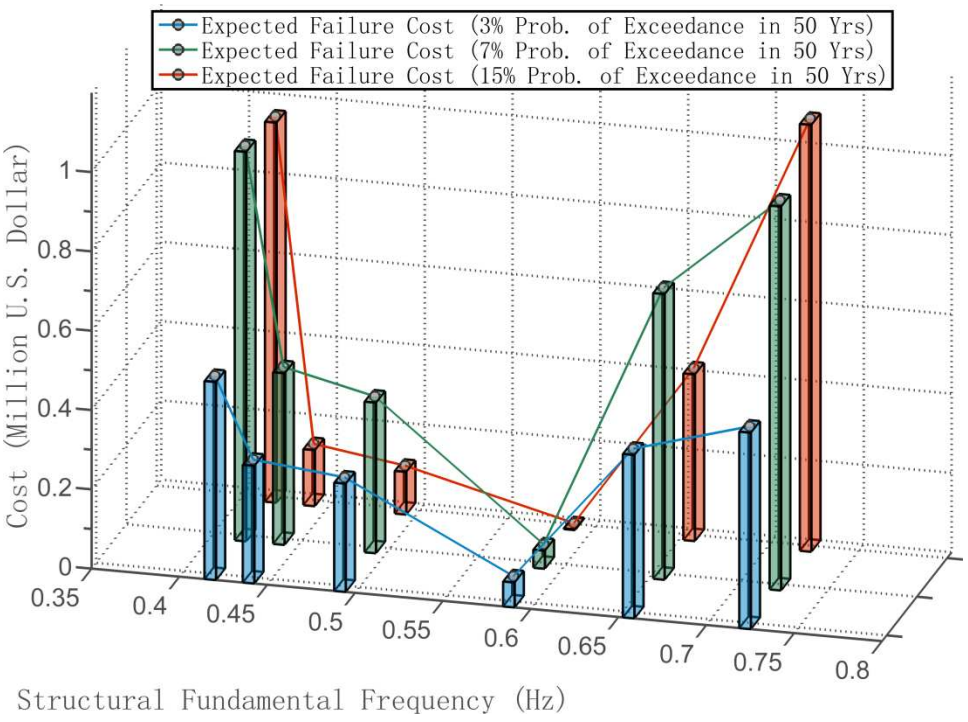


**Figure 5-15 Expected Failure Costs for BM-10 Considering Wind Hazard**

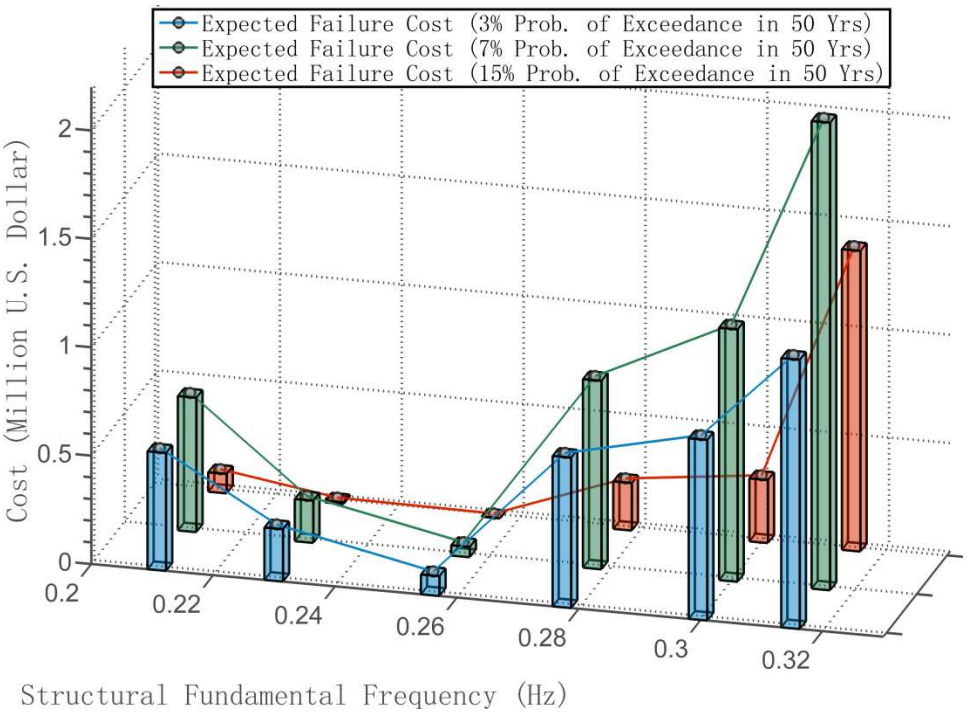


**Figure 5-16 Expected Failure Costs for BM-30 Considering Wind Hazard**

By comparing the failure cost results considering earthquake and wind hazard, it can be shown that the overall expected failure costs considering wind loading are much lower than the failure costs considering earthquake loading for both the 10-story and 30-story building model, which indicates that the seismic load can produce more severe financial consequence than wind load for medium to high rise building.

Additional studies for the failure cost considering earthquake and wind hazard are carried out in order to investigate the economic impact with different earthquake and wind intensity and the combination impact to the buildings. From a design prospective, one certain hazard level (earthquake or wind intensity) is usually determined to be considered prior to the structural design. Therefore, each of the failure costs led by three different earthquake intensities (2%, 5%, and 10% P.O.E in 50 years) is combined with each of the failure costs considering three different wind intensities (3%, 7%, and 15% P.O.E in 50 years) and their combinations are shown in Table 5-18.

**Table 5-18 The Combination of Earthquake and Wind intensity**

| Combinations | Earthquake Intensity (P.O.E) | Wind Intensity (P.O.E) |
|---|---|---|
| Combo 1 | 2% | 3% |
| Combo 2 | 2% | 7% |
| Combo 3 | 2% | 15% |
| Combo 4 | 5% | 3% |
| Combo 5 | 5% | 7% |
| Combo 6 | 5% | 15% |
| Combo 7 | 10% | 3% |
| Combo 8 | 10% | 7% |
| Combo 9 | 10% | 15% |

As long as the earthquake and wind intensity combinations are established, the corresponding failure costs should also be combined following these Combos. Figure 5-17 to Figure 5-19 present the failure costs considering different combinations of multi-hazards levels (earthquake and wind intensity) for BM-10.

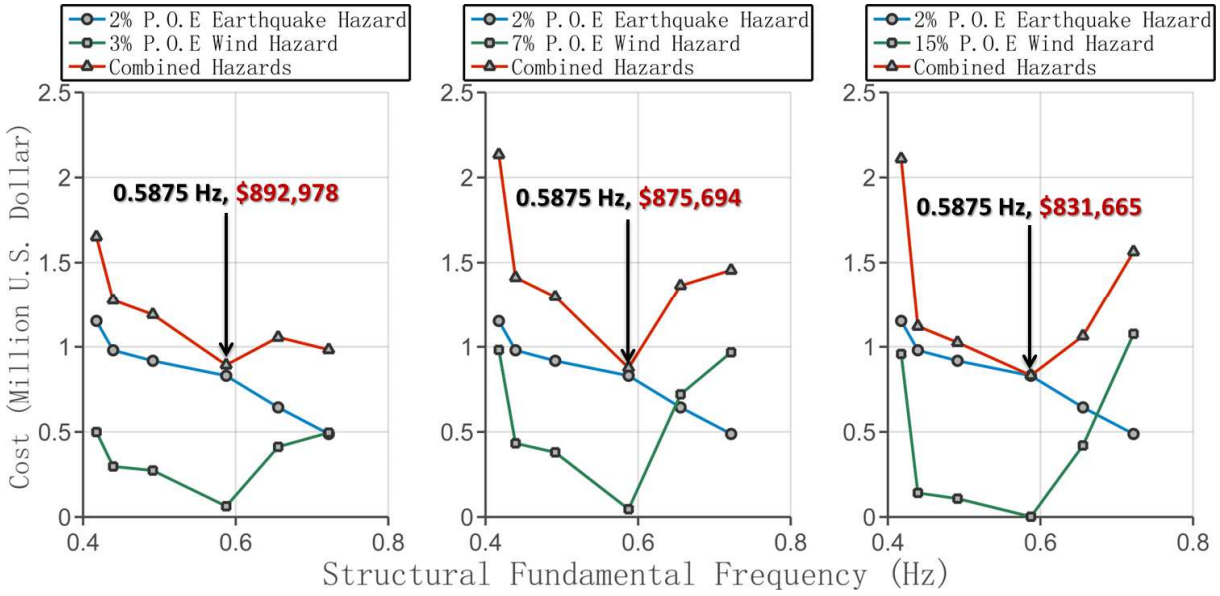


**Figure 5-17 Failure Cost Combination (Combo 1 to Combo 3) for BM-10**

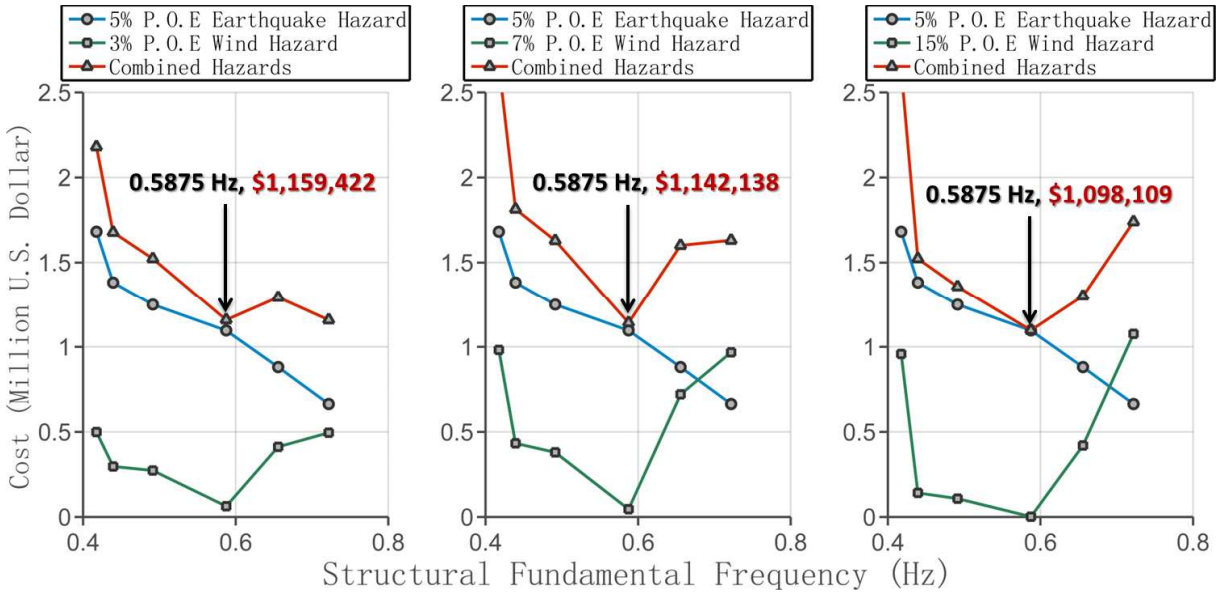


**Figure 5-18 Failure Cost Combination (Combo 4 to Combo 6) for BM-10**

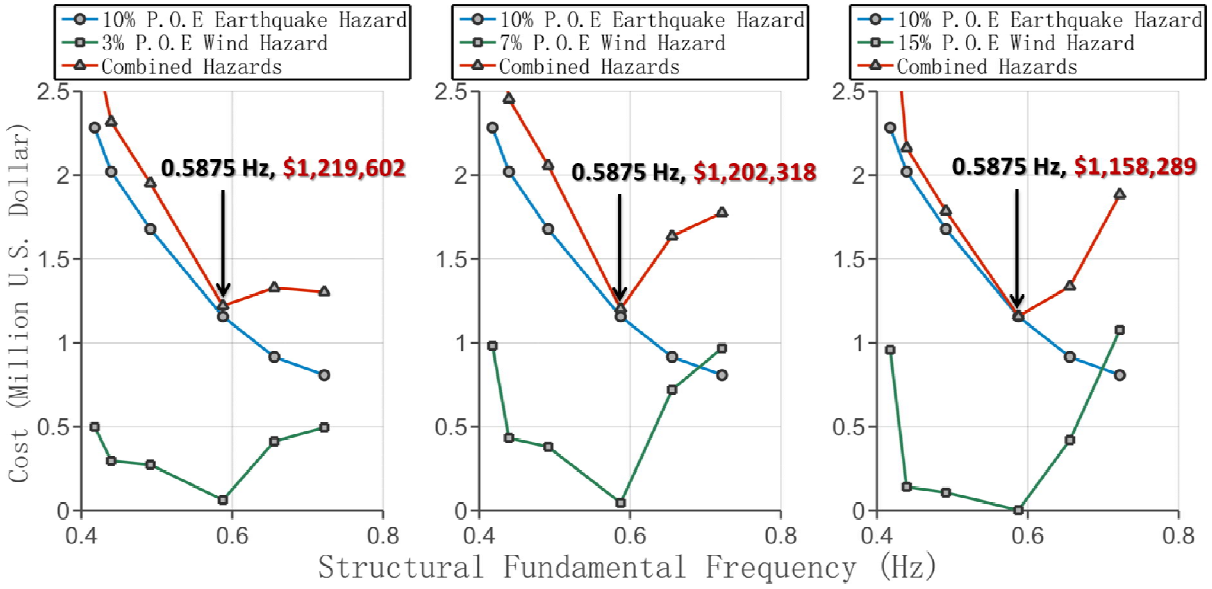


**Figure 5-19 Failure Cost Combination (Combo 7 to Combo 9) for BM-10**

According to the figures above, designers are able to identify the combination of earthquake and wind intensity and corresponding structural fundamental frequency based on their design objective. For design of BM-10, the design with consideration of combination of 2% P.O.E in 50 years earthquake intensity and 15% P.O.E in 50 years wind intensity considering structural fundamental frequency of 0.5875 Hz leads to the most economical failure cost. On the

other hand, the combination considering 10 % P.O.E in 50 years earthquake intensity and 3% P.O.E in 50 years wind intensity with structural fundamental frequency of 0.5875 Hz results in the most costly failure cost design. This finding provides designer an option to select the design hazard intensity combination according to different design purposes, e.g. economical design or conservative design from a financial perspective.

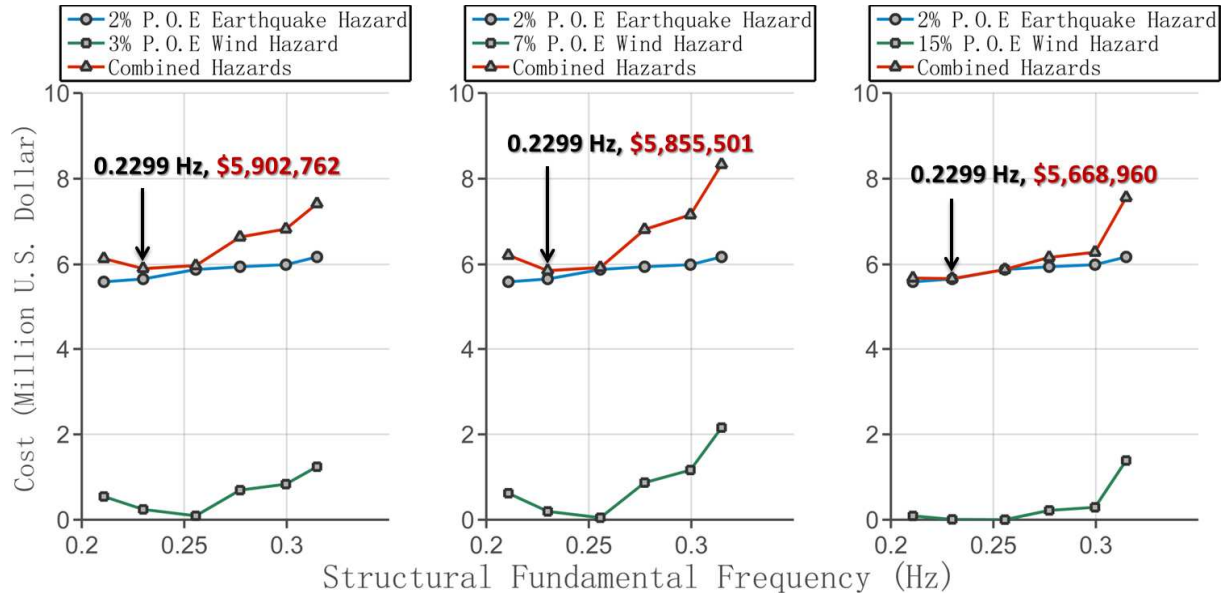


**Figure 5-20 Failure Cost Combination (Combo 1 to Combo 3) for BM-30**

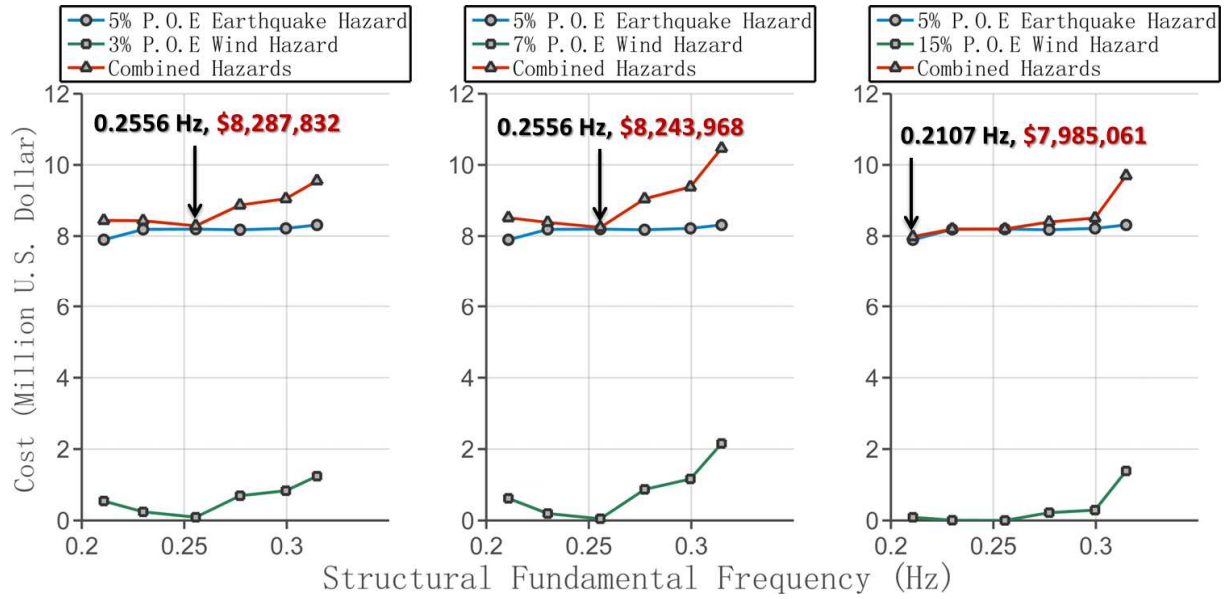


**Figure 5-21 Failure Cost Combination (Combo 4 to Combo 6) for BM-30**

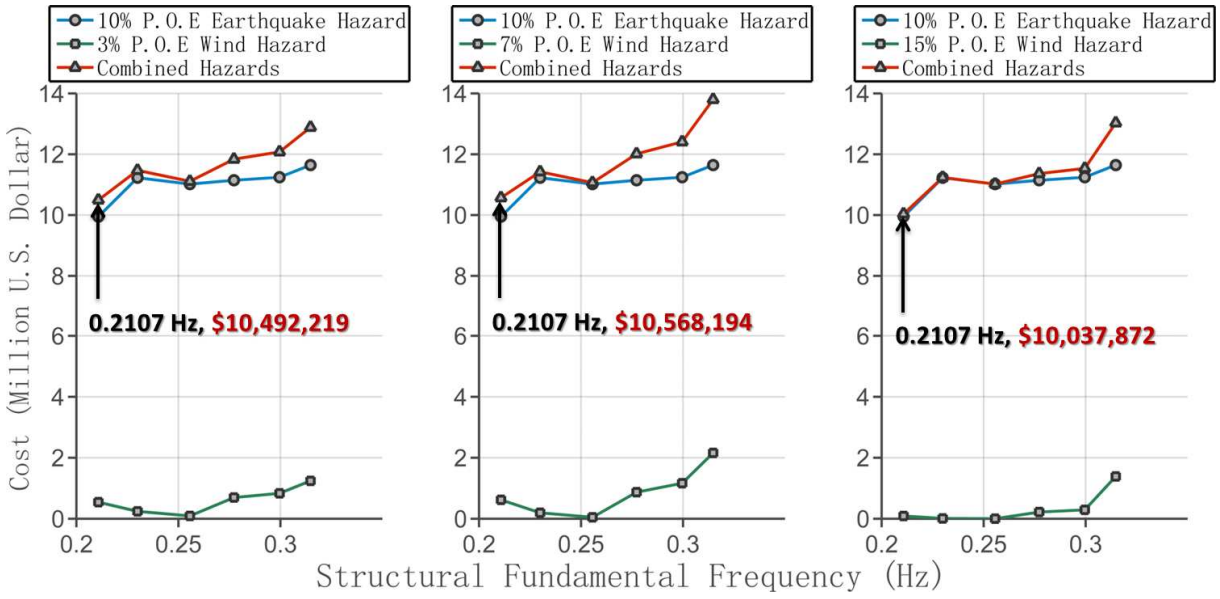


**Figure 5-22 Failure Cost Combination (Combo 7 to Combo 9) for BM-30**

The same investigation is also achieved for BM-30 and all the considered failure cost combinations are shown in Figure 5-20 to Figure 5-22. Similar to that has been found for BM-10, design considering structural fundamental frequency of 0.2299 Hz with combination considering 2% P.O.E in 50 years earthquake intensity and 15% P.O.E in 50 years wind intensity provides a more economical design and a more financially conservative design is ought to consider the combination considering 10 % P.O.E in 50 years earthquake intensity and 7% P.O.E in 50 years wind intensity for BM30 of structure with fundamental frequency of 0.2107 Hz.

### 5.5.2 Expected Life-cycle Costs Considering Single Hazard

In order to obtain a logical expected life-cycle cost results in this study, the total failure expected failure cost is defined as the summation of all the expected failure cost with consideration of earthquake intensities of 2%, 5%, and 10% P.O.E. It is because that the failure of the structure under seismic loading is identified as a series of potential economic loss or consumption (considering six permissible inter-story drift ratio), which can be generated by earthquake with intensities (2%, 5%, and 10% P.O.E) that may occur during the service time of

the building (assumed to be 50 years). In other words, these failure costs are generated during the building service time. Therefore, the total failure cost should include all the potential costs that might occur in this 50 years duration.

Figure 5-23 shows the final expected life-cycle costs, with the initial cost and total expected failure cost of 10-story building model subjected to earthquake hazard with considering of human injury and fatality.

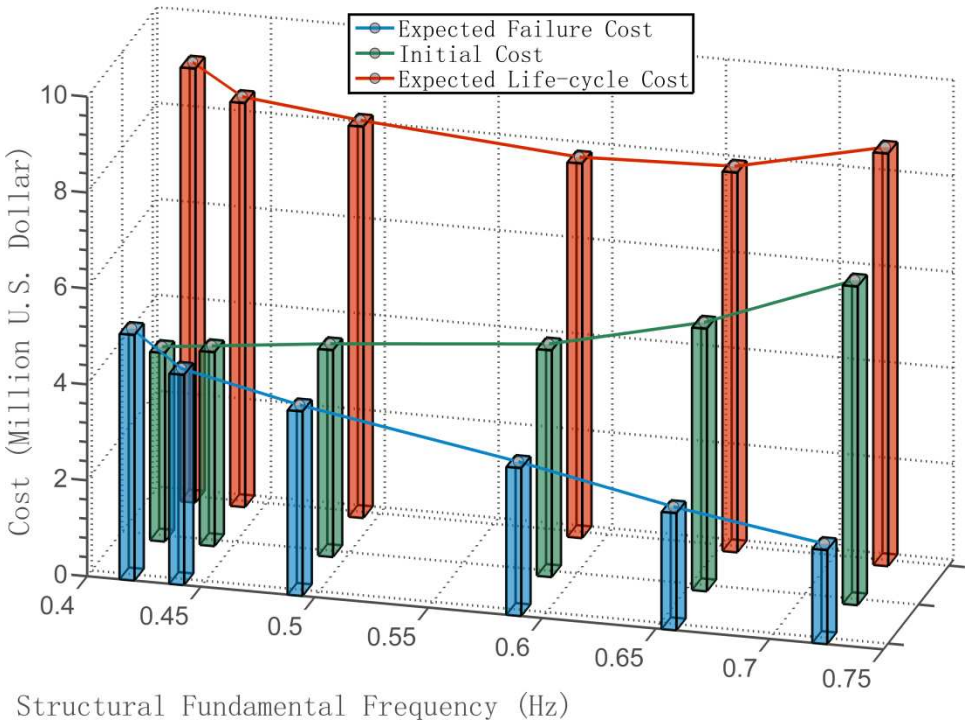


**Figure 5-23 Expected Life-cycle Cost for BM-10 Considering Earthquake Hazard**

As expected, the initial cost lessens as the overall structural lateral stiffness decreases since the reduction of column size. The expected failure cost, however, increases since the structural reliability reduces as the overall structural lateral stiffness decrease. The expected life-cycle cost equals the summation of initial cost and expected failure cost.

As can be seen in the figures, the column design scheme *II*, which has the approximated overall structural lateral stiffness f = 0.5875 Hz, results in the minimum expected life-cycle cost

and is considered as the column design scheme among all the six schemes for the 10-story building model considering earthquake risk only in San Francisco downtown area. The expected life-cycle cost for the 10-story building with the column design is estimated as $ 7,807,143 while considering human injury and death.

The final expected life-cycle costs, with the initial cost and total expected failure cost of the 30-story building model subjected to earthquake hazard with considering human injury and fatality are plotted in Figure 5-24.

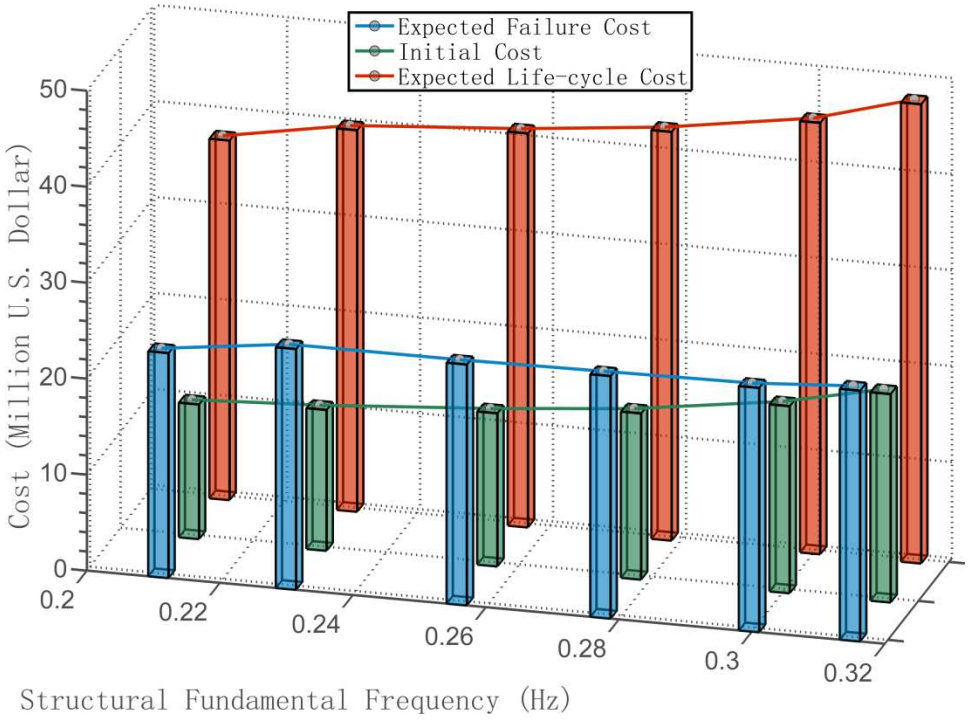


**Figure 5-24 Expected Life-cycle Cost for BM-30 Considering Earthquake Hazard**

For the design of 30-story building, the reduction in column sizes causes the structural overall lateral stiffness to decrease. Therefore, the initial cost is high when the overall structural lateral stiffness is large. The expected failure cost is increasing as the structure becomes stiffer. According to the expected life-cycle cost results, the column design scheme for 30-story building is obtained as the one with that consider earthquake risk only located in San Francisco downtown area can be selected as the one with smallest overall structural lateral stiffness as f = 0.2107 Hz

(Column design scheme *V*). The expected life-cycle cost of the 30-story building with the column design is estimated as $37,458,288 including the cost of human injury and death.

Cost of failure on the building subjected to wind hazard is defined as a potential initial cost on STMD system. Similar to the one considering earthquake hazard, the total failure cost for wind hazard should also include all the potential costs that might occur in the 50 building service years. It is because the failure costs considering different wind intensities were calculated by multiplying the probability of occurrence (3%, 7%, and 15%), which indicates each of these failure costs is considered as the potential initial cost for certain wind intensity. Therefore, the total failure costs considering wind intensities for the 50 building service years should combine the failure costs considering all of three wind intensities.

Figure 5-25 and Figure 5-26 show the expected life-cycle costs, with the initial cost and total expected failure cost of 10-story and 30-story building model, respectively, considering wind hazard only. According to the figures below, the optimal designs for BM-10 and BM-30 considering the wind hazard located in San Francisco downtown area are determined as the column design scheme *II* and *IV*, which have the approximated overall structural lateral stiffness f = 0.5875 Hz and f = 0.2299 Hz, respectively. Each of these two column design schemes respectively conducts the minimum expected life-cycle cost as $ 4,834,077 and $ 15,114,526 for BM-10 and BM-30.

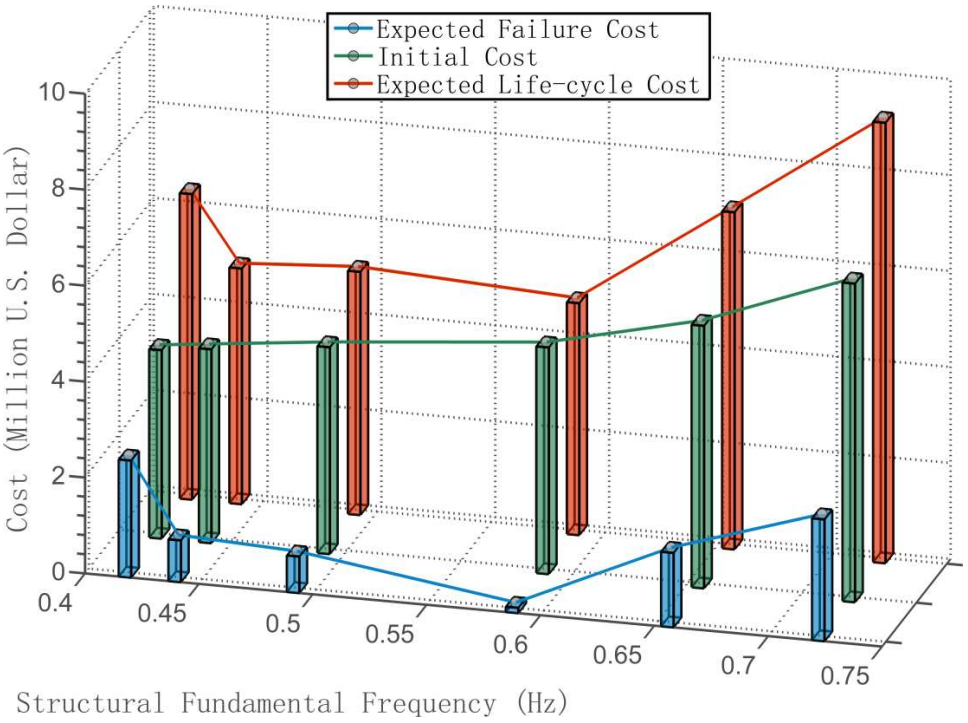


**Figure 5-25 Expected Life-cycle Cost for BM-10 Considering Wind Hazard**

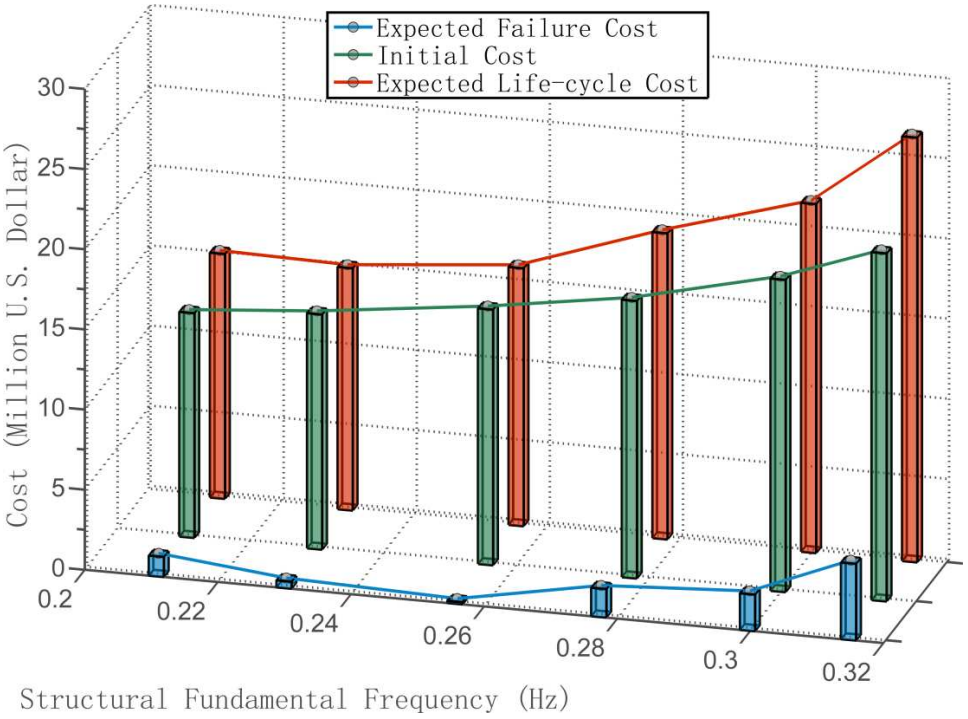


**Figure 5-26 Expected Life-cycle Cost for BM-30 Considering Wind Hazard**

### 5.5.3 Expected Life-cycle Costs Considering Multi-hazard

The expected life-cycle cost considering multi-hazard need to be defined carefully because irrationally combination of the probable economic losses may lead to underestimation or overestimation of the expected life-cycle cost. As mentioned previously, the definitions of failure for building subjected to earthquake and wind load are quite different. In spite of that, the expected life time failure costs for earthquake and wind hazard are calculated similarly as the summation of the expected failure costs considering different hazard intensities (earthquake intensity with 2%, 5%, and 10% P.O.E in 50 years and wind intensity with 3%, 7%, and 15% P.O.E in 50 years) during the building service years.

The expected failure cost herein, is defined as the summation of failure costs led by earthquake and wind hazards. Adding the expected failure cost to the initial construction cost conducts the final expected life-cycle cost considering multi-hazards. Figure 5-27 and Figure 5-28 present the expected life-cycle costs plotted with the initial construction cost and the expected failure cost considering multi-hazard for 10-story and 30-story building model, respectively.

As shown in the plots, the most economical column design schemes for both BM-10 and BM-30 can be selected. These design schemes obtain the minimum expected life-cycle costs considering both earthquake and wind hazard risks. As it has been mentioned that the failure cost made by wind hazard is much less effect on the total expected life-cycle cost compare to the one made by earthquake. Therefore, optimization decision considering multi-hazard risk keeps the same as the one considering earthquake hazard only (Column Design Scheme *II* for BM-10, and Column Design Scheme *V* for MB-30). Moreover, approximated structural fundamental frequencies f = 0.5875 Hz and f = 0.2107 Hz, can be determined as the optimizations in the structural fundamental frequencies region of 0.4 - 0.75 Hz and 0.2 – 0.32 Hz for 10-story and 30-

story building model, respectively. The corresponding minimum expected life-cycle costs considering multi-hazard are marked in the figures below.

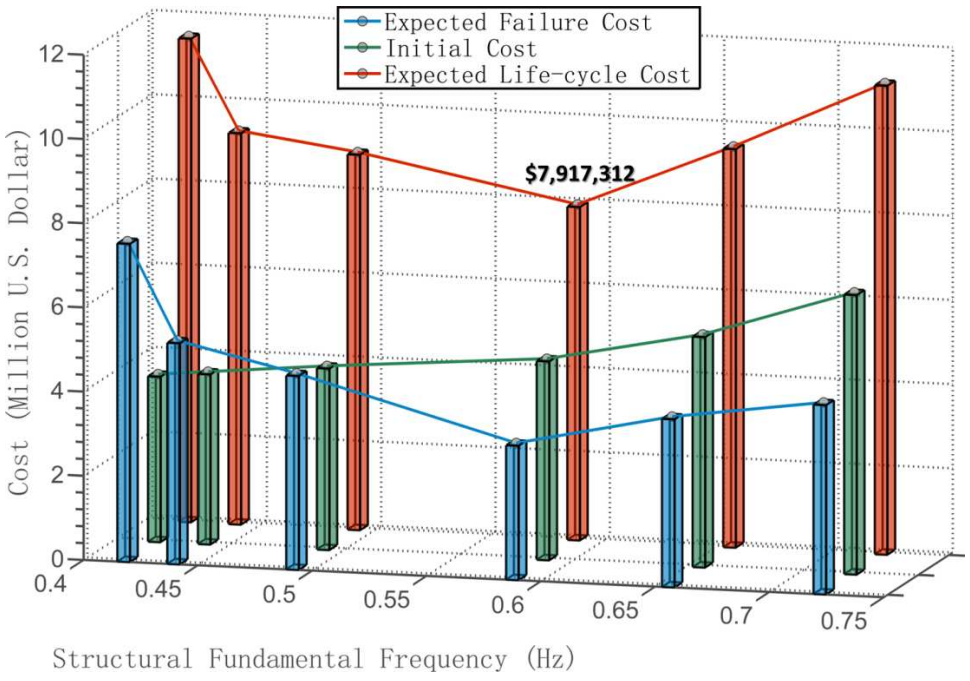


**Figure 5-27 Expected Life-cycle Cost for BM-10 Considering Multi- Hazard**

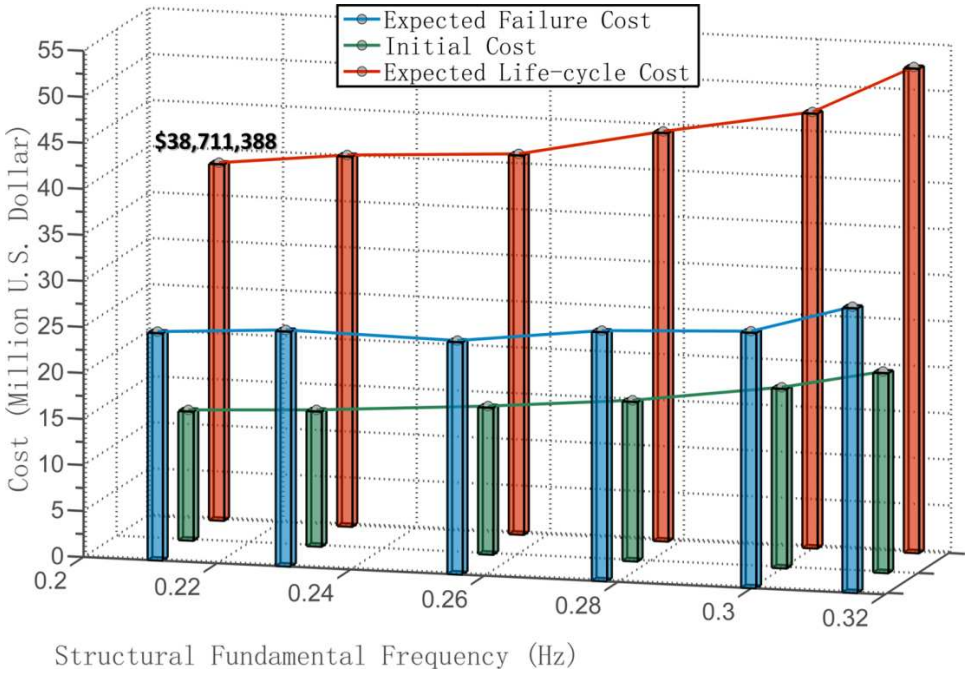


**Figure 5-28 Expected Life-cycle Cost for BM-30 Considering Multi- Hazard**

# CHAPTER 6

# CONCLUSION

## 6.1 Summary of the Work

In this thesis, a framework of expected life-cycle cost optimization design by considering reliability of buildings subjected to the combined hazard of earthquake and wind is proposed and tested. The framework includes finite element model development, limit state definition, cost function estimation, and methodology for interfacing MATLAB with ABAQUS for conducting a first order reliability method.

The 2D finite element models are developed to simulate typical medium- and high- rise residential building located in San Francisco downtown area, which is subjected to relatively higher risk from both strong earthquake and wind load. Six optimal design schemes (*Initial* and *I* to *V*) considering different column member sizes are developed according to design provisions. The initial design was developed such that the fundamental period of the buildings is roughly equal to 0.1×number of stories. This general rule ensures that drift requirements are met. The subsequent buildings designs are chosen as to introduce a reasonable perturbation in the initial period. The finite element simulation is conducted using ABAQUS with fine mesh to allow for accurate calculation of demand.

In order to offer a reliable assessment of the buildings subjected to multi-hazard, it is essential to provide a realistic definition of limit state. On the basis of current seismic and wind provisions as well as previous studies, six inter-story drift ratios are defined as the limit state for structure subjected to seismic loading and one limit state is defined for wind loading. For the seismic evaluation each of the inter-story drift ratios correspond to a damage level, which is

associated with a failure cost function. These cost functions and their parameters are determined in accordance with FEMA 229 (1992) and ATC 13 (1985). Other curtail factors, including for example discount rate and mean damage index, are also introduced. In this thesis, the reliability analysis considering structures subjected to dynamic loading is implemented by interfacing MATLAB and ABAQUS finite element simulation.

## 6.2 Significance and Conclusion

This study introduces an approach for investigating the expected life cycle cost for buildings subjected to multi-hazard risks. Medium and high-rise residential buildings subjected to low, medium, and high risk of earthquake and wind loads is selected for the study. The hazard levels represent 2%, 5%, and 10% probability of exceedance for the seismic hazard and 3%, 7%, and 15% for the wind. The following conclusion can be made from this study:

- The building structures are located at San Francisco downtown area are subjected to varying level of wind and seismic risks.
- The reliability index results, for the earthquake hazard only, it is found that when considering relatively more severe limit state (larger permissible inter-story drift ratio), a more intensive fluctuation of the reliability index value is obtained with respect to the different building designs (different fundamental frequencies). In other words, the structural reliability is more sensitive to structural fundamental frequency when larger limit state is considered.
- The expected failure cost has been rationally calculated and it is shown that the expected failure costs considering earthquake load only can be fitted into numerical function with the relationship between structural fundamental frequency and the

expected failure cost considering different intensity of seismic loading in a certain range of structural fundamental frequency. The prediction of the type of this numerical function is determined according to the FFT analysis of the earthquake time-history record.

- Failure cost with consideration to different hazards and intensities can be combined. The combined failure cost, which has minimum or maximum values over the range of frequencies investigated, can be viewed as design criterion where one might choose either an economical or a more conservative design.
- The final expected life-cycle cost can be calculated and presented as a function of the structural fundamental frequency for the individual and combined hazards.
- The results show that the an optimal design can be achieved to minimize the life-cycle cost under both hazards which would be otherwise not possible if the seismic hazard or wind hazards are evaluated independently.

## 6.3 Future Work Discussion

As previously mentioned, the main goal of this study is to develop and present the framework of an innovative method for investigating the expected life cycle cost optimization design considering structural reliability subjected to multi-hazard risks. There is significant work that can be conducted to both extend the investigation and improve the results. This includes the following:

- For providing more accurate analysis framework, 3D finite element models with cladding and slab components can be utilized to simulate the building, instead of the 2D models used in this study

- Only two random variables were considered in the reliability analysis. In reality, however, there are many inherent properties of the structure and loading cases that should be regard as random variables. For the realistic purpose based on this method, more random variables, e.g. material yield strength, moment of inertia of structural members, can be defined in order to obtain a more reasonable reliability analysis.

# REFERENCES


Ang, AH-S., and D. De Leon. "Determination of optimal target reliabilities for design and upgrading of structures." Structural Safety 19.1 (1997): 91-103.

AISC Committee. "Specification for Structural Steel Buildings (ANSI/AISC 360-10)." *American Institute of Steel Construction, Chicago-Illinois* (2010).

Applied Technology Council. *Earthquake damage evaluation data for California*. ATC-13, 1985.

ASCE 7-10. "Minimum design loads for building and other structures." (2010).

ASTM, A.6/A 6M, "Standard Specification for General Requirements for Rolled Structural Steel Bars, Plates, Shapes, and Sheet Piling. " (2010).

Beer, P.E. "Hurricane and Tornado Damage in Urban Areas – A Recent History." Pushing the Building Envelope, (2011) <http://buildingenvelope.wordpress.com/2011/05/24/hurricane-and-tornado-damage-in-urban-areas-%E2%80%93-a-recent-history/>

*RSMeans® Building Construction Cost Data* (BCCD), 54th Annual Edition, 1996.

*RSMeans® Building Construction Cost Data* (BCCD), 55th Annual Edition, 1997.

Chang, Fu-Kuei. "Human response to motions in tall buildings." *Journal of the Structural Division* 99.6 (1973): 1259-1272.

Coburn, A. and Spence, R. "Earthquake Protection", John Wiley, Chichester, U.K. (2002).

DeBlasio, Allen J., et al. "Effects of Catastrophic Events on Transportation System Management and Operations, Northridge Earthquake—January 17, 1994." *US Department of Transportation, Washington, DC* (2002).

Der Kiureghian, Armen. "First-and second-order reliability methods." *Engineering design reliability handbook* (2005): 1-47.

Duthinh, Dat, and Emil Simiu. "Safety of structures in strong winds and earthquakes: multi-hazard considerations." *Journal of structural engineering* 136.3 (2009): 330-333.

EQE International. "The January 17, 1995 Kobe Earthquake: An EQE Summary Report." (1995)

Estes, Allen C., and Dan M. Frangopol. "RELSYS: A computer program for structural system reliability." *Structural engineering and mechanics* 6.8 (1998): 901-919.

Ettouney, Mohammed M., and Norman J. Glover. "Engineering of architectural systems." *Journal of architectural engineering* 8.1 (2002): 7-9.

Ettouney, Mohammed, and Sreenivas Alampalli. "Blast hazard considerations within a multihazards environment: An application to the theory of multi-hazards." *Structures Congress 2006 @ sStructural Engineering and Public Safety*. ASCE, 2006.

Ettouney, Mohammed M., Sreenivas Alampalli, and Anil K. Agrawal. "Theory of multi-hazards for bridge structures." *Bridge Structures* 1.3 (2005): 281-291.

FEMA, P. 695. *Quantification of Building Seismic Performance Factors*, Federal Emergency Management Agency, (2009).

FEMA 174, *Establishing Programs and Priorities for the Seismic Rehabilitation of Buildings: A Handbook*, Federal Emergency Management Agency, (1989).

FEMA 227/228. *A Benefit–Cost Model for the Seismic Rehabilitation of Buildings, Volume 1: A User's Manual and Volume 2: Supporting Documentation*, Federal Emergency Management Agency, (1992).

Gollwitzer, S., et al. "PERMAS-RA/STRUREL system of programs for probabilistic reliability analysis." *Structural Safety* 28.1 (2006): 108-129.

GRIFFIS, LAWRENCE G. "Serviceability Limit States under Wind Load." *Engineering Journal/American Institute of Steel Construction* (2003).

Haukaas, Terje. *Finite element reliability and sensitivity methods for performance-based engineering*. Diss. UNIVERSITY of CALIFORNIA, 2003.

Haukaas, T., et al. "http://www. ce. berkeley. edu/haukaas/ferum/ferum. html. FERUM." *Department of Civil and Environmental Engineering, University of California, Berkeley, CA* (2003).

Horwich, George. "Economic lessons of the Kobe earthquake." *Economic development and cultural change* 48.3 (2000): 521-542.

Huh, Jungwon, and Achintya Haldar. "Stochastic finite-element-based seismic risk of nonlinear structures." *Journal of structural engineering* 127.3 (2001): 323-329.

Kam, T. Y. "Reliability of framed structures with initial imperfections." *Computers & structures* 25.5 (1987): 695-698.

Kam, Tai-Yan, Ross B. Corotis, and Edwin C. Rossow. "Reliability of nonlinear framed structures." *Journal of Structural Engineering* 109.7 (1983): 1585-1601.

Kang, Yong-Joong, and Y. K. Wen. *Minimum life-cycle cost structural design against natural hazards*. University of Illinois Engineering Experiment Station. College of Engineering. University of Illinois at Urbana-Champaign., 2000.

Kareem, Ahsan. "Reliability analysis of wind-sensitive structures." *Journal of wind engineering and industrial aerodynamics* 33.3 (1990): 495-514.

Lee, Young Joo. *Finite-element-based system reliability analysis and updating of fatigue-induced sequential failures*. Diss. University of Illinois at Urbana-Champaign, 2012.

Lin, Tzyy Shan, and Ross B. Corotis. "Reliability of ductile systems with random strengths." *Journal of Structural Engineering* 111.6 (1985): 1306-1325.

Liu, Shih Chi, and Farrokh Neghabat. "A cost optimization model for seismic design of structures." *Bell System Technical Journal* 51.10 (1972): 2209-2225.

Moses, F1. "System reliability developments in structural engineering." *Structural Safety* 1.1 (1983): 3-13.

O'Connor, Jennifer M., and Bruce Ellingwood. "Reliability of nonlinear structures with seismic loading." *Journal of Structural Engineering* 113.5 (1987): 1011-1028.

*Pacific Earthquake Engineering Research Ground Motion Database* (PEER), University of California, Berkeley, CA, (2010)

Russell, A. D., and K. T. Choudhary. "Cost optimisation of buildings." *Journal of the Structural Division* 106.ST1 (1980): 283-300.

Sarma, Kamal C., and Hojjat Adeli. "Cost optimization of concrete structures." *Journal of Structural Engineering* 124.5 (1998): 570-578.

Sfintesco, D. "Planning and environmental criteria for tall buildings." ASCE, 1981.

Song, J. *Decision and Risk Analysis*, Lecture notes, University of Illinois, Urbana, IL, (2007).

SwRI. *NESSUS (ver 9.0)*, http://www.nessus.swri.org/ Southwest Research Institute, (2009).

Tao, Zongwei, Ross B. Corotis, and J. Hugh Ellis. "Reliability-based bridge design and life cycle management with Markov decision processes." *Structural Safety* 16.1 (1994): 111-132.

Tse, K. T., K. C. S. Kwok, and Yukio Tamura. "Performance and cost evaluation of a smart tuned mass damper for suppressing wind-induced lateral-torsional motion of tall structures." *Journal of Structural Engineering* 138.4 (2012): 514-525.

*United States Geological Survey* (USGS), "Seismic Hazard Analysis Tools", Earthquake Hazards Program.

*United States Geological Survey* (USGS), "Seismic Hazard Maps and Data", Earthquake Hazards Program.

Vanmarcke, Erik, and Demosthenes Angelides. "Risk assessment for offshore structures: a review." *Journal of Structural Engineering* 109.2 (1983): 555-571.

Wang, Zifa. "A preliminary report on the Great Wenchuan Earthquake." *Earthquake Engineering and Engineering Vibration* 7.2 (2008): 225-234.

Warszawski, A., J. Gluck, and D. Segal. "Economic evaluation of design codes-case of seismic design." *Journal of Structural Engineering* 122.12 (1996): 1400-1408.

Wen, Y. K., and M. Shinozuka. "Cost-effectiveness in active structural control." *Engineering structures* 20.3 (1998): 216-221.

Whitman, Robert V., et al. "Seismic design decision analysis." *Journal of the Structural Division* 101.5 (1975): 1067-1084.

Zhou, Xiangming. "Multi-hazard performance assessment of a transfer-plate high-rise building." *Earthquake Engineering and Engineering Vibration* 6.4 (2007): 371-382.

# APPENDIX A

# STRUCTURAL MASS CALCULATION

The structural mass, in this study, is mainly considered as a structural inherent property for finite element dynamic time-history analysis using ABAQUS. In order to obtain a rational structural mass, the loading concept needs to be defined carefully.

First of all, the configuration of the structural is presented in Figure A-1. The shadow parts in the figure indicate the SMR Frame. For convenience of loading calculation, all the dimensions herein are indicated using ft.

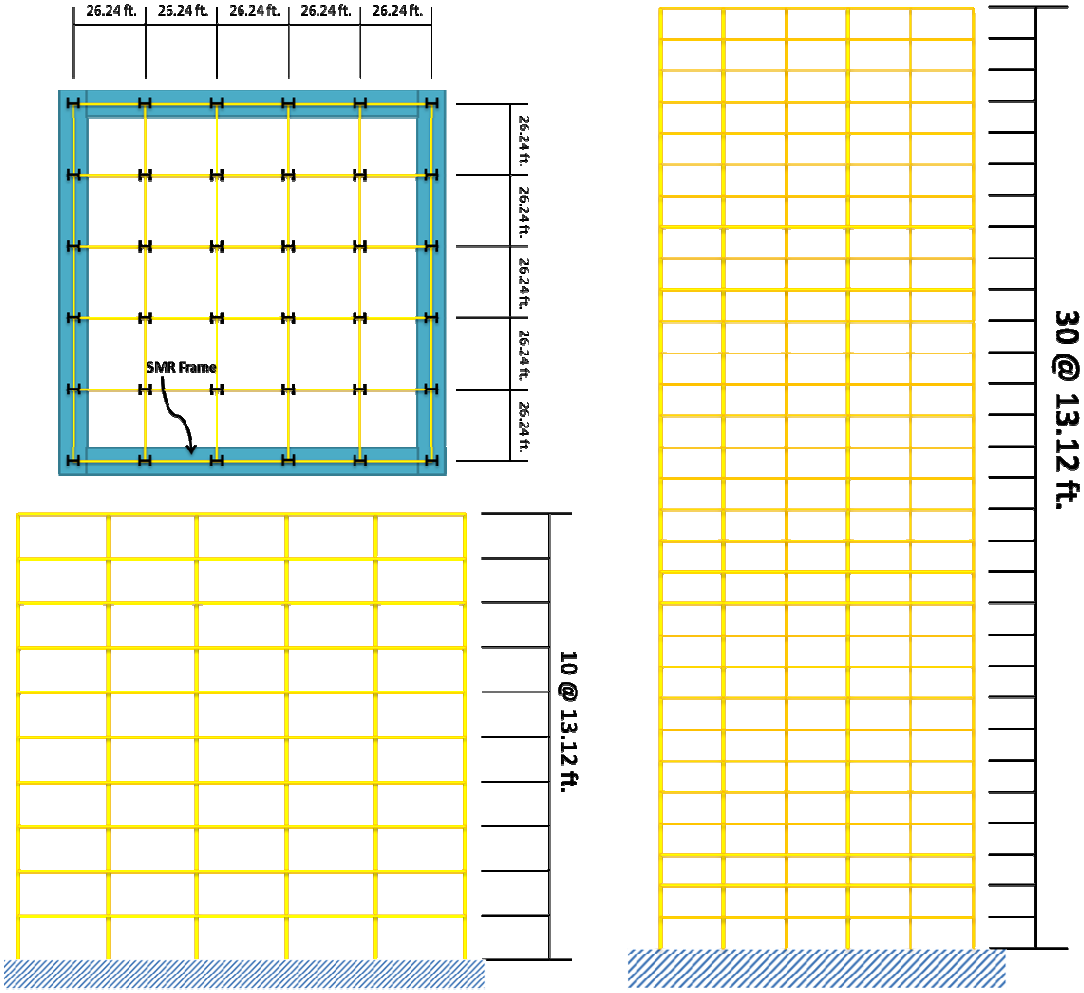


**Figure A- 1**

A rational loading case then is defined for dynamic time-history analysis and two assumptions are considered:

1. Total floor mass is distributed as lumped mass at the nodes of floor according to the tributary area as shown in Figure A-2.

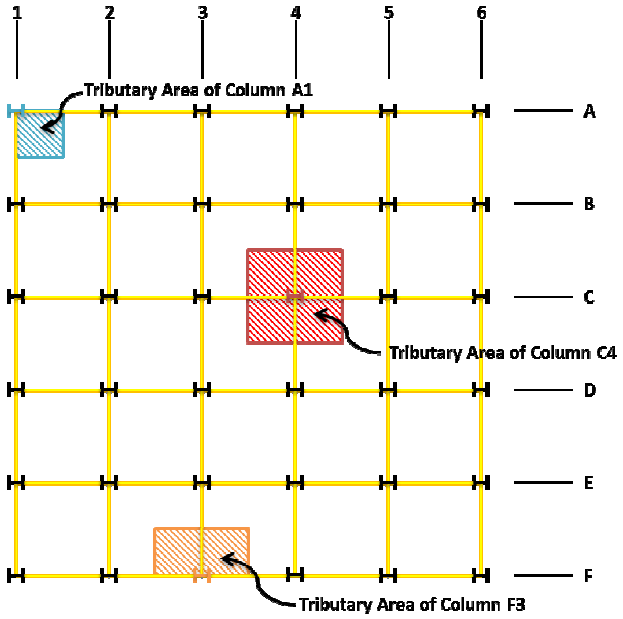


**Figure A-2 Tributary Area for Lumped Mass at the Nodes of Floor**

2. SMR Frames are considered to resist all the lateral inertia from the mass as demonstrated in Figure A-3. Each of the interest frames is assumed to absorb half of the lateral load from entire floor mass generated by ground motion.

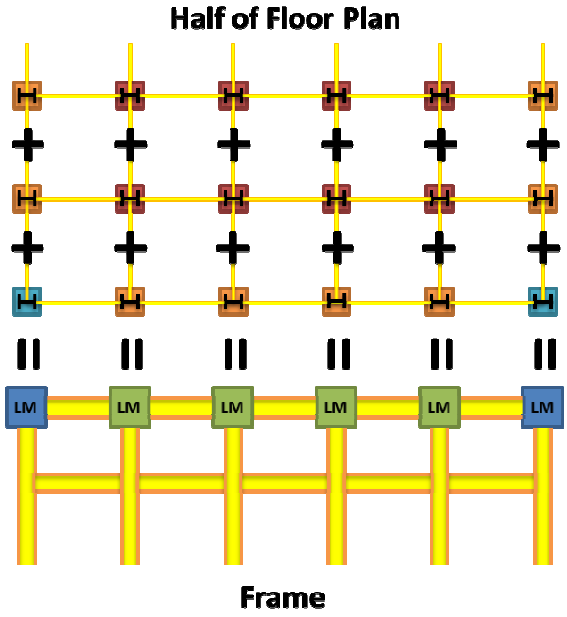


**Figure A-3 Assembly of Lumped Mass on the Node of SMRF**

3. Initial loading is assumed in follow:

$$Load\ Combination = 1.0DL + 10psf + 0.25LL$$

in which $DL = Dead\ Load$; $LL = Live\ Load$; and $10psf$ combines all the weights from exterior wall system

Then Table A-1 shows the unit weights of the dead load and live load, which are used in this study.

| **Roof Weight** | | | **Floor weight** | | |
|---|---|---|---|---|---|
| Dead load | 62.0 | psf | Dead load | 69.0 | psf |
| Exterior wall system weight: steel studs, gypsum board, fascia panels | | | | | |
| | 10.0 | psf | | 10.0 | psf |
| Live load | 20.0 | psf | Live load | 80.0 | psf |

Eventually, the calculations can be carried out and the details are shown in following.

***Initial Loads and Mass***

$Load\,(Roof) = [131.24 \times 131.24 \times (0.25 \times 20 + 62)] + 10 \times 10.5 \times (131.24 \times 4) = 1209125 lb$ *Note: exterior walls are distributed by tributary height. For the roof it is 4 ft. above the roof and 6.5 ft. below the roof.*

$Mass\,(Roof) = 548450\ kg$

$Load\,(Floor) = [131.24 \times 131.24 \times (0.25 \times 80 + 69)] + 10 \times 13.12 \times (131.24 \times 4) = 1601805 lb$
*Note: exterior walls are distributed by tributary height. For the floor it is full height of the floor 13.12ft.*

$Mass\,(Floor) = 726567\ kg$

***Lumped Mass at the Nodes***

According to the introduction of Figure A-2 and Figure A-3, the final lumped mass at the nodes of SME Frames for roof and floors can be determined.

At the first, the lumped mass of floor (or roof) is calculated according to the corresponding tributary area. Each of the interior nodes (with tributary area of red shadow in Figure A-2) is considered to take 4/100 of the total mass of the entire floor (or roof). Each of the edge nodes (with tributary area of orange shadow in Figure A-2) is considered to take 2/100 of the total mass of the entire floor (or roof). Each of the corner nodes (with tributary area of cyan shadow in Figure A-2) is considered to take 1/100 of the total mass of the entire floor (or roof).

As each of the SMR Frames is considered to resist half of the total lateral load, the lumped mass on the nodes of floor (or roof) will be assembled as the lumped mass on the nodes of SMR Frame and lumped mass values s calculated in follow.

1. Lumped mass at the interior nodes (marked by green box in Figure A-3)

$$\left(\frac{4}{100}+\frac{4}{100}+\frac{2}{100}\right)\times Mass(Floor,Roof)=\frac{Mass(Floor,Roof)}{10}$$

2. Lumped mass at the interior nodes (marked by blue box in Figure A-3)

$$\left(\frac{2}{100}+\frac{2}{100}+\frac{1}{100}\right)\times Mass(Floor,Roof)=\frac{Mass(Floor,Roof)}{20}$$

# APPENDIX B

# DETERMINATION OF COLUMN AND BEAM SIZES

## B.1. Determination of Beam Sizes

In order to determine a rational beam size for the structure, two basic criterions are needed to be considered: 1) the maximum flexural strength criterion, and 2) the maximum deformation criterion.

### B.1.1. Flexural Strength Criterion

The maximum flexural strength criterion indicates a condition that the flexural strength capacity of beam members must not exceed the required flexural strength. According to the AISC 360-10, Equation B-1 can be given here to demonstrate principle concept of the required flexural strength. In this equation, $M_u$ represents the required flexural strength for design of beam member; $M_n$ is the nominal flexural strength, which is determined later; and $\phi_b$ is consider as the resistance factor for flexure, which equals to 0.9.

$$M_u \leq \phi_b \cdot M_n \qquad \textbf{Equation B- 1}$$

For the design purpose, the required flexural strength $M_u$ can be determined considering structural load case consideration and the tributary area of beam members. Figure B-1 demonstrates the definition of the tributary area considered by beam member in this study. Then the $M_u$ can be calculated as follow.

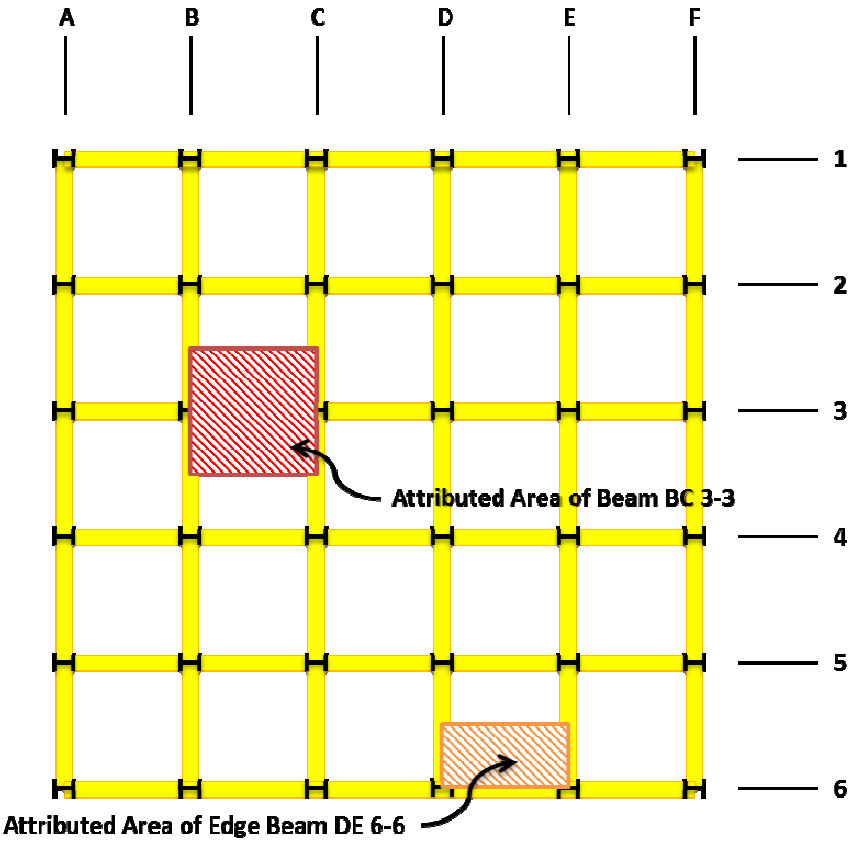


**Figure B-1**

***Load Calculation***

According to ASCE 7:

Minimum uniformly distributed live loads for building design

40 *psf* for residential dwellings, apartments, hotel rooms, school classrooms

50 *psf* for offices

60 *psf* for auditoriums with fixed seats

73 – 100 *psf* for retail stores

(ASCE 7-5)

***Required Flexural Strength Calculation***

Given

Live Load, $L = 40\ psf$

Dead Load, $D = 69\ psf$

Beam 3-3

Tributary Area, $A_T = 26.24 \times 26.24 = 689\ ft^2$

Influence Area, $A_I = 2 \cdot A_T = 2 \times 689 = 1378\ ft^2$

Live Load Reduction, $R_L = 0.25 + \left[15 / \sqrt{A_I}\right] = 0.25 + \left[15 / \sqrt{1378}\right] = 0.654$

Amplified Loads per linear ft.:

Dead Load, $1.2D = 1.2 \times (69\ psf) \times (26.24\ ft) = 2173 lb/\ ft$

Live Load, $1.6L = 1.6 \times (0.654) \times (40\ psf) \times (26.24\ ft) = 1098 lb/\ ft$

$W_u = 1.2D + 1.6L = 2173 + 1098 = 3271 lb/\ ft$

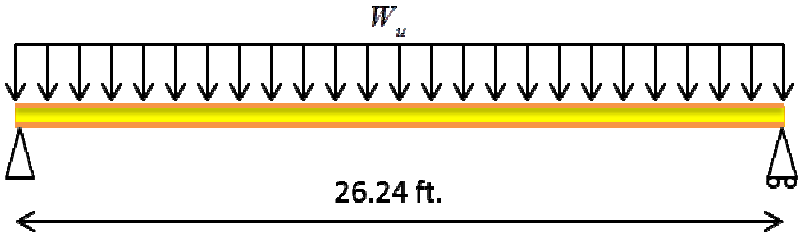


**Figure B-2**

As Figure B-2 has indicated the transformed linear load, the required flexural strength (moment) can be carried out as:

$$M_u = \frac{W_u L^2}{8} = \frac{3271 \times (26.24)^2}{8} = 281526\ lb \cdot\ ft$$

***Nominal Flexural Strength Calculation***

Yielding

$$M_n = M_p = F_y \cdot Z_x \qquad \textbf{Equation B- 2}$$

in which:

$M_p$ = Plastic bending moment

$F_y$ = Specified minimum yield stress of the type of steel being used, ($50\,ksi$)

$Z_x$ = Plastic section modulus about the x-axis, (according to ASTM 6A)

Lateral-Torsional Buckling

a) When $L_b \le L_p$, the limit state of lateral-torsional buckling does not apply.

b) When $L_p < L_b \le L_e$

$$M_n = C_b\left[M_p - \left(M_p - 0.7F_yS_x\right)\left(\frac{L_b - L_p}{L_r - L_p}\right)\right] \le M_p \qquad \textbf{Equation B- 3}$$

c) When $L_b > L_r$

$$M_n = F_{cr}S_x \le M_p \qquad \textbf{Equation B- 4}$$

in which:

$L_b$ = Length between points that area either braced against lateral displacement of the compression flange or braced against twist of the cross section, (length of beam or column member herein)

$L_p$ = Limiting laterally un-braced length for the limit state of yielding

$L_r$ = Limiting laterally un-braced length for the limit state of inelastic lateral-torsional buckling

$F_{cr}$ = Critical stress

$S_x$ = Elastic section modulus taken about the x-axis

In this study, all the beam members are assumed to be selected without consideration of the limit state of lateral-torsional buckling. Therefore, the selected beam members must satisfy the condition of $L_b \le L_p$ and the limiting length of $L_p$ can be determined as follow:

$$L_p = 1.76 r_y \sqrt{\frac{E}{F_y}} \qquad \textbf{Equation B- 5}$$

in which:

$r_y$ = Radius of gyration about the x-axis, (according to ASTM 6A)

$E$ = Modulus of elasticity of steel, ( $29{,}000\,ksi$ )

### B.1.2. Deflection Criterion

According to the AISC 360-10, a deflection limit for building serviceability design is given. The deformation limit indicates that the common deflection limits for horizontal members, e.g. beam members, have been summarized based on historical experiences. Deflection limits of 1/360 of the span for floors subjected to reduced live load and 1/240 of the span for roof members are identified and utilized as the minimum allowable deflection in this study. Equation B-6 offers the calculation of the minimum allowable deflection:

$$Minimum\,Allowable\,Delection = \frac{L_b}{360} = \frac{26.24}{360} = 0.073\ ft$$

## B.2. Determination of Columns Sizes

The determinations of column member sizes in this study are divided into two parts: 1) column member of interior frames (gravity resisting frames), and 2) column member of exterior frames (SMRF).

### B.2.1. Determination of Column Members in the Interior Frames

In this study, the column members located in the interior frames are considered to absorb the gravity load (Dead and Live load) only. Therefore, these column members can be design as the axially loaded compression members according to AISC 360-10.

At the beginning, the column members are defined as the flexural buckling members without slender elements. Therefore the selected column members must fulfill the limiting of width-to-thickness as non-slender consideration, which has been defined in AISC 360-10 (TABLE B4.1a). Then, the principle concept of column member design is given in Equation B-6

$$P_u \le \varphi_c P_n = \varphi_c A_g F_{cr} \qquad \textbf{Equation B- 6}$$

in which:

$P_u$ = Required axial compressive strength, (considering floor weight and column tributary areas in Appendix A)

$P_n$ = Nominal axial compressive strength

$\varphi_c$ = Resistance factor for compression members (0.90)

$A_g$ = Gross cross-sectional area, (according to ASTM 6A)

$F_{cr}$ = Critical compressive stress

The critical compressive stress, $F_{cr}$, is determined as follows:

a) When $\frac{KL}{r} \le 4.71\sqrt{\frac{E}{F_y}}$ (or $\frac{F_y}{F_e} \le 2.25$)

$$F_{cr} = \left[0.658^{\frac{F_y}{F_e}}\right] F_y \qquad \textbf{Equation B- 7}$$

b) When $\frac{KL}{r} > 4.71\sqrt{\frac{E}{F_y}}$ (or $\frac{F_y}{F_e} > 2.25$)

$$F_{cr} = 0.877 \cdot F_e \qquad \textbf{Equation B- 8}$$

in which:

$F_e$ = Elastic buckling stress determined according to Equation B-9

$$F_e = \frac{\pi^2 E}{\left(\frac{KL}{r}\right)^2} \qquad \textbf{Equation B- 9}$$

$K$ = Effective length factor, fixed ends are assumed, therefore $K = 0.5$ herein

$L$ = Laterally un-braced length of column member

$r$ = Governing radius of gyration about the axis of buckling

$F_y$ = Specified minimum yield stress, ($50\,ksi$)

$E$ = Modulus of elasticity of steel, ($29{,}000\,ksi$)

According to the floor and roof mass calculation and the tributary area determination in Appendix A, the required axial compressive strength $P_u$ can be carried out as the summed floor weight carried by the column members associated with the tributary areas, which is shown in Figure A-2.

The column members at the bottom floor are considered to take the entire upper floor weights as the required axial compressive strength for design. Therefore, column member size is considered to decrease from bottom to top.

### B.2.2. Determination of Column Members in the Exterior Frames

The exterior frames, in this study, play the role of the SMRF and are considered to resist the lateral loads including earthquake and wind loads. Therefore, the column members in the

exterior frames should be designed considering not only vertical loadings (gravity loads), but also the loadings result from earthquake and wind loads.

The seismic load is considered to be the principle effect for designing the column member of the SMRF. The design procedure will be presented in following:

1. The eigenvalue analyses are carried out with ABAQUS using the column member design considering only gravity loading as the initial column member sizes.
2. The fundamental frequencies of the frames, then, are used to find out the corresponding maximum considered peak ground acceleration ($PGA_{\max}$) using the Risk-adjusted Maximum Considered Earthquake design response spectrum (detail of this response spectrum has been introduced in Chapter 4).
3. The $PGA_{\max}$ values then will be used to calculate the maximum considered base moment ($M_{Base}$) by multiply it with the tributary mass and the length of column, e.g. the calculation process of the base moment is shown in Figure B-3 for the column size of the first 4 stories of BM-10.

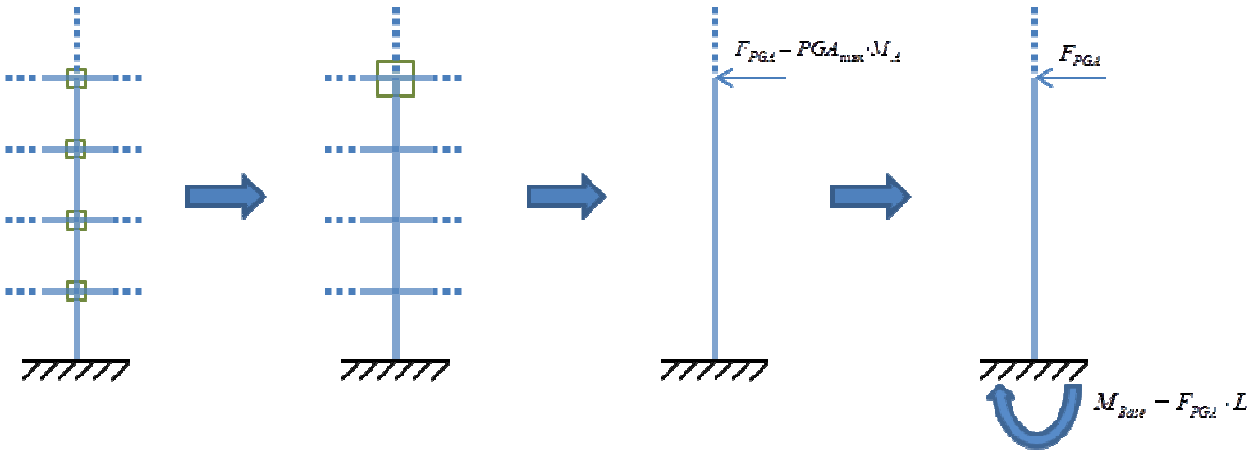


**Figure B- 3 Base Moment Calculation for the Columns of Frist 4 Story of BM-10**

4. The base moment ($M_{Base}$) then will be defined as the required moment and used to select a new column size for satisfying this moment requirement by using Equation B-2.
5. At last the new column size will be utilized in the frame model and steps from 1 to 4 are needed to repeat until the all the column sizes satisfy the requirement defined in Equation B-1.